

Master's thesis

NTNU
Norwegian University of Science and Technology

Isak Hammer

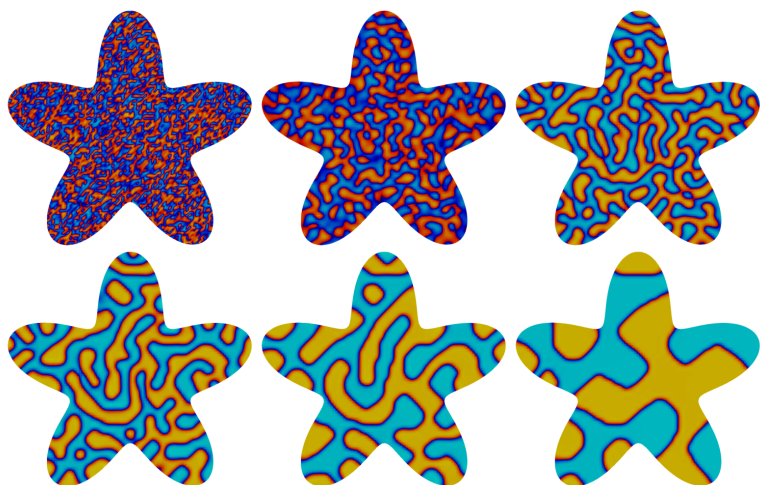
A cut finite element method for the biharmonic problem and its application to the Cahn-Hilliard equation

Master's thesis in Applied Physics and Mathematics

Main profile: Industrial Mathematics

Supervisor: André Massing

July 2023



Norwegian University of
Science and Technology

Isak Hammer

A cut finite element method for the biharmonic problem and its application to the Cahn-Hilliard equation

Master's thesis in Applied Physics and Mathematics
Main profile: Industrial Mathematics
Supervisor: André Massing
July 2023

Norwegian University of Science and Technology



Norwegian University of
Science and Technology

Contents

1	Introduction	7
1.1	The physical Cahn-Hilliard problem	7
1.2	Numerical methods	8
1.3	Outline of the report	10
2	Mathematical background	11
2.1	Sobolev spaces	11
2.2	Computational domains	12
2.3	Broken Sobolev spaces	14
2.4	Lax-Milgram lemma	15
2.5	Finite element methods	15
2.6	Condition number	19
2.7	Clément interpolation	20
2.8	Useful local inverse estimates	21
2.9	Abstract Nonconform Error Analysis	22
3	Continuous interior penalty methods for the biharmonic problem with Cahn-Hilliard type boundary conditions	23
3.1	The biharmonic equation	23
3.2	Detailed construction of Hessian and Laplacian Formulations	24
3.2.1	Construction of the Hessian formulation	24
3.2.2	Construction of the Laplacian formulation	27
3.2.3	Comments and earlier work	29
3.3	Note on the biharmonic mixed formulation	29
4	Cut continuous interior penalty methods for the biharmonic problem	30
4.1	Computational domain	31
4.2	Cut continuous interior penalty methods	31
4.3	Stability estimate	33
4.4	A priori error estimate	36
4.5	Constructing ghost penalties	40
4.6	Numerical experiments	44
4.6.1	Numerical setup	44
4.6.2	Validation of the a priori estimates	45
4.6.3	Translation test	48
5	Applications to the Cahn-Hilliard equation	50
5.1	Deriving the discrete formulation of the Cahn-Hilliard equation	50
5.2	Demonstration on the Cahn-Hilliard problem	51
5.3	Note on the manufactured solution	55
6	Conclusion	57

Abstract

The Cahn-Hilliard equation, with its wide range of applications in phase-separation, poses numerical challenges due to its non-linear and stiff nature and fourth-order derivatives. This thesis introduces a novel, stabilized, unfitted cut continuous interior penalty finite element method specifically designed for the biharmonic problem with Cahn-Hilliard type boundary conditions, which we have successfully extended to handle the Cahn-Hilliard equation. Our approach combines the theoretical cut discontinuous Galerkin framework for the Poisson problem, as proposed by [1], with the continuous interior penalty biharmonic formulation presented by [2, 3]. We prove that this method is well-posed and ensures optimal convergence. The theoretical results are further supported by presented numerical evidence. Finally, we demonstrate the applicability of the method by extending the formulation to handle the Cahn-Hilliard equation using a minimalist Implicit-Explicit (IMEX) time discretization scheme to manage the non-linearities.

Cahn-Hilliard-ligningen har et bredt av anvendelser innen fase-separasjon, men gir numeriske utfordringer på grunn av sin ikke-linearitet, stivhet og fjerdeordens deriverte. I denne avhandlingen introduserer vi en ny og stabilisert cut continuous interior penalty finite element metode spesifikt utviklet for det biharmoniske problemet med Cahn-Hilliard-liknende randbetingelser, og deretter utvidet for å håndtere Cahn-Hilliard-ligningen. Ideen er å anvende det teoretiske rammeverket for cut discontinuous Galerkin metoden for Poisson problemet, slik det er foreslått av [1], i kombinasjon med analysen av continuous interior penalty metoden for det biharmoniske problemet presentert av [2, 3]. Vi deretter gir teoretisk grunnlag for at denne metoden er veldefinert og har optimal konvergens. Videre validerer vi de teoretiske resultatene med numeriske eksperimenter. Til slutt demonstrerer vi at metoden kan bli utvidet til å håndtere Cahn-Hilliard-ligningen ved hjelp av en minimalistisk Implisitt-Eksplisitt (IMEX) tidsdiskretiseringsmetode for å håndtere ikke-lineariteter.

Acknowledgement

Nå som jeg sitter på bussen til Oppdal for å delta på et 10-dagers introduksjonskurs i fallskjermhopping, og samtidig skriver slutten på masteroppgaven, vil jeg også benytte anledningen til å takke rammeverket som har gjort denne mastergraden mulig.

Fra det siste året går nok den største takken til min masterveileder, André Massing. Det å skrive masteroppgave ble plutselig mye mer morsomt når man blir inkludert i forskningsgruppa og eksponert for forskjellige vinkler og utfordringer generelt i fagfeltet. Men absolutt det mest viktigste er oppfølging av dumme spørsmål og detaljert gjennomlesing av masteroppgaven. Selv om det er tidkrevende (og utmattende), er det nettopp gjennom disse diskusjonene jeg mener jeg har vokst mest innen matematikk!

Også en generell takk til ansatte på Institutt for matematiske fag på NTNU for å ikke bare opprettholde et høyt faglig og pedagogisk nivå, men også for å investere i studentene. Det er ikke alltid like lett med fire eksamener innen et kort tidsrom på to til tre uker, og da setter mang en student (les: meg) stor pris på at foreleserne er veldig positive og åpne for å legge opp til et nytt forsøk. Ut fra erfaring er det faktisk når man øver til andre (eller tredje) forsøk i stillhet i august at man virkelig lærer mest!

Selv om jeg tidlig byttet linje fra Industriell kjemi og bioteknologi til Fysikk og matematikk ble sjelen min fortsatt igjen i linjeforeningen. Derfor en stor takk til Høiskolen Chemikerforening (HC) for å gi meg en fantastisk sosial arena der jeg sikkert har brukt et par (tusen) timer på 'Kontoret' gjennom studieløpet. I tillegg vil jeg gi en kjempetakk til vennelinjeforeningen Kongliga Kemisektionen på KTH i Sverige for at de lar oss i HC komme på besøk en gang i året for å ha det gøy!

Sist, men ikke minst, stor takk til tålmodigheten til både Mamma og Pappa som fortsatt åpner husene sine og gir mat akkurat når jeg trenger det mest. Selv om jeg verken vasker eller lager middag, og til tross at dere knapt vet hva jeg faktisk studerer, er det en viktig trygghet!

Isak Hammer, 8. Juli 2023.

1 Introduction

The first application of the Cahn-Hilliard (CH) problem appeared when modelling phase separation of two-component incompressible fluids [4, 5, 6], but was quickly generalized to handle multi-component system as well [7, 8, 9, 10]. In engineering, CH is the critical component in the phase-field model, a mathematical framework to model transitions and interface dynamics in materials and fluid dynamics [11, 12]. From this, the equation found many interesting applications for a wide variety of problems. To mention a few, we have multiphase fluid dynamical problems [13, 14, 15, 16], solidification of binary or multi-component alloys [17, 18], and continuum modelling of fracture dynamics in materials [19, 20]. Perhaps an unexpected application is that CH can be used for in painting when recovering damaged parts of an image [21, 22, 7, 23] and modelling the origin of the irregular structure in Saturn's rings [24]. CH is also essential in many areas of biology and medicine. For example, from a macroscopic viewpoint, CH has been used to model tumour growth, wound healing and brain tumours [25, 26]. On the microscopic level on the biomembrane, there is an ongoing debate about the existence of the accumulation of lipids into so-called lipid rafts, which serve as a rigid platform for proteins with special properties such as signalling and intercellular trafficking [27, 28, 29, 30]. It turns out that the hypothesis can be tested by modelling the problem as a separation problem using CH [31, 32, 33].

1.1 The physical Cahn-Hilliard problem

The CH problem comes in many variants depending on its application, but we will in this report focus on the binary mixture version [10]. Let $\Omega \subset \mathbb{R}^d$ be a compact domain for $d = 2, 3$ with a sufficiently smooth boundary Γ , see Figure 1. We define the time duration parameter $T \in [0, \infty)$ and the so-called unknown phase-field function as the mapping $u : [0, T] \times \Omega \rightarrow [-1, 1]$, which denotes the local difference of a binary mixture of two concentrations $c_A, c_B \in [0, 1]$, i.e. $u = c_A - c_B$ and $c_A + c_B = 1$. Note that if a local point exists so u attains the extreme value $+1$, then it implies that the particular point has 100% concentration c_A and vice-versa for c_B . On the other hand, if u is zero, it implies that the mixture is 50% – 50%.

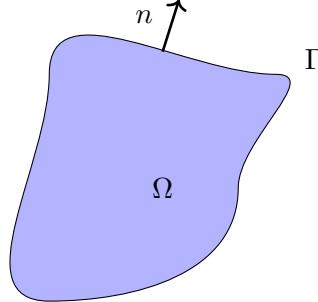


Figure 1: Illustration of the physical domain Ω for $d = 2$, the boundary Γ and the corresponding normal vector n .

Let $\varepsilon \ll 1$ be a small parameter. For an isotropic binary mixture non-uniform, the standard Ginzburg-Landay free energy functional is given by

$$E(u) = \int_{\Omega} \frac{\varepsilon^2}{2} |\nabla u|^2 + F(u) dx. \quad (1.1)$$

The nonlinear function $F(u)$ denotes the (Helmholtz) free energy density associated with the interaction dynamics between the components and thus comes in many forms depending on the thermodynamic properties, see [10]. However, we will in this article assume that $F(u) = (1/4)(u^2 - 1)^2$. The chemical potential μ is defined as the variational derivative,

$$\mu = \frac{\delta E(u)}{\delta u} = f(u) - \varepsilon^2 \Delta u, \quad (1.2)$$

where we used the notation $f(u) = F'(u) = u(u^2 - 1)$. First of all, to guarantee local mass conservation, we may enforce the continuity equation; that is,

$$\partial_t u + \nabla \cdot \mathcal{J} = 0, \quad (1.3)$$

where \mathcal{J} denotes the flux governed by the physical dynamics. Hence, this naturally leads to the no-flux and the Neumann boundary conditions,

$$\mathcal{J} \cdot n = 0 \text{ on } \Gamma, \quad (1.4)$$

$$\partial_n u = 0 \text{ on } \Gamma. \quad (1.5)$$

A well-accepted law for the flux is that it is proportional to the chemical energy gradient, $\mathcal{J} = -M\nabla\mu$ for a parameter M . For simplicity, we assume $M = 1$. This implies that we can rewrite the boundary condition (1.4) such that

$$\mathcal{J} \cdot n = \partial_n (\varepsilon^2 \Delta u - f(u)) = \varepsilon^2 \partial_n \Delta u - f'(u) \partial_n u = \varepsilon^2 \partial_n \Delta u, \quad (1.6)$$

for u evaluated on Γ . Here we used that $\partial_n f(u) = f'(u) \partial_n u = 0$ from the boundary condition (1.5). Hence, we now have an equivalent set of boundary conditions and can finally write the strong form of the Cahn-Hilliard equation. Let $u(x, 0) = u_0$, then is the dynamics of u governed by,

$$\begin{aligned} \partial_t u + \Delta (\varepsilon^2 \Delta u - f(u)) &= 0 && \text{in } \Omega, \\ \partial_n u &= 0 && \text{on } \Gamma, \\ \partial_n \Delta u &= 0 && \text{on } \Gamma. \end{aligned} \quad (1.7)$$

In this report, we will refer to this formulation as the Physical CH formulation due to the physical characteristics it embodies. Based on these laws and the boundary conditions, it becomes evident that the energy functional serves as a Lyapunov function in the sense that its time derivative is monotonically decreasing and that the global mass concentration is conserved, i.e.

$$\frac{d}{dt} E(u) \leq 0 \text{ and } \frac{d}{dt} \int_{\Omega} u dx = 0. \quad (1.8)$$

Note that the inequality computation utilizes the assumption of M to be constant, and both equations require the no-flux boundary condition $\mathcal{J} \cdot n = 0$. For details, see [34, Equation 17] and [35, Equation 1.7]. This is useful since we expect $E(u(\cdot, t_2)) \leq E(u(\cdot, t_1))$ for $0 < t_1 < t_2$ and that the global mass is conserved,

$$\int_{\Omega} u(x, t) dx = \int_{\Omega} u_0(x) dx. \quad (1.9)$$

These properties serve as a theoretical foundation for establishing the existence, uniqueness, and long-term behaviour of the CH problem. Consequently, these properties are well-comprehended from a mathematical standpoint. For references, see [36, 37, 38].

1.2 Numerical methods

One of the key challenges with the CH problem is that it involves fourth-order spatial derivatives. For simple domains, it has successfully been implemented using Finite Difference Methods [39, 40] and Spectral Methods [41, 42]. However, these methods are generally constrained to simple domains (with some notable exceptions [43, 44, 45]).

As a further evolution to address the CH problem, it is common to consider a corresponding biharmonic (BH) problem as a numerical testbed in the spatial discretization schemes. This problem is defined as follows: Find $u : \Omega \rightarrow \mathbb{R}$ such that

$$\begin{aligned} \alpha u + \Delta^2 u &= f(x) && \text{in } \Omega, \\ \partial_n u &= g_1(x) && \text{on } \Gamma, \\ \partial_n \Delta u &= g_2(x) && \text{on } \Gamma, \end{aligned} \quad (1.10)$$

for given $f, g_1, g_2 : \Omega \rightarrow \mathbb{R}$ and constant $\alpha > 0$. The BH problem holds relevance since it provides a proper spatial-discretization test framework prior to moving on solving the non-linearities and time-integration.

The early Finite Element Methods (FEM) for CH were proposed in [46, 38] utilizing global C^1 and C^2 in one spatial dimension, but later it has been shown that making C^1 (or higher order) elements in multiple space dimensions is far from being trivial. For reference, see [47, 48, 49].

There exist several promising alternative methods that guarantee C^1 continuity, and these have shown potential for solving the CH problem. A notable mention is isogeometric analysis (IGA), a technique that leverages Non-Uniform Rational B-Splines (NURBS) to efficiently handle complex geometries and smooth boundaries without the need for translating CAD-based geometry descriptions into classical FEM meshes. Thus, IGA presents a desirable alternative for problems dealing with intricate and smooth domains [50]. Specifically for the CH problem, IGA has successfully been implemented [51, 52]. Another rising method is the virtual finite element method (VFEM), which has applied so-called virtual C^1 elements to handle the C^1 continuity requirement [53].

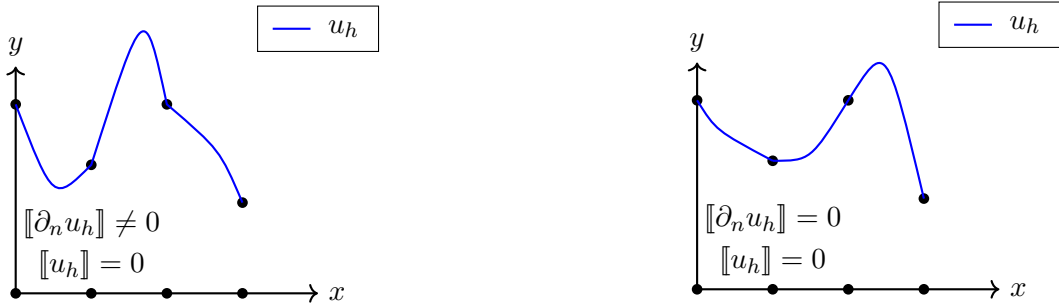


Figure 2: Illustration of global C^0 continuous elements (left) and global C^1 elements (right) in 1 dimension. Here, u_h is a discrete solution , where the jump between the elements is denoted as $\llbracket u_h \rrbracket = u_+ - u_-$.

An alternative approach is to avoid global C^1 continuity and weaken it to global C^0 continuity, see Figure 2 . As a result, this strategy has led to the development of two distinct families of methods for solving the CH problem. The first involves the Continuous Interior Penalty (CIP) methods, which uses the standard weak formulation but penalizes the discontinuity of the derivative between elements as a form of regularization. The method has been designed for several interesting stable variants for the BH problem, that is [2, 54, 55, 56, 57], and recently also for tri-harmonic problems [58]. This method is advantageous due to its symmetry and relationship with discontinuous Galerkin (DG) methods [59], renowned for their natural way of handling inhomogeneous boundary conditions, flexibility with unstructured meshes, efficient parallelization, and strong stability. This connection lends robust stability analysis tools, making the method highly suitable for intricate computational problems. The CIP formulation has also then been adapted to solve CH by applying the Newton-Raphson scheme to handle the non-linearities [60] or utilizing an implicit-explicit (IMEX) time integration scheme, where the stiff part is treated implicitly (such as backward Euler) and the nonlinear part explicitly (such as the forward Euler or explicit Runge-Kutta) [3].

Another popular variant is to rewrite the BH problem as a system of second-order problems in a mixed formulation. This strategy not only broadens the problem's flexibility but also provides a more natural means to incorporate boundary conditions, see [61, 62, 63, 64]. This approach also leverages the general saddle point theory for mixed FEM methods, which provide a mathematical framework to ensure numerical stability [65]. Moreover, this approach adapts well to the CH problem [60, 66, 67], and some methods even apply a so-called convex splitting scheme approach in a way that preserves the convexity of the energy functional, making the system easier to solve [68, 69]. A combination of these methods, the DG and mixed formulation for the CH problem, has recently been considered [70, 71].

Creating a high-quality mesh in two and three dimensions for realistic problems is a challenging

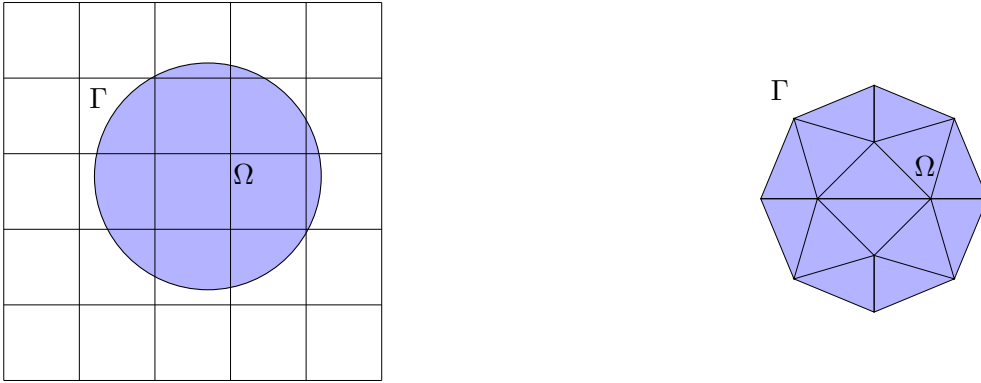


Figure 3: Mesh comparison: unfitted mesh (left) adheres to domain and boundary, while fitted mesh (right) employs a triangular mesh for polygonal approximation of the circular domain.

task that can consume a significant amount of time in the simulation workflow. It is also difficult to scale properly on distributed platforms, making it less suitable for moving domains, highly complex meshes, or smooth boundaries. An interesting class to approach the problem is the so-called unfitted finite element method, which utilizes a background mesh and does not align with the physical boundary. For an illustration see Figure 3. This greatly reduces the need to generate an unstructured mesh and makes it very applicable for parallelization and moving domains since it avoids the need for remeshing entirely. However, without paying attention to the so-called cut cells, which are the elements intersecting with the boundary, the method quickly leads to instability and ill-conditioning. One of the methods to counter this is the cut finite element method (CutFEM), where the focus is to penalize the cut-cells weakly by adding an additional ghost penalty term to ensure well-posedness and optimal convergence properties [72]. Notably, there exist related methods, sometimes considered equivalent, named Extended FEM and Trace FEM [73, 74]. This method has been successfully implemented for the BH problem for the mixed formulation [75], the CIP formulation [76, 73] or using so-called C^1 continuous Bogner-Fox-Schmit elements [77]. However, both implementations consider an interface problem between two domains. Specifically for the CH problem, the mixed formulation [78] has been shown to be successful. Aggregated unfitted finite element method (AgFEM) is a close relative to CutFEM and has also shown to be promising [79, 80]. The method is an alternative way to the ghost penalty, which instead applies a so-called cell aggregation with respect to a cut cell (assuming each cell has enough support with interior elements) and, thus, the badly cut cells are removed, ensuring robustness and well-posedness. Recent results have shown that investigations on unfitted versions of IGA [81] and its applicability to moving surfaces [82] is also possible.

1.3 Outline of the report

In this thesis, we propose a novel stabilized unfitted cut continuous interior penalty method (Cut-CIP) specifically for the BH problem with Cahn-Hilliard type boundary conditions, which incorporates the CutFEM methodology in combination with a CIP formulation. We then extend this method to a CIP CutFEM solver for CH, giving the first CIP CutFEM formulation applied for the problem. Our approach is inspired by the theoretical procedure as presented in the DG Poisson formulation proposed by [1], but instead apply the CIP BH formulation while taking into account and extending the analytical results provided in [3, 54].

The structure of this thesis is as follows. Firstly, in Section 2, we aim to establish notation by reviewing necessary mathematical tools. In Section 3 the basic construction of the CIP BH formulations and their related properties are reviewed. The discussion of the derivation for the standard/fitted CIP is a revised and enhanced version based on the presentation featured in the author's project thesis [83]. Subsequently, in Section 4, we propose the corresponding CutCIP BH method and provide a theoretical analysis showing that the stability and convergence properties

from the original CIP method are conserved. To verify these theoretical properties, we also presented numerical experiments as validation. Finally, in Section 5, we demonstrate how to extend the method to handle the CH problem.

2 Mathematical background

In this section, we revisit the established definitions and briefly overview Sobolev spaces. Afterwards, we briefly review the finite element method and discuss the necessary tools required for calculating a priori estimates. We will generally follow the formulations presented in [84, 85].

2.1 Sobolev spaces

We will, in this thesis, assume Ω to be a compact and open set in \mathbb{R}^d . Let $p \in \mathbb{R}$, $1 \leq p \leq \infty$, and define the space $L^p(\Omega)$ to be the set of all measurable functions $u : \Omega \mapsto \mathbb{R}$ such that $|f|^p$ is Lebesgue integrable, i.e,

$$L^p(\Omega) = \left\{ u : \Omega \mapsto \mathbb{R} \mid \int_{\Omega} |u|^p d\Omega < \infty \right\}.$$

Let $u \in L^p(\Omega)$. We define the integral norm of order p to be

$$\|u\|_{L^p(\Omega)} = \left(\int_{\Omega} |u|^p dx \right)^{\frac{1}{p}}.$$

The following definition for derivatives is employed. For d dimensions of order k we define the multi-index $\alpha = (\alpha_1, \dots, \alpha_d)$ with the absolute value $|\alpha| = \sum_{i=1}^d \alpha_i = k$ such that

$$\partial^\alpha u = \frac{\partial^{\alpha_1}}{\partial x_1^{\alpha_1}} \cdots \frac{\partial^{\alpha_d}}{\partial x_d^{\alpha_d}} u \quad \text{for } u \in C^{|\alpha|}(\Omega). \quad (2.1)$$

Let $k \geq 0$ be an integer and let $1 \leq p < \infty$ be a real number, then the Sobolev space $W^{k,p}(\Omega)$ is defined by

$$W^{k,p}(\Omega) = \{u \in L^p(\Omega) \mid \partial^\alpha u \in L^p(\Omega) \forall \alpha : |\alpha| \leq k\}. \quad (2.2)$$

with the corresponding norm

$$\|u\|_{W^{k,p}(\Omega)} = \left(\sum_{j=0}^k \|u\|_{W^{j,p}(\Omega)}^p \right)^{\frac{1}{p}}. \quad (2.3)$$

Here the seminorm is defined such that $|u|_{W^{k,p}(\Omega)} = (\sum_{|\alpha|=k} \|\partial^\alpha u\|_{L^p(\Omega)}^p)^{\frac{1}{p}}$.

For shorthand notation, we denote

$$\begin{aligned} \|\cdot\|_{k,p} &= \|\cdot\|_{k,p,\Omega} = \|\cdot\|_{W^{k,p}(\Omega)}, \\ |\cdot|_{k,p} &= |\cdot|_{k,p,\Omega} = |\cdot|_{W^{k,p}(\Omega)}. \end{aligned} \quad (2.4)$$

Since $p = 2$ is frequently used in this report, we also define for convenience a compact notation $\|u\|_\Omega = \|u\|_{L^2(\Omega)}$ and $H^m(\Omega) = W^{m,2}(\Omega)$ such that,

$$\begin{aligned} \|\cdot\|_{H^m(\Omega)} &= \|\cdot\|_{k,\Omega} = \|\cdot\|_{k,2,\Omega}, \\ |\cdot|_{H^m(\Omega)} &= |\cdot|_{k,\Omega} = |\cdot|_{k,2,\Omega}. \end{aligned} \quad (2.5)$$

Recall that $L^2(\Omega)$ and $H^m(\Omega)$ are Hilbert spaces equipped with the inner products

$$\begin{aligned}(u, v)_\Omega &= (u, v)_{L^2(\Omega)} = \int_\Omega uv dx, \quad \forall u, v \in L^2(\Omega), \\ (u, v)_{m, \Omega} &= \sum_{|\alpha| \leq m} (\partial^\alpha u, \partial^\alpha v)_\Omega, \quad \forall u, v \in H^m(\Omega).\end{aligned}\tag{2.6}$$

Let $u, v \in H^2(\Omega)$ be scalar functions. The following is the definition for their corresponding operator inner products.

$$\begin{aligned}(\nabla v, \nabla u)_\Omega &= \int_\Omega \nabla v \cdot \nabla u \, dx, \\ (\Delta v, \Delta u)_\Omega &= \int_\Omega \Delta v \Delta u \, dx, \\ (D^2 v, D^2 u)_\Omega &= \int_\Omega D^2 v : D^2 u \, dx.\end{aligned}\tag{2.7}$$

Also, $\|\nabla v\|_\Omega^2 = (\nabla v, \nabla v)_\Omega$, $\|\Delta v\|_\Omega^2 = (\Delta v, \Delta v)_\Omega$, and $\|D^2 v\|_\Omega^2 = (D^2 v, D^2 v)_\Omega$. Here, $\nabla v \cdot \nabla u$ and $D^2 v : D^2 u$ represent the inner product of the gradients and the Frobenius inner product ¹ of Hessian matrices, respectively.

Let $v \in H^r(\Omega)$, we define $D^r v$ to be a tensor of order r such that

$$[D^r v]_{i_1 \dots i_r} = \frac{\partial^r v}{\partial x_{i_1} \dots \partial x_{i_r}} \quad \forall i_1, \dots, i_r \in \{1, \dots, d\}.\tag{2.8}$$

where the norm $\|D^r v\|_\Omega^2 = \int_\Omega D^r v : D^r v \, dx$ is defined via the standard Frobenius inner product. Observe that this notation holds such that $D^0 v = v$, $D^1 v = \nabla v$ and $D^2 v = J(\nabla v) = \text{Hess}(v)$, where J is the Jacobian operator .

Given the context of Sobolev spaces, we consider the functions $u \in H^2(\Omega)$ and $v \in H^1(\Omega)$. We can denote the Greens theorem, which links integrals over a volume and its boundary, as follows,

$$(\Delta u, v)_\Omega = -(\nabla u, \nabla v)_\Omega + (u, \partial_n v)_\Gamma.\tag{2.9}$$

This identity serves as an essential tool for the calculations done.

2.2 Computational domains

Assume that $\Omega \subset \mathbb{R}^d$ is an open and bounded domain with a boundary Γ . In standard FEM methods, a key assumption is that the set Ω is a polyhedra. This is useful since a polyhedra can be fully covered by a collection of polyhedra and, hence, motivating us to define a fitted mesh. We define a fitted mesh \mathcal{T} of the domain Ω to be a collection of closed polyhedra $\{T\}$ with disjoint interior forming a partition of Ω such that $\overline{\Omega} = \bigcup_{T \in \mathcal{T}} T$, for illustration see Figure 3. We say that each $T \in \mathcal{T}$ is a mesh element or an element. The mesh size is defined as the maximum diameter $h := h_{\max}$ of any polyhedra in the mesh $\mathcal{T} = \{T\}$, that is, $h_{\max} = \max_{T \in \mathcal{T}} h_T$ s.t. $h_T = \text{diam}(T) = \max_{x_1, x_2 \in T} \text{dist}(x_1, x_2)$. Hence, motivates us to use the notation \mathcal{T}_h for a mesh \mathcal{T} with size h .

For simplicity, we restrict ourselves to simplicial and quadrilateral elements. A mesh \mathcal{T}_h in \mathbb{R}^d is said to be matching if for all neighbouring elements $T_1, T_2 \in \mathcal{T}_h$ such that the intersection is non-empty, $T_1 \cap T_2 \neq \emptyset$, then $T_1 \cap T_2$ is for $d = 2$ either a common vertex, edge, and for $d = 3$ a common vertex, edge or a face.

¹The Frobenius inner product for two tensors $A, B \in \mathbb{R}^{n \times n \times \dots \times n}$ is defined such that $A : B = \sum_{1 \leq i_1, \dots, i_r \leq d} A_{i_1 \dots i_r} B_{i_1 \dots i_r}$.

Let the chunkiness parameter $c_T := h_T/r_T$, where r_T is the largest ball that be inscribed inside a element $T \in \mathcal{T}_h$. A mesh is said to be shape regular if $c_T \leq c$ is independent of T and h . We also say that the mesh is quasi-uniform only if it is shape regular and $h_{\max} \leq ch_{\min}$. For a more complete description of meshes, see [85, Chapter 8].

In this thesis, we will assume that a mesh \mathcal{T}_h is matching, shape regular and quasi-uniform unless specified. The fact that the mesh is conform makes it an useful property since the interface between mesh elements has come into contact in the sense that it is either a vertex or a facet. This, with the combination of shape regularity and quasi-uniformity, is a major key to prove important inequalities in broken Sobolev spaces [84, Chapter 1.4.1]. Hence, the assumptions are convenient when proving convergence.

Let $\mathcal{T}_h = \{T\}$ be a mesh of $\Omega \subset \mathbb{R}^d$ consisting of polygons $T \in \mathbb{R}^d$. The set of all facets is the union of external and internal facets, $\mathcal{F}_h = \mathcal{F}_h^{ext} \cup \mathcal{F}_h^{int}$, where each is defined by

$$\mathcal{F}_h^{int} = \{F = T^+ \cap T^- \mid T^+, T^- \in \mathcal{T}_h\} \text{ and } \mathcal{F}_h^{ext} = \{F = \partial T \cap \partial \Omega \mid T \in \mathcal{T}_h\}.$$

Assume $T^+ \neq T^-$. Next, we define the following normal vectors.

- 1) We define $n = n_{\partial T}$ to be unit outward normal on ∂T for each $T \in \mathcal{T}_h$
- 2) Let $F \in \mathcal{F}_h^{int}$. We define n to be the facet normal $n = n_F = n|_{\partial T^+}$ from T^+ to T^- , illustrated in Figure 4.
- 3) Let $F \in \mathcal{F}_h^{ext}$. Then we define the facet normal $n|_F = n|_{\partial T}$ to be the unit outward normal.

Please note that we, for convenience, employ the notation n when it is clear what entity the normal is associated with.

Let $v \in L^2(\Omega)$ be a scalar function on Ω with a corresponding shape regular and quasi-uniform mesh \mathcal{T}_h . We will use the following definitions.

- 1) Let $F \in \mathcal{F}_h^{int}$ and $v^\pm|_F = \lim_{t \rightarrow 0^+} v(x \mp tn)$ for $x \in F$. We define the mean as $\{v\}|_F = \frac{1}{2}(v_F^+ + v_F^-)$ and the jump as $[v]|_F = v_F^+ - v_F^-$.
- 2) Let $F \in \mathcal{F}_h^{ext}$ and let $v(x) = v(x)|_F$ for $x \in F$. We define the mean as $\{v\}|_F = v$ and the jump as $[v]|_F = v$.

To simplify will we use the notation $\{v\} = \{v\}|_F$ and $[v] = [v]|_F$ for all $F \in \mathcal{F}_h$. Remark that if we have two functions u, v , for which $u^\pm(x)$ and $v^\pm(x)$ are defined, then the following identity holds $[uv] = [u]\{v\} + \{u\}[v]$ along all facets \mathcal{F}_h associated with the triangulation \mathcal{T}_h .

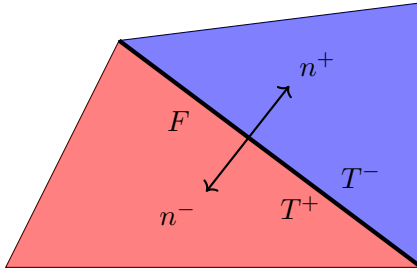


Figure 4: Facet $F \in \mathcal{F}_h^{int}$ shared by the triangles $T^+, T^- \in \mathcal{T}_h$ and the normal unit vector n^+ and n^- . If we pick $T = T^+$ and want to evaluate the normal vector n along a facet F , then we define $n = n|_F = n^+$.

2.3 Broken Sobolev spaces

In this work, we will compute norms on discontinuous elements and, thus, it will be necessary to define broken Sobolev spaces. Let \mathcal{T}_h be a mesh and some integer $m \leq n$. Then we define the broken Sobolev space to be

$$\begin{aligned} H^m(\mathcal{T}_h) &:= \{v \in L^2(\Omega) \mid v|_T \in H^m(T) \quad \forall T \in \mathcal{T}_h\}, \\ L^2(\mathcal{F}_h) &:= \{v \in L^2(\mathcal{T}_h) \mid v|_F \in L^2(F) \quad \forall F \in \mathcal{F}_h\}. \end{aligned}$$

This motivates us to define broken Sobolev norms and inner products using summation over mesh elements,

$$\|v\|_{H^m(\mathcal{T}_h)}^2 = \sum_{T \in \mathcal{T}_h} \|v\|_{H^m(T)}^2 \quad \text{and} \quad (v, w)_{m, \mathcal{T}_h} = \sum_{T \in \mathcal{T}_h} (v, w)_{m, T}.$$

As before, we use the shorthand notation, $\|v\|_{\mathcal{T}_h} = \|v\|_{L^2(\mathcal{T}_h)}$ and $(v, w)_{\mathcal{T}_h} = (v, w)_{L^2(\mathcal{T}_h)}$. That is,

$$\|v\|_{L^2(\mathcal{F}_h)}^2 = \sum_{F \in \mathcal{F}_h} \|v\|_{L^2(F)}^2 \quad \text{and} \quad (v, w)_{L^2(\mathcal{F}_h)} = \sum_{T \in \mathcal{T}_h} (v, w)_{L^2(F)}.$$

Again, we often use the more compact notation $\|v\|_{\mathcal{F}_h} = \|v\|_{L^2(\mathcal{F}_h)}$ and $(v, w)_{\mathcal{F}_h} = (v, w)_{L^2(\mathcal{F}_h)}$. Often it is needed to integrate over boundaries of elements $\partial\mathcal{T}_h = \{\partial T \mid \forall T \in \mathcal{T}_h\}$, hence, we also denote the notation $\|\cdot\|_{\partial\mathcal{T}_h} = \sum_{T \in \mathcal{T}_h} \|\cdot\|_{\partial T} = \sum_{T \in \mathcal{T}_h} \sum_{F \in \partial T} \|\cdot\|_F$.

A very useful lemma when working with estimates on broken Sobolev spaces is that if a function is continuous, then the jump between the mesh elements is zero. Keep in mind a function $v \in H^1(\mathcal{T}_h)$ belongs to $H^1(\Omega)$ if and only if $\llbracket v \rrbracket = 0 \forall F \in \mathcal{F}_h^{int}$, see [84, Lemma 1.23].

Recall the " \lesssim " symbol denotes an inequality up to a constant factor. That is, given $a, b > 0$, the statement $a \lesssim b$ is true if there exists a constant $C > 0$ such that $a \leq Cb$. Generally, this constant will contain information related to the properties of the mesh, such as shape regularity and quasi-uniformity, but it often also includes the maximum finite number or measure of a quantity. For instance, let $w, v_i \in L^2(\Omega)$, $a_i \in \mathbb{R}$ for $i = 1, \dots, N$ and $\|w\|_\Omega = \|\sum_i^N a_i v_i\|_\Omega$, then is $\|w\|_\Omega \lesssim \sum_i^N \|v_i\|_\Omega$. To maintain clarity and avoid unnecessary complexity, we will not delve into this particular detail related to the constant.

We can express several general useful basic inequalities and estimates.

(i) A fundamental property of the inner-product the so-called Cauchy-Schwarz inequality

$$(u, v)_{m, \Omega} \leq \|u\|_{m, \Omega} \|v\|_{m, \Omega} \quad \forall u, v \in H^m(\Omega). \quad (2.10)$$

(ii) Let $v \in H^m(\Omega)$, then is

$$\|D^m v\|_\Omega \lesssim \|v\|_{m, \Omega}. \quad (2.11)$$

Similarly is $\|\Delta v\|_\Omega \lesssim \|v\|_{2, \Omega}$.

(iii) For all $u \in L^2(\mathcal{T}_h)$ we have,

$$\begin{aligned} \|\llbracket u \rrbracket\|_{\mathcal{F}_h} &\leq \|u^+\|_{\mathcal{F}_h} + \|u^-\|_{\mathcal{F}_h} \lesssim \|u\|_{\partial\mathcal{T}_h}, \\ \|\{\{u\}\}_{\mathcal{F}_h} &\leq \|u^+\|_{\mathcal{F}_h} + \|u^-\|_{\mathcal{F}_h} \lesssim \|u\|_{\partial\mathcal{T}_h}. \end{aligned} \quad (2.12)$$

(iv) For any $a, b > 0$ the well known Young's ε -inequality is on the form,

$$2ab \leq \varepsilon a^2 + \frac{1}{\varepsilon} b^2. \quad (2.13)$$

2.4 Lax-Milgram lemma

The intention is to introduce an abstract framework which can handle various types of partial differential equations (PDE). Let $\mathcal{A} : X \rightarrow Y$ be an abstract linear operator encoding the structure of any linear PDE, including boundary conditions and X, Y are spaces of functions. Then we denote the abstract strong formulation as the equation

$$\mathcal{A}u = f, \quad (2.14)$$

for a given function $f : \Omega \subset \mathbb{R}^d \mapsto \mathbb{R}$. We assume that the function $u : \Omega \rightarrow \mathbb{R}$ satisfies the relation (2.14) pointwise so that $\mathcal{A}u(x) = f(x) \forall x \in \Omega$. We will discover that Sobolev spaces are specifically engineered to study these kinds of problems.

Definition 2.1 (Linear bounded functional). *Let V be a Hilbert space. Furthermore, we define the dual space V' to be the space of linear and bounded functionals $F : V \mapsto \mathbb{R}$, i.e.,*

$$V' = \{F : V \rightarrow \mathbb{R} \mid F \text{ is linear and bounded}\}. \quad (2.15)$$

Problem 2.2 (Abstract linear problem). *Assume X and Y to be two Hilbert spaces. Let the vector space $\mathcal{L}(X, Y)$ be all linear bounded operators spanned from V to Y . We define the abstract linear problem as follows; find $u \in V$ such that*

$$a(u, v) = l(v) := \langle f, v \rangle_{V', V} \quad \forall v \in V, \quad (2.16)$$

where $a \in \mathcal{L}(V, V, \mathbb{R})$ is a bounded bilinear form and $f \in V' := \mathcal{L}(V, \mathbb{R})$ is a bounded linear form associated with the abstract strong formulation (2.14). Here we denote by $\langle \cdot, \cdot \rangle_{V', V}$ the duality pairing between V' and V .

Definition 2.3 (Coercivity and Boundedness). *Let V be a Hilbert space and let $a(\cdot, \cdot) \in \mathcal{L}(V, V, \mathbb{R})$. Recall that the bilinear form $a(\cdot, \cdot)$ is coercive if*

$$a(v, v) \gtrsim \|v\|_V \quad \forall v \in V.$$

The bilinear form $a(\cdot, \cdot)$ is said to bounded if

$$a(w, v) \lesssim \|w\|_V \|v\|_V \quad \forall w, v \in V.$$

Lemma 2.4 (Lax-Milgram). *The abstract linear problem 2.2 is well-posed if $a(\cdot, \cdot)$ is bounded and coercive. Moreover, the following a priori estimate holds.*

$$\|u\|_V \lesssim \|f\|_{V'}. \quad (2.17)$$

Proof. The problem can easily be proved using a special case of the Banach–Nečas–Babuška theorem. See [84, Lemma 1.4] \square

2.5 Finite element methods

The finite element method (FEM) is a numerical method to solve partial differential equations by finding an approximation of the Problem 2.2. Let V_h be a finite-dimensional (polynomial) approximation space on the mesh \mathcal{T}_h . We say that a method is conform if $V_h \subset V$ and non-conform if $V_h \not\subset V$. In this thesis, our primary focus will be on the non-conforming methods. We define the approximate problem as follows.

Problem 2.5 (The approximate problem). *Let $V_h \not\subset V$ be a non-conform finite-dimensional space. Find $u_h \in V_h$ such that,*

$$a_h(u_h, v_h) = l_h(v_h) := \langle f, v_h \rangle \quad \forall v_h \in V_h. \quad (2.18)$$

We denote the bilinear form $a_h : V_h \times V_h \rightarrow \mathbb{R}$ as approximation of $a : V \times V \rightarrow \mathbb{R}$, and similarly for the right-hand side $l_h : V_h \rightarrow \mathbb{R}$ as an approximation of $l : V \rightarrow \mathbb{R}$. Note that since the discrete is non-conformal, $V_h \not\subset V$, implies that boundedness and coercivity is not inherited from the continuous bilinear form $a(\cdot, \cdot)$. Hence, the discrete formulation $a_h : V_h \times V_h \rightarrow \mathbb{R}$ well-posed if it is coercive and bounded,

$$\begin{aligned} a_h(v_h, w_h) &\lesssim \|v_h\|_{V_h} \|w_h\|_{V_h} \quad \forall w_h, v_h \in V_h, \\ a_h(v_h, v_h) &\gtrsim \|v_h\|_{V_h}^2 \quad \forall v_h \in V_h. \end{aligned} \tag{2.19}$$

Note that we have relaxed the boundedness of $l_h(\cdot)$, which arises from the finite dimensional property of V_h .

Strictly speaking, if $a_h(\cdot, \cdot)$ is well-posed does not necessarily imply that it is consistent. However this detail will be addressed in Section 2.9. Following, we will establish a theoretical framework for finite element analysis.

Definition 2.6 (Local polynomial space). *Let T be a element in a mesh \mathcal{T}_h , $x = [x_1, \dots, x_d]$ be a vector, and $\alpha = [\alpha_1, \dots, \alpha_d] \in \mathbb{N}^d$ be a multi index. The local polynomial space $\mathcal{P}^k(T)$ for a simplex is denoted as*

$$\mathcal{P}^k(T) = \text{span } \{x^\alpha \text{ for } x \in T \text{ and } 0 \leq \alpha_i \leq k\}. \tag{2.20}$$

where x^α is a monomial such that $x^\alpha = x_1^{\alpha_1} \dots x_d^{\alpha_d}$.

Let T be a cuboid, i.e., $T = \prod_{i=1}^d [z_i^-, z_i^+]$ where $z_i^- < z_i^+$ for $z_i^\pm \in \mathbb{R}$. Then the polynomial space $\mathcal{Q}^k(T)$ in \mathbb{R}^d is defined as the tensor product of 1-dimensional finite elements, i.e.,

$$\mathcal{Q}^k(T) := \mathcal{P}^k([z_1^-, z_1^+]) \otimes \dots \otimes \mathcal{P}^k([z_d^-, z_d^+]).$$

For more information about the local polynomial spaces, see [85, Chapter 6.4, 7.3]

Following Ciarlet [86, pp.93], the abstract definition of a finite element is defined as the triplet (T, \mathcal{P}, Σ) . In our case, T represents either a simplex or a quadrilateral geometry, and \mathcal{P} denotes a finite-dimensional polynomial space consisting of N shape functions $\{\phi_i\}_{i \in \mathcal{I}}$, where $\mathcal{I} = \{1, \dots, N\}$, as depicted in Definition 2.6. On the other hand, Σ is the so-called dual of \mathcal{P} , that is, the set of linear forms $\{\sigma_i\}_{i \in \mathcal{I}}$ such that $\sigma_j(\phi_i) = \delta_{ij}$ and $p(x) = \sum_{i \in \mathcal{I}} \sigma_i(p)p_i$. If there is a set of points $\{a_i\}_{i \in \mathcal{I}}$ in T such that $\sigma_i(p) = p(a_i) \forall p \in \mathcal{P}$, then the triple (T, \mathcal{P}, Σ) is called a Lagrangian finite element. The set of points $\{a_i\}_{i \in \mathcal{I}}$ is called nodes and is associated with the so-called nodal basis of \mathcal{P} such that $\phi(a_i) = \delta_{ij} \forall i, j \in \mathcal{I}$

As anticipated, the local node configuration of the polynomial space is influenced by the form of T . For our discussion, let us represent the polynomial basis for a simplicial element and a quadrilateral element as $\mathcal{P}^k(T)$ and $\mathcal{Q}^k(T)$, both of polynomial order k . Figure 5 illustrates how the node configuration evolves for $k = 1, 2, 3$ in dimension $d = 2$

We may introduce the reference element \hat{T} in d dimensions. The reference for a quadrilateral is denoted as $\hat{T} = [0, 1]^d$. The reference for a simplex is defined by the convex hull spanned by the points (z_0, e_1, \dots, e_d) where $z_0 := 0$ is the origin and $\{e_i\}_{i=1}^d$ is the standard Cartesian unit basis in \mathbb{R}^d . A corresponding reference finite element is defined as $(\hat{T}, \hat{\mathcal{P}}, \hat{\Sigma})$.

Let the mapping $\mathcal{G} : \hat{T} \rightarrow T$ an affine mapping, i.e. $\mathcal{G}(x) = Ax + b$. The important property of affine transformations is the preservation of parallelism. Hence, for any two vectors $x, y \in \hat{T}$ that are parallel in the reference element, their images $\mathcal{G}(x)$ and $\mathcal{G}(y)$ will also be parallel. Generally speaking, an affine transformation of the reference simplex is a transformation to any other simplex of the same dimension. However, for any quadrilateral, an affine transformation preserves the parallelism of opposite sides. For an illustration, see Figure 6 and for a counterexample see Figure 7.

Following [85, Example 9.4], the $(\hat{T}, \hat{\mathcal{P}}, \hat{\Sigma})$ is denoted as the reference finite element associated with the nodes $\{\hat{a}_i\}_{i \in N}$. Let the mapping ψ be function in $\mathcal{L}(\mathcal{P}^k(T), \mathcal{P}^k(\hat{T}))$ such that is an

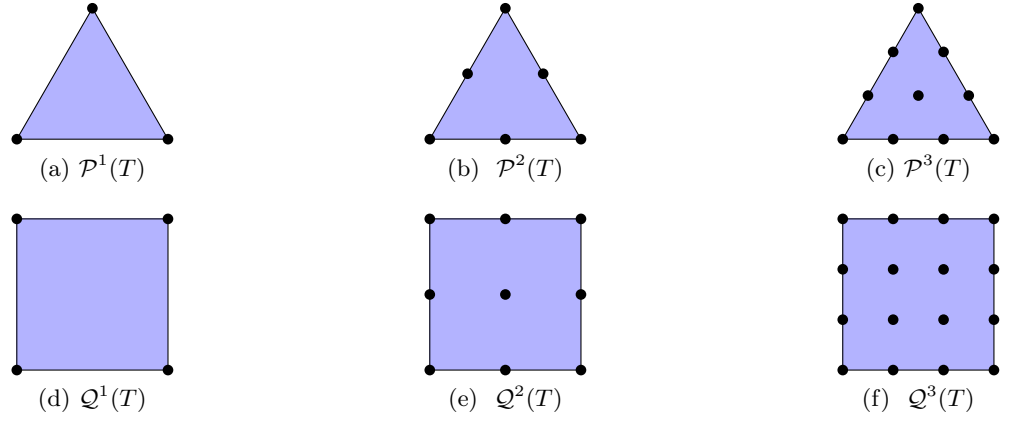


Figure 5: Illustration of the nodes for the element of a simplex and a quadrilateral for dimension $d = 2$ for polynomial orders $k = 1, 2, 3$.

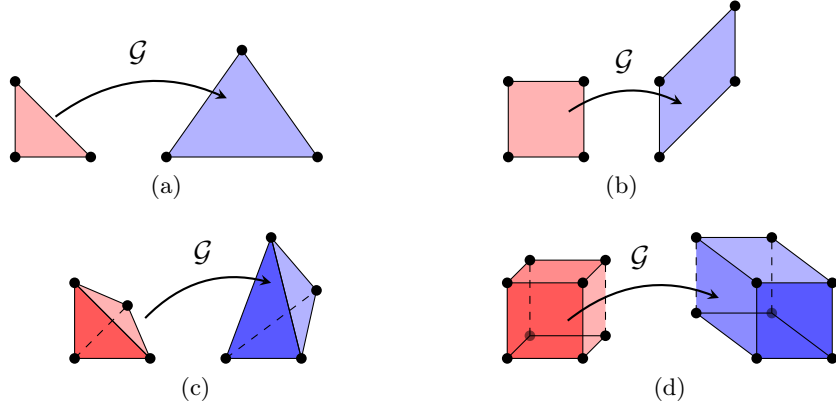


Figure 6: Illustration of affine mapping $\mathcal{G} : \hat{T} \rightarrow T$ in dimensions $d = 2, 3$ from a reference element \hat{T} to element T for simplexes and quadrilaterals.



Figure 7: Illustration of an affine mapping $\mathcal{G} : \hat{T} \mapsto T$ versus a non-affine transformation. The left figure preserves parallel lines before and after the transformation, indicating an affine transformation. However, the right figure does not maintain parallelism, making it a non-affine transformation.

isomorphic from $\psi : \mathcal{P}^k(T) \rightarrow \mathcal{P}^k(\hat{T})$. Then $\sigma(p) = \hat{\sigma}(\psi(p))(a_i) = (p \circ \mathcal{G})(\hat{a}_i)$ for all $p \in \mathcal{P}^k(T)$. Then the Lagrange interpolation follows,

$$p(x) = \sum_{i \in N} \sigma(a_i)\phi_i(x) \quad \text{for } a_i = \mathcal{G}(\hat{a}_i) \quad \forall i \in N.$$

Hence, the finite element (T, \mathcal{P}, Σ) , associated with the notes $\{a_i\}_{i \in N}$, is reconstructed via the reference finite element $(\hat{T}, \hat{\mathcal{P}}, \hat{\Sigma})$. Thus, the definition of the local polynomial space can be extended

to using the affine transformation depending on the reference element. That is,

$$\mathcal{P}^k(T) = \left\{ \hat{v} \circ \mathcal{G}^{-1}(T) \mid \hat{v} \in \mathcal{P}^k(\hat{T}) \right\}, \quad (2.21)$$

$$\mathcal{Q}^k(T) = \left\{ \hat{v} \circ \mathcal{G}^{-1}(T) \mid \hat{v} \in \mathcal{Q}^k(\hat{T}) \right\}. \quad (2.22)$$

Working on shape-regular and affine geometries has been shown to greatly simplify and generalise local interpolation estimates, see [85, Theorem 11.12], and thus is very useful for deriving a priori estimates. Please note that workarounds exist for proving non-affine local interpolation estimates. However, they require key assumptions on the relationship between the nodes a_i and the regularity of the mapping \mathcal{G} [85, Chapter 13]. Hence, affine meshes are essential for the error analysis, which utilize the interpolation estimates, but it limits us to work on structure mesh if we specifically choose quadrilateral meshes.

Definition 2.7 (Broken polynomial spaces). *Let \mathcal{T}_h be a mesh of $\Omega \in \mathbb{R}^d$ and $\Omega_h = \bigcup_{T \in \mathcal{T}_h} T$. Let $\mathcal{P}^k(T)$ be the space of all polynomials of order k in the mesh element T in \mathcal{T}_h . We define the broken polynomial space and the global C^0 continuous polynomial space as*

$$\begin{aligned} \mathcal{P}^k(\mathcal{T}_h) &:= \left\{ v \in L^2(\Omega_h) \mid v|_T \in \mathcal{P}^k(T) \quad \forall T \in \mathcal{T}_h \right\}, \\ \mathcal{P}_c^k(\mathcal{T}_h) &:= \left\{ v \in C^0(\Omega_h) \mid v|_T \in \mathcal{P}^k(T) \quad \forall T \in \mathcal{T}_h \right\}. \end{aligned} \quad (2.23)$$

Similarly, for quadrilateral elements is the polynomial spaces defined as,

$$\begin{aligned} \mathcal{Q}^k(\mathcal{T}_h) &:= \left\{ v \in L^2(\Omega_h) \mid v|_T \in \mathcal{Q}^k(T) \quad \forall T \in \mathcal{T}_h \right\}, \\ \mathcal{Q}_c^k(\mathcal{T}_h) &:= \left\{ v \in C^0(\Omega_h) \mid v|_T \in \mathcal{Q}^k(T) \quad \forall T \in \mathcal{T}_h \right\}. \end{aligned} \quad (2.24)$$

In this thesis, we will generally utilize the global C^0 continuity. Thus, for the rest of the thesis do we define

$$V_h = \left\{ P_c^k(\mathcal{T}_h) \text{ or } Q_c^k(\mathcal{T}_h) \right\}. \quad (2.25)$$

Hence, all results hold for both polynomial spaces.

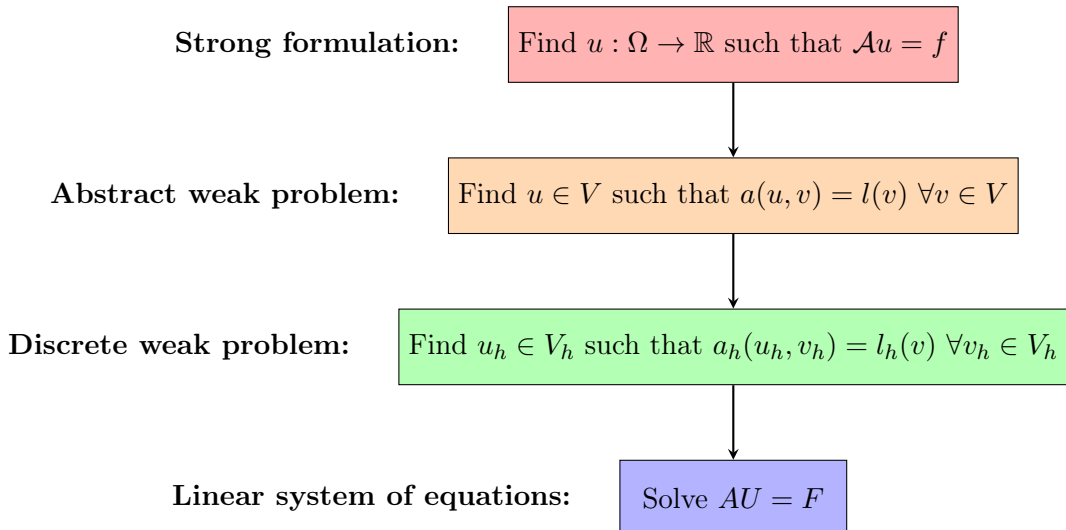


Figure 8: Workflow of solving linear PDEs using the FEM method.

We now have a well-defined discrete global space V_h consisting of the finite set of basis functions $\{\phi_i\}_{i=1}^N$ associated with the Lagrangian nodes $\{a_i\}_{i=1}^N$. The degree of freedoms, also known as

ndofs, is denoted as $\dim(V_h) = N$. Let $U_j = u_h(a_j)$, so that $u_h = \sum_{j=1}^N U_j \phi_j$. Then the Problem 2.5 is equivalent to

$$\sum_{j=1}^N u_j a_h(\phi_j, \phi_i) = l_h(\phi_i). \quad (2.26)$$

Hence, by letting $U = [U_j]$, $F = [(f, \phi_i)_\Omega]$ and $A = [a_h(\phi_j, \phi_i)]$ can we construct a linear system,

$$AU = F. \quad (2.27)$$

Ultimately, the matrix A is shown to be symmetric positive definite only if $a_h(\cdot, \cdot)$ is well-posed.

To summarize the workflow of solving linear PDEs using the FEM method, see Figure 8.

2.6 Condition number

Recall the discrete l^p norm for a vector,

$$\forall U \in \mathbb{R}^N, \quad \|U\|_p = \begin{cases} \left(\sum_{i=1}^N |U_i|^p \right)^{\frac{1}{p}}, & 1 \leq p < \infty \\ \max_i |U_i|, & p = \infty \end{cases}. \quad (2.28)$$

Also, recall the definition of the matrix norm,

$$\forall A \in \mathbb{R}^{N \times N}, 1 \leq p \leq \infty, \quad \|A\|_p = \max_{U \in \mathbb{R}^N \setminus 0} \frac{\|AU\|_p}{\|U\|_p}. \quad (2.29)$$

Remark that this notation is not to be confused with Sobolev norms. Assume that A is invertible, then we define the condition number for a matrix in l^p norm defined such that

$$\forall A \in \mathbb{R}^{N \times N}, 1 \leq p \leq \infty, \quad \kappa_p(A) = \|A\|_p \|A^{-1}\|_p. \quad (2.30)$$

From basic theory, it is known that $\|A\|_2$ is equal to the maximum singular value of A , where singular values of A are the square roots of the eigenvalues of $A^T A$ [87, Theorem 2.9]. Because of the connection between $\|A\|_2$ norms and its singular values, $\kappa_2(A)$ is often in preferred numerical analysis. A challenge is that the computations generally involve performing Singular Value Decomposition (SVD) or power iteration, which can be expensive particularly for large sparse matrices. However, $\|A\|_\infty$ is computed as the maximum absolute row sum and, hence, only necessary to compute the sum for the non-zero elements in each row. Thus, we seek to estimate $\kappa_2(A)$ using $\kappa_\infty(A)$.

It is well established that $\frac{1}{\sqrt{N}} \|A\|_\infty \leq \|A\|_2 \leq \sqrt{N} \|A\|_\infty$ for any matrix $A \in \mathbb{R}^{N \times N}$ ². Applying this identity, we obtain the upper and lower bounds for $\kappa_2(A)$. Specifically, we have

$$\frac{1}{N} \kappa_\infty(A) \leq \kappa_2(A) \leq N \kappa_\infty(A). \quad (2.31)$$

Thus, since these norms are equivalent, will we in this thesis focus on $\kappa_\infty(A)$ because of the efficiency of computing $\|A\|_\infty$.

²The identity naturally appears from the standard inequality $\|v\|_\infty \leq \|v\|_2 \leq \sqrt{N} \|v\|_\infty$ for $v \in \mathbb{R}^N$, which simply comes from the fact that $\|v\|_\infty^2 = \max_i |v_i|^2 \leq \sum_i^n |v_i|^2 = \|v\|_2^2 \leq N \max_i |v_i|^2 = N \|v\|_\infty^2$. Now let $A \in \mathbb{R}^{N \times N}$ be any matrix. We can then deduce that $\|A\|_2 = \max_{v \in \mathbb{R}^N} \frac{\|Av\|_2}{\|v\|_2} \geq \max_{v \in \mathbb{R}^N} \frac{\|Av\|_\infty}{\sqrt{N} \|v\|_\infty} = \frac{1}{\sqrt{N}} \|A\|_\infty$ and $\|A\|_2 = \max_{v \in \mathbb{R}^N} \frac{\|Av\|_2}{\|v\|_2} \leq \max_{v \in \mathbb{R}^N} \frac{\sqrt{N} \|Av\|_\infty}{\|v\|_\infty} = \sqrt{N} \|A\|_\infty$. Hence, the identity $\frac{1}{\sqrt{N}} \|A\|_\infty \leq \|A\|_2 \leq \sqrt{N} \|A\|_\infty$ is proven.

2.7 Clément interpolation

Our goal is to utilize interpolation estimates to compute convergence rates. An important tool in the process is the so-called Clément interpolation operator, C_h . It is used for interpolation on non-smooth functions by regularizing so-called macroelements. However, we need to define affine operations on so-called macroelements before proceeding with the error estimates.

A patch for an element $\omega(T)$ is denoted as the set of elements in \mathcal{T}_h sharing at least one vertex with $T \in \mathcal{T}_h$. Similarly, a patch of a facet $\omega(F)$ is defined as the set of all elements in \mathcal{T}_h sharing at least one vertex with $F \in \mathcal{F}_h$. For an illustrative example of patches in a two-dimensional triangular mesh, please refer to Figure 9.

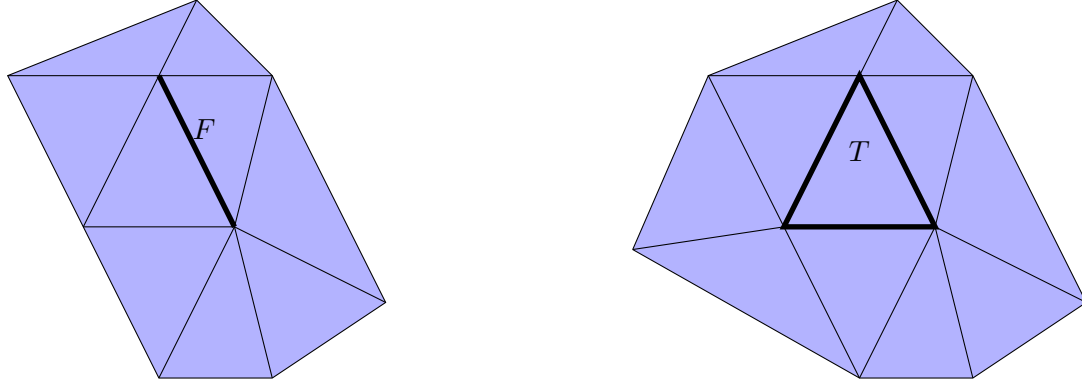


Figure 9: Illustration of the patch $\omega(F)$ on the left-hand side and $\omega(T)$ on the right-hand side.

Let the set $\{a_i\}_{i \in N}$ be all Lagrange nodes on the mesh \mathcal{T}_h . Associated with each node a_i , we denote the macroelement A_i to consist of all elements containing a_i . Let n_{cf} be the number of configurations for the macroelement. We define the index $j : \{1, \dots, N\} \rightarrow \{1, \dots, n_{cf}\}$ such that $j(i)$ is the index associated with the reference configuration $\hat{A}_{j(i)}$ for corresponding macroelement A_i . Let us define a C^0 -diffeomorphism $\mathcal{G}_{A_i} : \hat{A}_{j(i)} \rightarrow A_i$ on the reference macroelements such that for all $\hat{T} \in \hat{A}_{j(i)}$ is the restriction $\mathcal{G}_{A_i}|_{\hat{T}}$ affine. For an illustration of the reference macroelement $\hat{A}_{j(i)}$ and how it related to a_i , see Figure 10.

The Clément interpolation operator C_h is the L^2 -projection onto the macroelements. That is, given a reference macroelement $\hat{A}_{j(i)}$ and a function $\hat{v} \in L^1(\hat{A}_{j(i)})$, then $\hat{C}_{j(i)}\hat{v}$ is the unique polynomial in $\mathcal{P}^k(\hat{A}_{j(i)})$ such that

$$\int_{\hat{A}_{j(i)}} (\hat{C}_{j(i)}\hat{v} - \hat{v})p \, dx = 0 \quad \forall p \in \mathcal{P}^k(\hat{A}_{j(i)}).$$

Finally, the Clément interpolator is defined as the mapping $C_h : L^1(\Omega) \rightarrow \mathcal{P}_c^k(\mathcal{T}_h)$ such that

$$C_h v = \sum_{i=1}^N \hat{C}_{j(i)}(v(\mathcal{G}_{A_i})(\mathcal{G}_{A_i}^{-1}(a_i)))\phi_i,$$

where ϕ_i is the corresponding polynomial basis associated with the node a_i .

Finally, we have the following a priori estimate.

Lemma 2.8. *Let $v \in H^s(\Omega)$. We define the Clement interpolation as the mapping $C_h : L^2(\Omega) \rightarrow V_h$, where V_h has the order k . Then does the following stability estimate hold,*

$$\|C_h v\|_{s,\Omega} \lesssim \|v\|_{s,\Omega} \quad \forall v \in H^s(\Omega). \tag{2.32}$$

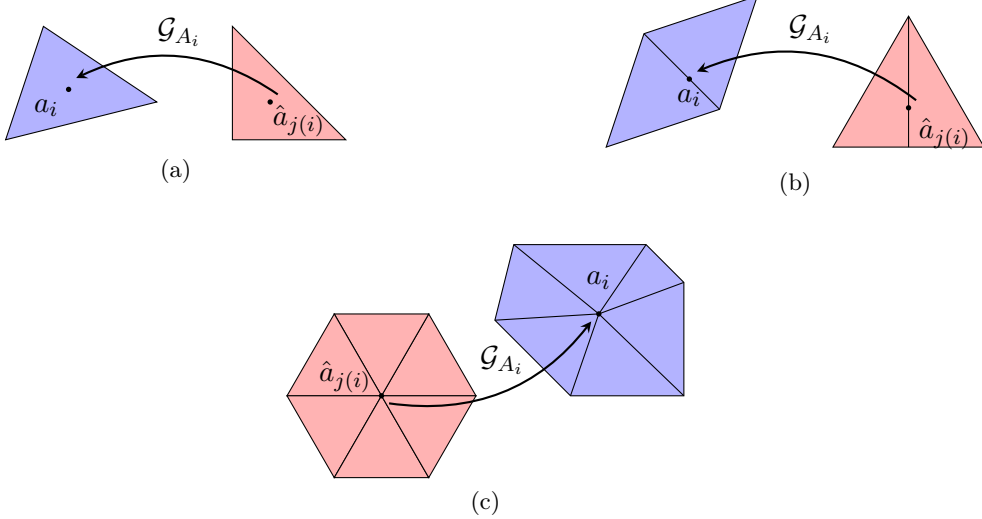


Figure 10: Illustration of the different cases when mapping from the reference macroelement $\widehat{A}_{j(i)}$ to the domain A_i , $\mathcal{G}_{A_i} : \widehat{A}_{j(i)} \rightarrow A_i$. Here we have defined $\widehat{a}_{j(i)} \in \widehat{A}_{j(i)}$ s.t. $\mathcal{G}_{A_i}(\widehat{a}_{j(i)}) = a_i$.

Let $r = \min(s, k + 1)$. If the following conditions for a parameter l is satisfied, it exists error estimates such that

$$\begin{aligned} 0 \leq l \leq r &\implies \|v - C_h v\|_{m,T} \lesssim h_T^{r-l} \|v\|_{l,\omega(T)} \quad \forall T \in \mathcal{T}_h, \forall v \in H^l(\omega(T)), \\ 0 \leq l \leq r - \frac{1}{2} &\implies \|v - C_h v\|_{m,F} \lesssim h_T^{r-l-\frac{1}{2}} \|v\|_{l,\omega(F)} \quad \forall \partial T \in \mathcal{T}_h, \forall v \in H^l(\omega(F)). \end{aligned} \quad (2.33)$$

Corollary 2.9. Let $0 \leq l \leq k + 1$ and let $0 \leq m \leq \min(1, l)$. Given Lemma 2.8, then does the following estimate hold

$$\inf_{v_h \in V_h} \|v - v_h\|_{m,\Omega} \lesssim h^{l-m} \|v\|_{l,\Omega} \quad \forall v \in H^l(\Omega). \quad (2.34)$$

This result is very useful since it is now sufficient to show that a priori estimates holds to prove the convergence rate. For further detailed information about the Clément interpolation, please investigate [88, Chapter 1.6].

2.8 Useful local inverse estimates

Choose any element $T \in \mathcal{T}_h$ and let $v_h \in \mathcal{P}^m(T)$. Then does the local inverse estimate hold,

$$|v_h|_{H^l(T)} \lesssim h^{m-l} |v_h|_{H^m(T)} \text{ for } l \leq m. \quad (2.35)$$

For proof, see [85, Lemma 12.1]. An essential example is the following inequality.

$$\|D^2 v_h\|_T \lesssim h^{-1} \|\nabla v_h\|_T \lesssim h^{-2} \|v_h\|_T. \quad (2.36)$$

Another advantageous inequality is the so-called trace inequality which connects the relationship of evaluating the norm on element T and with any of the corresponding facets $F \in \partial T$. The general form is

$$\|v_h\|_F \lesssim h^{-\frac{1}{2}} \|v_h\|_T. \quad (2.37)$$

For proof, see [85, Lemma 12.8].

Let $\partial_n v = \nabla v \cdot n$ and $\partial_{nn} v = n^T D^2 v \cdot n$. Keeping in mind that the normal vector has a unit length and, thus, evidently applying the trace inverse inequality, we have two present useful examples,

$$\begin{aligned} \|\partial_n v_h\|_F &\leq \|\nabla v_h\|_F \leq h^{-\frac{1}{2}} \|\nabla v_h\|_T, \\ \|\partial_{nn} v_h\|_F &\leq \|D^2 v_h\|_F \leq h^{-\frac{1}{2}} \|D^2 v_h\|_T. \end{aligned} \quad (2.38)$$

Combining (2.35) and (2.37), we establish that

$$|v_h|_{l,F} \lesssim h^{m-l-\frac{1}{2}} |v_h|_{m,T} \text{ for } l \leq m. \quad (2.39)$$

2.9 Abstract Nonconform Error Analysis

Our goal is to construct abstract error estimates for the discrete bilinear form $a_h(\cdot, \cdot)$. Since $V_h \not\subset V$, it is clear that we cannot directly employ the standard Cea's lemma [89, p. 66]. Hence, we have to review how a non-conform variant can be derived, see for instance [90][Chapter 27]. To successfully achieve this, a critical assumption for $a_h(\cdot, \cdot)$ is its consistency. Assume that the discrete bilinear form can be extended to a mapping $a_h : W \times V_h \rightarrow \mathbb{R}$ for an sufficiently regular subspace $W \subset V$. We say that the bilinear form is consistent if it exists an exact solution $u \in W$ for which it holds that $a_h(u, v_h) = l_h(v_h)$. This inherently implies the so-called Galerkin orthogonality,

$$a_h(u - u_h, v_h) = 0. \quad (2.40)$$

For more information, see [84, Definition 1.31].

Let $v + v_h \in W \oplus V_h$ be associated with a corresponding norm $\|\cdot\|_{V,*}$. Here the symbol \oplus is denoted the direct sum of the spaces V_h and W . A necessary assumption is that the discrete bilinear form $a_h(\cdot, \cdot)$ is bounded in $W \oplus V_h \times V_h$ and that $\|v_h\|_{V,*} \lesssim \|v_h\|_{V_h} \forall v_h \in V_h$, i.e.

$$\begin{aligned} a_h(v + v_h, w_h) &\lesssim \|v + v_h\|_{V,*} \|w_h\|_{V_h} \quad \forall v + v_h \in W \oplus V_h, \quad w_h \in V_h, \\ a_h(v_h, w_h) &\lesssim \|v_h\|_{V,*} \|w_h\|_{V_h} \lesssim \|v_h\|_{V_h} \|w_h\|_{V_h} \quad \forall v_h, w_h \in V_h. \end{aligned} \quad (2.41)$$

We can now utilize these boundedness assumptions in combination with the stability and coercivity results presented in (2.19).

Lemma 2.10 (Nonconform Cea's Lemma). *Let $u \in W \subset V$ be the exact solution and let $V_h \not\subset V$. Assume that the discrete bilinear form $a_h(\cdot, \cdot)$ is well-posed in $W \oplus V_h \times V_h$. Additionally, assume that both the stability estimates (2.41) and Galerkin orthogonality (as outlined in (2.40)) are valid. Then the following error estimate hold,*

$$\|u - u_h\|_{V,*} \lesssim \inf_{v_h \in V_h} \|u - v_h\|_{V_h,*}. \quad (2.42)$$

Proof. Applying the triangle inequality to the error $\|u - u_h\|_{V,*}$ and then the assumption $\|v_h\|_{V,*} \lesssim \|v_h\|_{V_h} \forall v_h \in V_h$, we have

$$\begin{aligned} \|u - u_h\|_{V,*} &\lesssim \|u - v_h\|_{V,*} + \|v_h - u_h\|_{V,*}, \\ &\lesssim \|u - v_h\|_{V,*} + \|v_h - u_h\|_{V_h}. \end{aligned} \quad (2.43)$$

By employing the discrete coercivity as defined in equation (2.19), and then applying the Galerkin orthogonality from equation (2.40), followed by the stability condition from equation (2.41), we can derive the following estimate,

$$\begin{aligned} \|v_h - u_h\|_{V_h}^2 &\lesssim a_h(v_h - u_h, v_h - u_h) \\ &= a_h(v_h - u, v_h - u_h) + a_h(u - u_h, v_h - u_h) \\ &\lesssim \|v_h - u\|_{V,*} \|v_h - u_h\|_{V_h}. \end{aligned} \quad (2.44)$$

Dividing $\|v_h - u_h\|_{V_h}$ on both sides we have $\|v_h - u_h\|_{V_h} \lesssim \|u - v_h\|_{V,*}$. Combing this with (2.43) we obtain the following abstract error estimate.

$$\|u - u_h\|_{V,*} \lesssim \inf_{v_h \in V_h} \|u - v_h\|_{V,*}. \quad (2.45)$$

□

A useful property is that for a nonconformal numerical method to converge, we can now simply require

$$\lim_{h \rightarrow 0} \inf_{v_h \in V_h} \|u - v_h\|_{V,*} = 0. \quad (2.46)$$

In that case will $\|u - u_h\|_{V_h,*} \rightarrow 0$, $h \rightarrow 0$. Hence, if this requirement is fulfilled, the numerical methods will converge towards the unique solution. Note that in combination with Corollary 2.9 this is very useful for estimating a priori estimates. For further details on nonconformal error analysis, refer to [84, Chapter 1.3]

3 Continuous interior penalty methods for the biharmonic problem with Cahn-Hilliard type boundary conditions

One of the objectives of this section is to discuss the strong formulation for the biharmonic problem. Following this, we will present both the continuous weak formulation and the derivation of the two proposed discrete weak formulations, specifically the continuous interior penalty methods. We then present a short discussion of the current status of the properties of the methods.

3.1 The biharmonic equation

Let $\Omega \subseteq \mathbb{R}^d$ be a bounded polygonal domain and Γ be its corresponding boundary. Also let $\mathcal{T}_h = \{T\}$ be a shape-regular fitted mesh s.t. $\mathcal{T}_h = \Omega$. Let the biharmonic problem have the form,

$$\Delta^2 u + \alpha u = f(x) \quad \text{in } \Omega, \quad (3.1a)$$

$$\partial_n u = g_1(x) \quad \text{on } \Gamma, \quad (3.1b)$$

$$\partial_n \Delta u = g_2(x) \quad \text{on } \Gamma. \quad (3.1c)$$

Here $\Delta^2 = \Delta(\Delta)$ is the biharmonic operator, also known as the bilaplacian. We will assume for the strong form that $u \in H^4(\Omega)$, $\alpha > 0$ and $f \in L^2(\Omega)$. The functions $g_1, g_2 : \Omega \rightarrow \mathbb{R}$ are denoted as boundary conditions similar to the CH problem.

Remark. It is worth noting that the problem is closely related to the Kirchhoff's plate problem by changing the boundary conditions such that $u = \partial_n u = 0$ on Γ , which is in the literature known as so-called clamped boundary conditions. Many of the papers we refer to may consider clamped boundary conditions, not CH boundary conditions. The main difference relies on if the problem is treated with homogeneous or non-homogeneous boundary conditions and if the discrete space is imposing the Dirichlet and Neumann conditions strongly in the discrete solution space or weakly using the Nitsche's method [91].

We want to construct a weak form for the strong biharmonic problem (3.1). Let $v \in H^2(\Omega)$. Using Greens Theorem is it obvious that $(\Delta^2 u, v)_\Omega = (\partial_n \Delta u, v)_\Gamma - (\nabla(\Delta u), \nabla v)_\Omega$. Next, applying a new iteration of the Greens theorem, we get $-(\nabla(\Delta u), \nabla v)_\Omega = (\Delta u, \Delta v)_\Omega - (\Delta u, \partial_n v)_\Gamma$. Hence, we obtain the identity

$$(\Delta^2 u, v)_\Omega = (\Delta u, \Delta v)_\Omega + (\partial_n \Delta u, v)_\Gamma - (\partial_n v, \Delta u)_\Gamma. \quad (3.2)$$

We now see that boundary condition (3.1c) can be naturally included in the variational formulation by simply replacing $\partial_n \Delta u$ with g_2 in the third term of (3.2). The remaining boundary condition (3.1b) on the other hand needs to be built into the function space and thus presents an essential boundary condition. As a consequence, the corresponding test function space will consist of functions with zero normal flux, i.e., $\partial_n v = 0$ on Γ and therefore the last contribution in (3.2) disappears. We end up with the following corresponding weak formulation of the biharmonic problem (3.1):

$$\text{Find } u \in V_{g_1} \text{ such that } a(u, v) = l(v) \quad \forall v \in V_0. \quad (3.3)$$

with

$$\begin{aligned} a(u, v) &= (\Delta u, \Delta v)_\Omega + (\alpha u, v)_\Omega, \\ l(v) &= (f, v)_\Omega - (g_2, v)_\Omega, \end{aligned} \quad (3.4)$$

where we introduced for general $g \in H^{1/2}(\Gamma)$ the function space

$$V_{g_1} := \{v \in H^2(\Omega) \mid \partial_n v = g_1 \text{ on } \Gamma\}. \quad (3.5)$$

3.2 Detailed construction of Hessian and Laplacian Formulations

The goal is to construct two CIP formulations for the problem (3.3), that is: Find $u_h \in V_h \not\subseteq V$ such that $a_h(u_h, v_h) = l_h(v_h)$ for all $v_h \in V_h$. We will follow the ideas presented in [2] and [3]. A necessary property is that when we have a bilinear form and replace the exact solution with $u_h \in V_h$, the system remains consistent in V . Hence, we guarantee consistency of the discrete weak formulation by assuming during the construction that $u \in H^4(\Omega)$ and $v_h \in V_h$. However, due to the nonconformal nature of V_h , it becomes necessary to introduce penalty terms to ensure the discrete system is well-posed when we replace it with $u_h \in V_h$. Keep in mind that the C^1 continuity is imposed weakly and, in the same way, are the Neumann conditions also imposed weakly.

Our goal is to achieve the objective of constructing the Hessian and Laplacian formulations. The following lemmas will be the primary components.

3.2.1 Construction of the Hessian formulation

Lemma 3.1. *Assume the homogeneous Neumann conditions $g_1 = 0$. Let $u \in H^4(\Omega)$ be the solution to (3.1), let $v_h \in V_h$ and a constant $\gamma > 0$. Then does the following identity hold.*

$$\begin{aligned} (\Delta^2 u, v_h)_\Omega &= (D^2 u, D^2 v_h)_\Omega + (g_2, v_h)_\Gamma \\ &\quad - (\{\partial_{nn} u\}, [\partial_n v_h])_{\mathcal{F}_h^{int}} - ([\partial_n u], \{\partial_{nn} v_h\})_{\mathcal{F}_h^{int}} + \frac{\gamma}{h} ([\partial_n u], \{\partial_{nn} v_h\})_{\mathcal{F}_h^{int}} \\ &\quad - (\partial_{nn} u, \partial_n v_h)_\Gamma - (\partial_n u, \partial_{nn} v_h)_\Gamma + \frac{\gamma}{h} (\partial_n u, \partial_n v_h)_\Gamma. \end{aligned} \quad (3.6)$$

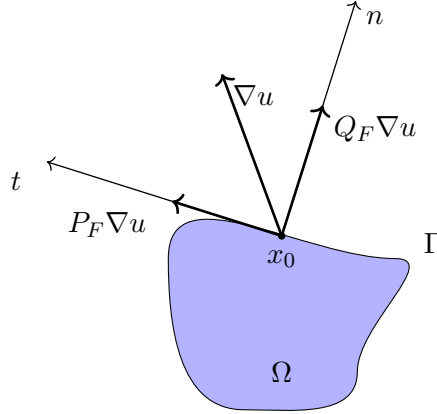


Figure 11: Let x_0 be a point at the boundary Γ for dimension $d = 2$. Here is an illustration of the gradient ∇u with the corresponding normal and tangential decomposition, $Q_F \nabla u$ and $P_F \nabla u$.

Proof. We will start constructing a local theory for an element T and then extend it to the full mesh \mathcal{T}_h . Using Greens Theorem, it is obvious that

$$(\Delta^2 u, v_h)_T = (\partial_n \Delta u, v_h)_{\partial T} - (\nabla(\Delta u), \nabla v_h)_T. \quad (3.7)$$

We can expand the second term in the following way.

$$\begin{aligned}
(\nabla(\Delta u), \nabla v_h)_T &= \sum_{i=1}^d (\Delta \partial_{x_i} u, \partial_{x_i} v_h)_T = \sum_{i=1}^d (\nabla \cdot (\nabla \partial_{x_i} u), \partial_{x_i} v_h)_T \\
&= \sum_{i=1}^d ((\partial_n \partial_{x_i} u, \partial_{x_i} v_h)_{\partial T} - (\nabla \partial_{x_i} u, \nabla \partial_{x_i} v_h)_T) \\
&= (\partial_n \nabla u, \nabla v_h)_{\partial T} - (D^2 u, D^2 v_h)_T.
\end{aligned} \tag{3.8}$$

Hence, the normal flux of Δu appears naturally in the formulation. It can be denoted that D^2 is the Hessian matrix operator. Also, remark that we apply the notation $(D^2 u, D^2 v_h)_\Omega = \int_\Omega D^2 u : D^2 v_h dx$ for the inner product $D^2 u : D^2 v_h$.

Next, we want to decompose the evaluation of ∇u on the boundary ∂T in the tangential and normal direction. Pick a facet $F \in \partial T$, then we define the following decomposition of linear transformation $\nabla u = P_F \nabla u + Q_F \nabla u$ s.t. the orthogonality, $P_F \nabla u \cdot Q_F \nabla u = 0$, holds. Here, the normal projection matrix is defined as $Q_F = n \otimes n$ and the tangential decomposition follows from $P_F = I - Q_F = I - n \otimes n = \sum_{i=1}^{d-1} t_i \otimes t_i$, where we defined a orthonormal basis t_i , $i = 1, \dots, d-1$ for the space orthogonal to the outer normal vector n on a facet F . For demonstration in $d = 2$, see Figure 11. Let $a_1, a_2, a_3 \in \mathbb{R}^d$ be any vectors, and then it is well known that the following identity holds $(a_1 \otimes a_2)a_3 = (a_2^T a_3)a_1$. Hence, we have

$$\begin{aligned}
Q_F \nabla u &= (n \otimes n) \nabla u = (n^T \nabla u)n, \\
P_F \nabla u &= (I - n \otimes n) \nabla u = \nabla u - (n^T \nabla u)n = \sum_{i=1}^{d-1} (t_i^T \nabla u)t_i.
\end{aligned} \tag{3.9}$$

Given that u is evaluated only on ∂T can we write $\nabla u = (n^T \nabla u)n + \sum_{i=1}^{d-1} (t_i^T \nabla u)t_i$ such that,

$$\begin{aligned}
(\partial_n \nabla u, \nabla v_h)_{\partial T} &= (\partial_n(\partial_n u n), \partial_n v_h n)_{\partial T} + \sum_{i,j=1}^{d-1} (\partial_n(\partial_{t_i} u t_i), \partial_{t_j} v_h t_j)_{\partial T} \\
&= (\partial_{nn} u, \partial_n v_h)_{\partial T} + \sum_{i=1}^{d-1} (\partial_{nt_i} u, \partial_{t_i} v_h)_{\partial T}.
\end{aligned} \tag{3.10}$$

Here we used that $n^T n = 1$ and $t_i^T t_j = \delta_{ij}$. Remark that simple relation was applied,

$$\begin{aligned}
\partial_n(\partial_n u) &= n^T \nabla(\partial_n u) = n^T (D^2 u n) = n^T D^2 u n = \partial_{nn} u, \\
\partial_n(\partial_{t_i} u) &= t_i^T \nabla(\partial_n u) = t_i^T (D^2 u n) = n^T D^2 u t_i = \partial_{nt_i} u.
\end{aligned}$$

We may also deduce the relationship $\partial_{nt_i} u = \partial_{t_i n} u$ which arise from the fact that $n^T D^2 u t_i = (t_i^T D^2 u n)^T = t_i^T D^2 u n$, where we utilized the symmetry $D^2 u = (D^2 u)^T$ and that the product is a scalar. Combining (3.7), (3.8) and (3.10) we see that,

$$(\Delta^2 u, v_h)_T = (D^2 u, D^2 v_h)_T + (\partial_n \Delta u, v_h)_{\partial T} - (\partial_{nn} u, \partial_n v_h)_{\partial T} - \sum_{i=1}^{d-1} (\partial_{nt_i} u, \partial_{t_i} v_h)_{\partial T}.$$

Since we aim constructing an identity for the full mesh \mathcal{T}_h , we sum over the elements.

$$(\Delta^2 u, v_h)_\Omega = \sum_{T \in \mathcal{T}_h} (D^2 u, D^2 v_h)_T + (\partial_n \Delta u, v_h)_{\partial T} - (\partial_{nn} u, \partial_n v_h)_{\partial T} - \sum_{i=1}^{d-1} (\partial_{nt_i} u, \partial_{t_i} v_h)_{\partial T}. \tag{3.11}$$

Our goal is to simplify the equation above so we can take account for discontinuities of the derivatives. By integrating over exterior facets \mathcal{F}_h^{ext} and interior facets \mathcal{F}_h^{int} , we will get e more suitable

formulation which makes it easier to control the jumps between the elements, hence makes it possible to penalize discontinuities.

$$\begin{aligned}
(\Delta^2 u, v_h)_\Omega &= \sum_{T \in \mathcal{T}_h} (D^2 u, D^2 v_h)_T + (\partial_n \Delta u, v_h)_{\partial T} - (\partial_{nn} u, \partial_n v_h)_{\partial T} - \sum_{i=1}^{d-1} (\partial_{t_i n} u, \partial_{t_i} v_h)_{\partial T} \\
&= \sum_{T \in \mathcal{T}_h} (D^2 u, D^2 v_h)_T + \sum_{F \in \mathcal{F}_h^{ext}} (\partial_n \Delta u, v_h)_F - (\partial_{nn} u, \partial_n v_h)_F - \sum_{i=1}^{d-1} (\partial_{t_i n} u, \partial_{t_i} v_h)_F \\
&\quad + \underbrace{\sum_{F \in \mathcal{F}_h^{int}} ((\partial_{n+} \Delta u^+, v_h^+)_F + (\partial_{n-} \Delta u^+, v_h^-)_F)}_{\text{I}} \\
&\quad - \underbrace{((\partial_{n+n+} u^+, \partial_{n+} v_h^+)_F + (\partial_{n-n-} u^-, \partial_{n-} v_h^-)_F)}_{\text{II}} \\
&\quad - \underbrace{\sum_{i=1}^{d-1} ((\partial_{n+t_i} u^+, \partial_{t_i} v_h^+)_F + (\partial_{n-t_i} u^-, \partial_{t_i} v_h^-)_F)}_{\text{III}}.
\end{aligned} \tag{3.12}$$

Where the integration of the interior facets is computed in the following fashion.

$$\begin{aligned}
\text{I} &= (\partial_{n+} \Delta u^+, v_h^+)_F + (\partial_{n-} \Delta u^-, v_h^-)_F \\
&= \int_F [\![\partial_n \Delta u \cdot v_h]\!] = \int_F \{\!\{\partial_n \Delta u\}\!\} \underbrace{[\![v_h]\!]}_{=0} + \underbrace{[\![\partial_n \Delta u]\!]}_{=0} \{\!\{v_h\}\!\} = 0, \\
\text{II} &= (\partial_{n+n+} u^+, \partial_{n+} v_h^+)_F + (\partial_{n-n-} u^-, \partial_{n-} v_h^-)_F \\
&= \int_F [\![\partial_{nn} u \cdot \partial_n v_h]\!] = \int_F \{\!\{\partial_{nn} u\}\!\} \underbrace{[\![\partial_n v_h]\!]}_{\neq 0} + \underbrace{[\![\partial_{nn} u]\!]}_{=0} \{\!\{\partial_n v_h\}\!\}, \\
\text{III} &= (\partial_{n+t_i} u^+, \partial_{t_i} v_h^+)_F + (\partial_{n-t_i} u^-, \partial_{t_i} v_h^-)_F \\
&= \int_F [\![\partial_{nt_i} u \cdot \partial_{t_i} v_h]\!] = \int_F \{\!\{\partial_{nt_i} u\}\!\} \underbrace{[\![\partial_{t_i} v_h]\!]}_{=0} + \underbrace{[\![\partial_{nt_i} u]\!]}_{=0} \{\!\{\partial_{t_i} v_h\}\!\} = 0.
\end{aligned} \tag{3.13}$$

Observe that the cancellations in the term I and term III appear of the continuity of $v_h \in V_h$ and $u \in H^4(\Omega)$, which makes the jumps and derivative jumps zero. On the other hand, the second term II does not vanish since the derivative of $v_h \in V_h$ has a nonzero jump. It can also be raised that $\{\!\{\partial_{nn} u\}\!\} = \partial_{nn} u$ holds of $H^4(\Omega)$.

Combining (3.13) and inserting the boundary condition $g_2 = \partial_n \Delta u$ is it clear that the formulation presented in (3.11) is equivalent to the following formulation.

$$\begin{aligned}
(\Delta^2 u, v_h)_\Omega &= (D^2 u, D^2 v_h)_{\mathcal{T}_h} + (g_2, v_h)_\Gamma - (\{\!\{\partial_{nn} u\}\!\}, [\![\partial_n v_h]\!])_{\mathcal{F}_h^{int}} \\
&\quad - (\partial_{nn} u, \partial_n v_h)_{\mathcal{F}_h^{ext}} - \sum_{i=1}^{d-1} (\partial_{t_i n} u, \partial_{t_i} v_h)_{\mathcal{F}_h^{ext}}.
\end{aligned} \tag{3.14}$$

Under the assumption that $g_1 = 0$ on Γ , and given that the tangential decomposition is orthogonal to n , we can assert that $\partial_{t_i n} u = \partial_{t_i}(\partial_n u) = \partial_{t_i}(g_1) = 0$ holds for any $i = 1, \dots, d-1$. This implies that the last term of the equation vanishes.

We also note that we add consistent symmetry terms $(\{\!\{\partial_{nn} v_h\}\!\}, [\![\partial_n u]\!])_{\mathcal{F}_h^{int}}$ and $(\partial_{nn} v_h, \partial_n u)_\Gamma$ in addition to the penalty terms $\frac{\gamma}{h}(\partial_n u, \partial_n v)_\Gamma$ and $\frac{\gamma}{h}([\![\partial_n u]\!], [\![\partial_n v]\!])_{\mathcal{F}_h^{int}}$. Since $u \in H^4(\Omega)$ and the boundary condition, $\partial_n u = g_1 = 0$ on Γ , is each of these terms effectively zero, but does provide

symmetry and will later be proven to be essential for the well-posedness of the discrete problem. Finally, we have

$$\begin{aligned} (\Delta^2 u, v_h)_\Omega &= (D^2 u, D^2 v_h)_\Omega + (g_2, v_h)_\Gamma \\ &\quad - (\{\partial_{nn} u\}, [\partial_n v_h])_{\mathcal{F}_h^{int}} - ([\partial_n u], \{\partial_{nn} v_h\})_{\mathcal{F}_h^{int}} + \frac{\gamma}{h} ([\partial_n u], [\partial_n v_h])_{\mathcal{F}_h^{int}} \quad (3.15) \\ &\quad - (\partial_{nn} u, \partial_n v_h)_\Gamma - (\partial_n u, \partial_{nn} v_h)_\Gamma + \frac{\gamma}{h} (\partial_n u, \partial_n v)_\Gamma. \end{aligned}$$

The proof is complete. \square

Note that since $V_h \not\subset V$ is it necessary to define the space $V \oplus V_h$, which essentially is the direct sum of these two spaces. This new space includes all elements from V and V_h and all possible linear combinations of these elements. i.e., let $u \in V$ and $u_h \in V_h$, then $u + u_h \in V \oplus V_h$.

We will now assemble the Hessian CIP formulation. Assume that the homogeneous boundary condition $g_1 = 0$. The discrete problem is as follows:

$$\text{Find } u_h \in V_h \text{ such that } a^H(u_h, v_h) = l_h^H(v_h) \quad \forall v_h \in V_h. \quad (3.16)$$

Here is the corresponding bilinear and linear form defined as,

$$\begin{aligned} a_h^H(u_h, v_h) &= (\alpha u_h, v_h)_\Omega + (D^2 u_h, D^2 v_h)_\Omega \\ &\quad - (\{\partial_{nn} u_h\}, [\partial_n v_h])_{\mathcal{F}_h^{int}} - ([\partial_n u_h], \{\partial_{nn} v_h\})_{\mathcal{F}_h^{int}} + \frac{\gamma}{h} ([\partial_n u_h], [\partial_n v_h])_{\mathcal{F}_h^{int}} \quad (3.17) \\ &\quad - (\partial_{nn} u_h, \partial_n v_h)_\Gamma - (\partial_n u_h, \partial_{nn} v_h)_\Gamma + \frac{\gamma}{h} (\partial_n u_h, \partial_n v_h)_\Gamma, \\ l_h^H(v_h) &= (f, v_h)_\Omega - (g_2, v_h)_\Gamma. \end{aligned}$$

With the corresponding energy norms,

$$\begin{aligned} \|v_h\|_{a_h^H}^2 &= \alpha \|v_h\|_\Omega^2 + \|D^2 v_h\|_\Omega^2 + \|h^{-\frac{1}{2}} [\partial_n v_h]\|_{\mathcal{F}_h^{int}}^2 + \|h^{-\frac{1}{2}} \partial_n v_h\|_\Gamma^2, \quad v_h \in V_h, \\ \|v\|_{a_h^H, *}^2 &= \|v\|_{a_h}^2 + \|h^{\frac{1}{2}} \{\partial_{nn} v\}\|_{\mathcal{F}_h^{int}}^2 + \|h^{\frac{1}{2}} \partial_{nn} v\|_\Gamma^2, \quad v \in V \oplus V_h. \end{aligned} \quad (3.18)$$

Remark. This formulation accommodates the nonconformity of V_h by factoring in the discontinuities among the facets, yet it preserves consistency when u exhibits sufficient regularity, specifically when $u \in H^s(\Omega)$, $s \geq \frac{5}{2} + \varepsilon$. This implies that the solution u is continuous across the boundaries of interior elements, i.e., $[\partial_n u] = 0$ and $\{\partial_{nn} u\} = \partial_{nn} u$ on any $F \in \mathcal{F}_h^{int}$.

It is noteworthy that we have the consistent terms $(\{\partial_{nn} u_h\}, [\partial_n v_h])_{\mathcal{F}_h^{int}}$ and $(\partial_{nn} u_h, \partial_n v_h)_\Gamma$ naturally appear in the derivation. However, we also added two symmetry terms, $(\{\partial_{nn} u_h\}, [\partial_n v_h])_{\mathcal{F}_h^{int}}$ and $(\partial_{nn} u_h, \partial_n v_h)_\Gamma$, and the so-called penalty terms, $\frac{\gamma}{h} ([\partial_n u_h], [\partial_n v_h])_{\mathcal{F}_h^{int}}$ and $\frac{\gamma}{h} (\partial_n u_h, \partial_n v_h)_\Gamma$. These terms are essential for making the problem well-posed, hence, the name interior penalty method or symmetric interior penalty method. For more information of nonconformal CIP error analysis, see [84, Chapter 1.3].

3.2.2 Construction of the Laplacian formulation

Lemma 3.2. *Let $u \in H^4(\Omega)$ the solution of (3.1), $v_h \in V_h$ and a constant $\gamma > 0$. Then we have the following identity.*

$$\begin{aligned} (\Delta^2 u, v_h)_\Omega &= (\Delta u, \Delta v_h)_{\mathcal{T}_h} + (g_2, v_h)_\Gamma - (g_1, \Delta v_h)_\Gamma + \frac{\gamma}{h} (g_1, \partial_n v_h)_\Gamma \\ &\quad - ([\partial_n u], \{\Delta v_h\})_{\mathcal{F}_h^{int}} - (\{\Delta u\}, [\partial_n v_h])_{\mathcal{F}_h^{int}} + \frac{\gamma}{h} ([\partial_n u], [\partial_n v_h])_{\mathcal{F}_h^{int}} \quad (3.19) \\ &\quad - (\Delta u, \partial_n v_h)_\Gamma - (\partial_n u, \Delta v_h)_\Gamma + \frac{\gamma}{h} (\partial_n u, \partial_n v_h)_\Gamma. \end{aligned}$$

Proof. Similarly, we start by constructing integration by parts identities locally for an element T and then extend it to the entire mesh \mathcal{T}_h . Utilizing (3.2) can we see that

$$(\Delta^2 u, v_h)_T = (\Delta u, \Delta v_h) + (\partial_n \Delta u, v_h)_{\partial T} - (\partial_n v_h, \Delta u)_{\partial T}.$$

Now, summing over all elements, we get

$$\begin{aligned} (\Delta^2 u, v_h)_\Omega &= \sum_{T \in \mathcal{T}_h} ((\Delta u, \Delta v_h)_T + (\partial_n \Delta u, v_h)_{\partial T} - (\partial_n v_h, \Delta u)_{\partial T}) \\ &= (\Delta u, \Delta v_h)_{\mathcal{T}_h} + \sum_{F \in \mathcal{F}_h^{ext}} \overbrace{((\partial_n \Delta u, v_h)_F)}^{=(g_2, v_h)_F} - (\partial_n v_h, \Delta u)_F \\ &\quad + \sum_{F \in \mathcal{F}_h^{int}} \underbrace{((\partial_{n+} \Delta u, v_h)_F + (\partial_{n-} \Delta u, v_h)_F)}_{I} - \underbrace{((\partial_{n+} v_h, \Delta u)_F + (\partial_{n-} v_h, \Delta u)_F)}_{II}. \end{aligned} \quad (3.20)$$

Decomposing the terms and utilizing the regularity of $u \in H^4(\Omega)$ and the C^0 continuity of $v_h \in V_h$ is it easy to see that,

$$\begin{aligned} I &= (\partial_{n+} \Delta u, v_h)_F + (\partial_{n-} \Delta u, v_h)_F = \int_F [\partial_n \Delta u \ v_h] \\ &= (\{\!\!\{\partial_n \Delta u\}\!\!\}, \underbrace{[v_h]}_{=0})_F + (\underbrace{[\partial_n \Delta u]}_{=0}, \{\!\!\{v_h\}\!\!\})_F, \\ II &= (\partial_{n+} v_h, \Delta u)_F + (\partial_{n-} v_h, \Delta u)_F = \int_F [\partial_n v_h \ \Delta u] \\ &= (\underbrace{[\partial_n v_h]}_{\neq 0}, \{\!\!\{\Delta u\}\!\!\})_F + (\{\!\!\{\partial_n v_h\}\!\!\}, \underbrace{[\Delta u]}_{=0})_F. \end{aligned} \quad (3.21)$$

Hence, we end up with the identity,

$$(\Delta^2 u, v_h)_\Omega = (\Delta u, \Delta v_h)_{\mathcal{T}_h} + ([\partial_n v_h], \{\!\!\{\Delta u\}\!\!\})_{\mathcal{F}_h} + (g_2, v_h)_\Gamma - (\partial_n v_h, \Delta u)_\Gamma. \quad (3.22)$$

Similarly as for Lemma 3.1, we add consistent symmetry terms $([\partial_n u], \{\!\!\{\Delta v_h\}\!\!\})_{\mathcal{F}_h^{int}}$ and $(\partial_n u, \Delta v_h)_\Gamma - (g_1, \Delta v_h)_\Gamma$ and the penalty terms $\frac{\gamma}{h}(\partial_n u, \partial_n v_h)_\Gamma - \frac{\gamma}{h}(g_1, \partial_n v_h)_\Gamma$ and $\frac{\gamma}{h}([\partial_n u], [\partial_n v_h])_{\mathcal{F}_h^{int}}$. Effectively, the terms adding zero because of the regularity $u \in H^4(\Omega)$ and the boundary condition $\partial_n u = g_1$. Finally, we have

$$\begin{aligned} (\Delta^2 u, v_h)_\Omega &= (\Delta u, \Delta v_h)_{\mathcal{T}_h} + (g_2, v_h)_\Gamma - (g_1, \Delta v_h)_\Gamma + \frac{\gamma}{h}(g_1, \partial_n v_h)_\Gamma \\ &\quad - ([\partial_n u], \{\!\!\{\Delta v_h\}\!\!\})_{\mathcal{F}_h^{int}} - (\{\!\!\{\Delta u\}\!\!\}, [\partial_n v_h])_{\mathcal{F}_h^{int}} + \frac{\gamma}{h}([\partial_n u], [\partial_n v_h])_{\mathcal{F}_h^{int}} \\ &\quad - (\Delta u, \partial_n v_h)_\Gamma - (\partial_n u, \Delta v_h)_\Gamma + \frac{\gamma}{h}(\partial_n u, \partial_n v_h)_\Gamma. \end{aligned} \quad (3.23)$$

And the proof is complete. \square

We will now assemble the Laplace CIP formulation. The discrete problem is as follows:

$$\text{Find } u_h \in V_h \text{ such that } a^L(u_h, v_h) = l_h^L(v_h) \quad \forall v_h \in V_h. \quad (3.24)$$

The corresponding bilinear and linear form is defined as,

$$\begin{aligned} a_h^L(u_h, v_h) &= (\alpha u_h, v_h)_\Omega + (\Delta u_h, \Delta v_h)_\Omega \\ &\quad - (\{\!\!\{\Delta u_h\}\!\!\}, [\partial_n v_h])_{\mathcal{F}_h^{int}} - (\{\!\!\{\Delta v_h\}\!\!\}, [\partial_n u_h])_{\mathcal{F}_h^{int}} + \frac{\gamma}{h}([\partial_n u_h], [\partial_n v_h])_{\mathcal{F}_h^{int}} \\ &\quad - (\Delta u_h, \partial_n v_h)_\Gamma - (\partial_n u_h, \Delta v_h)_\Gamma + \frac{\gamma}{h}(\partial_n u_h, \partial_n v_h)_\Gamma, \\ l_h^L(v_h) &= (f, v_h)_\Omega - (g_2, v_h)_\Gamma - (g_1, \Delta v_h)_\Gamma + \frac{\gamma}{h}(g_1, \partial_n v_h)_\Gamma. \end{aligned} \quad (3.25)$$

With the corresponding energy norms

$$\begin{aligned}\|v\|_{a_h^L}^2 &= \alpha\|v\|_\Omega^2 + \|\Delta v\|_\Omega^2 + \|h^{-\frac{1}{2}}[\partial_n v]\|_{\mathcal{F}_h^{int}}^2 + \|h^{-\frac{1}{2}}\partial_n v\|_\Gamma^2 \quad v \in V_h, \\ \|v\|_{a_h^L,*}^2 &= \|v\|_{a_h}^2 + \|h^{\frac{1}{2}}\{\partial_{nn} v\}\|_{\mathcal{F}_h^{int}}^2 + \|h^{\frac{1}{2}}\partial_{nn} v\|_\Gamma^2 \quad v \in V \oplus V_h.\end{aligned}\tag{3.26}$$

Remark. Again, note that we have the consistent terms $(\{\Delta u_h\}, [\partial_n v_h])_{\mathcal{F}_h^{int}}$ and $(\Delta u_h, \partial_n v_h)_\Gamma$ naturally appearing in the derivation. Also recall the symmetry terms, $([\partial_n u_h], \{\Delta v_h\})_{\mathcal{F}_h^{int}}$ and $(\partial_n u_h - g_1, \Delta v_h)_\Gamma$, with corresponding Nitsche penalty terms, $\frac{\gamma}{h}(\partial_n u_h - g_1, \partial_n v_h)_\Gamma$ and $\frac{\gamma}{h}([\partial_n u_h], [\partial_n v_h])_{\mathcal{F}_h^{int}}$, thus making the bilinear form $a^L(\cdot, \cdot)$ symmetric and well-posed.

3.2.3 Comments and earlier work

It should be noted that the Hessian formulation has a substantial limitation in that it is only valid for homogeneous Neumann conditions. This constraint arises from the challenges associated with imposing g_1 via the tangential derivative terms in Equation (3.14) during the proof of Lemma 3.1. From a physical perspective, this is manageable as it aligns with the boundary conditions of the original CH problem (1.7). However, from the standpoint of numerical validation, the homogeneous Neumann condition enforces strict rules on the design of manufactured solutions on arbitrary domains. One way to fix this is to enforce tangential derivatives of g_1 , i.e., inserting $\partial_n u = g_1$ for $(\partial_{t_i}(\partial_n u), \partial_n v)_\Gamma$ into (3.14). A downside with this method is that we must require g_1 in $H^{\frac{3}{2}}(\Gamma)$. Consequently, the examples illustrated in section 4.6 are only demonstrated on simple domains. This particular constraint does not apply to the Laplace formulation.

The Hessian formulation is well investigated by Susanne Brenner in several papers for [2, 54, 55] with corresponding analysis and numerical validation. Similarly, variants of the Laplace formulation can be found here [3, 57]. In these articles there also is good theoretical and experimental evidence that both formulation have the following expected a priori estimates. Let $u \in H^s(\Omega)$ for $s \geq \frac{5}{2} + \varepsilon$, and $u_h \in V_h$ of order $k \geq 2$. Then with $r = \min\{s, k+2\}$ the a priori estimates are

$$\begin{aligned}\|u - u_h\|_{a_h,*} &\lesssim h^{r-2}\|u\|_{r,\Omega}, \\ \|u - u_h\|_\Omega &\lesssim h^{r-\max\{0, 3-k\}}\|u\|_{r,\Omega}.\end{aligned}\tag{3.27}$$

Be aware that the $\|\cdot\|_\Omega$ norm estimates is suboptimal for $k = 2$. It is worth noting that technically is the interior regularisation equivalent to do a Nitsche's method in all interior boundaries of the elements with boundary conditions of each element weakly imposed to zero. Thus, we expect the penalty parameter γ to be the same interior and exterior elements. Let where $k \geq 2$ is the polynomial order, then for the Hessian formulation is it theoretically proven that $\gamma = 2k(k-1)$ [54, 2]. However, we still prefer to experimentally verify the best parameter.

3.3 Note on the biharmonic mixed formulation

It is easy to see that the biharmonic problem can be rewritten into an equivalent mixed formulation, that is, to find $\sigma, \tau \in H^2(\Omega)$ such that

$$\Delta\sigma = f \quad \text{in } \Omega, \tag{3.28a}$$

$$\sigma = \Delta u \quad \text{in } \Omega, \tag{3.28b}$$

$$\partial_n\sigma = g_1 \quad \text{on } \Gamma, \tag{3.28c}$$

$$\partial_n u = g_2 \quad \text{on } \Gamma. \tag{3.28d}$$

The goal is to obtain an useful weak formulation. Using Greens theorem on the first equation we get,

$$(\sigma, v)_\Omega = (\nabla u, \nabla v)_\Omega - (\nabla_n u, v)_\Gamma. \tag{3.29}$$

Similarly for the second equation we obtain

$$(\nabla\sigma, \nabla\varphi)_\Omega - (\partial_n\sigma, \varphi)_\Gamma = (f, \varphi)_\Omega. \quad (3.30)$$

Putting it all together we have the following mixed weak formulation; Find $(u, \sigma) \in H^1(\Omega) \times H^1(\Omega)$ such that

$$\begin{aligned} (\nabla u, \nabla v)_\Omega - (\sigma, v)_\Omega &= (g_1, v)_\Gamma \quad \forall v \in H^1(\Omega), \\ (\nabla\sigma, \nabla\varphi)_\Omega &= (f, \varphi)_\Omega + (g_2, \varphi)_\Gamma \quad \forall \varphi \in H^1(\Omega). \end{aligned} \quad (3.31)$$

Now we want to relate this formulation to the abstract saddle point problem (SPP). Let $V = H^1(\Omega)$ and $W = H^1(\Omega)$ be Hilbert spaces and define the bilinear form $a : V \times V \rightarrow \mathbb{R}$ and $b : V \times W \rightarrow \mathbb{R}$ s.t. $a(\sigma, v) = -(\sigma, v)_\Omega$ and $b(u, v) = (\nabla u, \nabla v)_\Omega$. We also may define the linear forms, $G, F : V \rightarrow \mathbb{R}$ such that $G(v) = (g_1, v)_\Gamma$ and $F(\varphi) = (f, \varphi)_\Omega + (g_2, \varphi)_\Gamma$.

Hence, we obtain the following SPP. Find $(u, \sigma) \in V \times W$ such that

$$\begin{cases} a(\sigma, v) + b(u, v) &= G(v) \quad \forall v \in V, \\ b(u, \varphi) &= F(\varphi) \quad \forall \varphi \in W. \end{cases} \quad (3.32)$$

This is useful since we can now apply standard saddle point theory to do an analysis for the problem. We will see that it is now easier to handle the boundary constraints naturally, but with the cost of a more challenging time discretization procedure. For more information about the biharmonic mixed formulation, see [92, 75]. However, in this thesis is the focus on solving the biharmonic equation avoiding the mixed formulation using the CIP formulation, which does in fact handle the downsides with the SPP problem.

4 Cut continuous interior penalty methods for the biharmonic problem

Questions arise when we want to allow for complex geometries where some physical domain Ω has a smooth boundary Γ . A method would be to generate a structured background mesh which fully covers Ω , but does not necessarily fit to the boundary perfectly. For consistency, integration of the contribution is performed on the physical domain, but the involved discrete test and trial functions in V_h are defined on the background mesh. However, we will run into geometrical problems when so-called cut finite elements have a very small intersection of the physical domain, i.e., $|T \cap \Omega|_d \ll |T|_d \lesssim h^d$ and $|\Gamma \cap T|_{d-1} \ll h^{d-1}$, where $|\cdot|_d$ is the measure of the volume in dimension d . The cut elements are identified as a crucial geometric issue since the inverse inequalities outlined in Section 2.8 do not generalize well to these elements. This identifies the challenges in establishing theoretical stability and a priori estimates for any geometric arrangement.

One way to handle this issue is to introduce the so-called cut finite element method (CutFEM). The method involves adding a stabilization term, commonly referred to as the ghost penalty term. This term serves the purpose of controlling the energy norm associated with the bilinear form, utilizing the entire background mesh to ensure stabilization and geometric robustness. For more information, see [72, 93, 94, 95]. Inspired by the corresponding CutFEM DG elliptic framework outlined in [1], the objective of this section is to engineer suitable stabilized ghost penalty terms for the biharmonic problem, starting from the CIP methods introduced in Section 3. We will show what assumptions are needed for the ghost-penalty method for the discrete problem to be stable in Section 4.3 and derive optimal convergence in Section 4.4. Once this is fulfilled we propose a ghost penalty which fulfills these assumptions in Section 4.5. Lastly, we provide numerical experiments to validate the theoretical results in Section 4.6

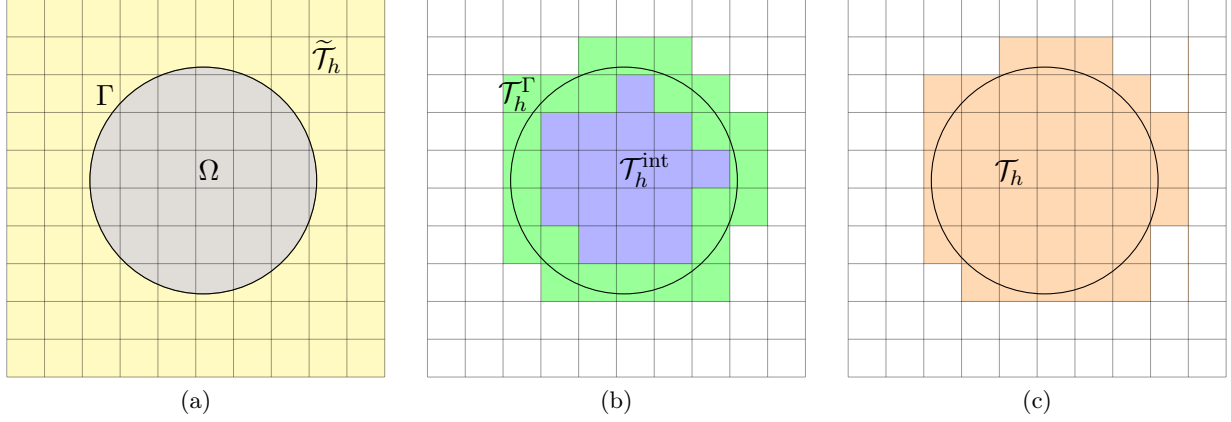


Figure 12: Illustration of the domain Ω with the corresponding boundary Γ , the background mesh $\tilde{\mathcal{T}}_h$, the cut cells \mathcal{T}_h^Γ , the interior cells \mathcal{T}_h^{int} and the active set $\mathcal{T}_h = \mathcal{T}_h^{int} \cup \mathcal{T}_h^\Gamma$.

4.1 Computational domain

We want to devise a CutFEM based on the CIP formulation for the biharmonic problem. Assume that the physical domain $\Omega \subseteq \mathbb{R}^d$ to be open and bounded with a corresponding sufficiently smooth boundary Γ . Let $\tilde{\mathcal{T}}_h$ be a shape-regular and quasi-uniform mesh which covers Ω , but does not need to fit the domain. Let us denote the active set $\mathcal{T}_h \subseteq \tilde{\mathcal{T}}_h$ which intersects the interior of the active domain Ω , that is

$$\mathcal{T}_h = \left\{ T \in \tilde{\mathcal{T}}_h \mid T \cap \Omega \neq \emptyset \right\}. \quad (4.1)$$

We define the corresponding set of interior facets,

$$\mathcal{F}_h^{int} = \left\{ F = T^+ \cap T^- \mid T^+, T^- \in \mathcal{T}_h \text{ and } T^+ \neq T^- \right\},$$

and the set of elements cut by the boundary

$$\mathcal{T}_h^\Gamma = \left\{ T \in \mathcal{T}_h \mid T \cap \Gamma \neq \emptyset \right\}.$$

For convenience, we will also define the interior of the active set as \mathcal{T}_h^{int} .

$$\mathcal{T}_h^{int} = \left\{ T \in \mathcal{T}_h \mid T \cap \text{Int}(\Omega) \neq \emptyset \right\}.$$

Hence, we have that the active set is the union of the interior and cut elements, $\mathcal{T}_h = \mathcal{T}_h^{int} \cup \mathcal{T}_h^\Gamma$. For an illustration, see Figure 12.

4.2 Cut continuous interior penalty methods

As Ω is static, it is easy to observe that having a polynomial basis on the full mesh $\tilde{\mathcal{T}}_h$ is not necessary. Restricting us to the active set, we define the domain $\Omega_h = \bigcup_{T \in \mathcal{T}_h} T$. Hence, we define the polynomial space only on the active set \mathcal{T}_h from (4.1),

$$V_h = \left\{ v \in C^0(\Omega_h) \mid v|_T \in \left\{ \mathcal{P}^k(T) \text{ or } \mathcal{Q}^k(T) \right\} \forall T \in \mathcal{T}_h \right\}. \quad (4.2)$$

Here is k the polynomial order and $\mathcal{P}^k(\cdot)$ and $\mathcal{Q}^k(\cdot)$ is defined in Definition 2.6. Furthermore, drawing on the principles outlined in Section 3, we can indeed recall two CIP formulations for the biharmonic equation: the Hessian formulation (3.16) and the Laplace formulation (3.24).

To make sure the problem is stabilized will we add a consistent symmetric positive semi-definite bilinear ghost-penalty term $g_h : V_h \times V_h \rightarrow \mathbb{R}$ to our bilinear form. That is, we define the discrete problem to be:

$$\text{Find } u_h \in V_h \text{ such that } A_h(u_h, v_h) := a_h(u_h, v_h) + g_h(u_h, v_h) = l_h(v_h) \quad \forall v_h \in V_h. \quad (4.3)$$

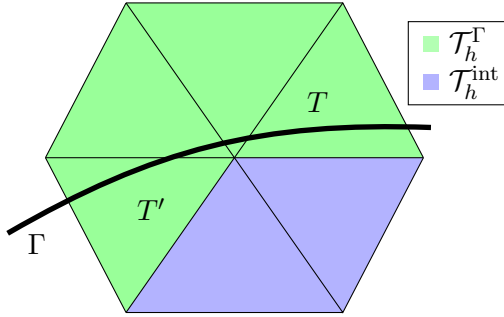


Figure 13: Illustration of the fat intersection property. Let $T \in \mathcal{T}_h^\Gamma$. It shows a patch $\omega(T)$ contains elements $T \in \mathcal{T}_h^\Gamma$ and $T' \in \mathcal{T}^{\text{int}} \cup \mathcal{T}_h^\Gamma = \mathcal{T}_h$, with T' having a sufficiently large intersection with Ω .

Here $a_h(\cdot, \cdot)$ stand for either $a_h^L(\cdot, \cdot)$ or $a_h^H(\cdot, \cdot)$.

In this section, we provide a full proof for the Hessian formulation, however, the proof of the Laplace formulation is similar. For simplification will we use the notation $a_h(\cdot, \cdot) = a_h^H(\cdot, \cdot)$ and $l_h(\cdot) = l_h^H(\cdot)$ for the rest of the stability and convergence analysis.

Keep in mind that our proposed method is defined on an unfitted mesh in contrast to the standard CIP methods. As we will see in the analysis, the ghost penalty is a method to ensure numerical stability on cut cell \mathcal{T}_h^Γ . The main reason why this numerical instability happens for an unfitted mesh happens when a cell is badly cut, see examples in Figure 14. In other words, when a cell is "badly cut," it means that it is intersected by the boundary Γ in such a way that only an almost vanishing part of the interior of an element T intersects with the physical domain Ω , i.e. $|\Omega \cap T|_d \ll h^d$. This can lead to stability issues and a very poor condition number of the system matrix causing numerical instability.

The ghost penalty stabilization technique is designed to tackle this issue. Essentially, this approach introduces additional terms into the finite element method that penalize jumps in the discrete solution and its gradients across cell interfaces, typically the cut-cells. This penalty not only improves the conditioning of the system matrix but also enhances the robustness of the method with respect to the location of the boundary inside each cell. However, to make this possible, we assume a so-called fat-intersection property, which will be relevant in Section 4.5.

Our first assumption is as follows; for a $T \in \mathcal{T}_h^\Gamma$ there always exists a patch $\omega(T)$ which contains T and an element T' with a so-called fat intersection $|T' \cap \Omega|_d \gtrsim |T'|_d$, where $|\cdot|_d$ is the measure of an element of dimensions $d = 2, 3$. For an illustration, see Figure 13.

We define the underlying norms for $v_h \in V_h$ as

$$\|v_h\|_{a_h}^2 = \alpha \|v_h\|_{\mathcal{T}_h \cap \Omega}^2 + \|D^2 v_h\|_{\mathcal{T}_h \cap \Omega}^2 + \|h^{-\frac{1}{2}} [\partial_n v_h]\|_{\mathcal{F}_h \cap \Omega}^2 + \|h^{-\frac{1}{2}} \partial_n v_h\|_\Gamma^2, \quad (4.4)$$

$$|v|_{g_h}^2 = g(v_h, v_h), \quad (4.5)$$

$$\|v_h\|_{A_h}^2 = \|v_h\|_{a_h}^2 + |v_h|_{g_h}^2, \quad (4.6)$$

$$(4.7)$$

and for $v \in V \oplus V_h$ we also introduce,

$$\|v\|_{a_h,*}^2 = \|v\|_{a_h}^2 + \|h^{\frac{1}{2}} \{\partial_{nn} v\}\|_{\mathcal{F}_h \cap \Omega}^2 + \|h^{\frac{1}{2}} \partial_{nn} v\|_\Gamma^2. \quad (4.8)$$

Remark. Note that it holds that $\mathcal{T}_h \cap \Omega = \Omega$ and $\mathcal{T}_h \cap \Gamma = \Gamma$. Depending on context, we choose the best suitable notation.

Remark. The necessity to define the supplementary terms in the $\|\cdot\|_{a_h,*}$ may raise certain questions. The reason is because when v is continuous, i.e. $v \in V$, the local inverse estimates 2.38 does not hold for $\{\partial_{nn} v\}_{\mathcal{F}_h \cap \Omega}$ and $\|\partial_{nn} v\|_\Gamma$ when evaluating $a_h(v, v)$. Hence, this leads necessity adding the additional terms into the norm when we later need to bound $a_h(u - C_h u, v_h)$ as part of the a priori error estimate derivation in Section 4.4.

4.3 Stability estimate

In Section 2.8, we discussed standard local inverse estimates, which plays a crucial role in the theoretical analysis of the classical CIP method for biharmonic problems. Similarly, for cut elements, is it easy to see that this must hold,

$$\|\partial_{nn}v_h\|_{F \cap \Omega} \lesssim \|\partial_{nn}v_h\|_F \lesssim \|h_T^{-\frac{1}{2}} D^2 v_h\|_T. \quad (4.9)$$

A useful variant is the following inequality that is,

$$\|\partial_{nn}v_h\|_{\Gamma \cap T} \lesssim h^{-\frac{1}{2}} \|D^2 v_h\|_T. \quad (4.10)$$

For the proposed unfitted version, it may be natural to instead look at $\|\partial_{nn}v_h\|_{\Gamma \cap T} \lesssim h^{-\frac{1}{2}} \|D^2 v_h\|_{T \cap \Omega}$, however, this cannot hold for an arbitrary cut configuration for an unfitted mesh. To demonstrate this, let $\varepsilon \ll 1$ be a small length. For the examples provided in Figure 14 we have two cases: i) $|\Gamma \cap \Omega|_{d-1} \lesssim \varepsilon h^{d-1}$ and $|T \cap \Omega|_{d-1} \lesssim \varepsilon h^{d-1}$, and ii) $|\Gamma \cap \Omega|_{d-1} \lesssim h^{d-1}$ and $|T \cap \Omega|_{d-1} \lesssim \varepsilon h^{d-1}$. The first case impacts the condition number since it introduces almost vanishing entries in the system matrix from (2.27). The second case is bad for inverse estimates and, thus, problematic for proving discrete coercivity. To recover, we must incorporate the full element T into the inverse estimate as done in (4.10) and (4.9).

Since the inequalities above hold for all elements locally, it is natural to work with norms defined by the full mesh \mathcal{T}_h .

$$\|\partial_{nn}v_h\|_{\mathcal{T}_h \cap \Gamma} \lesssim h^{-\frac{1}{2}} \|D^2 v_h\|_{\mathcal{T}_h}, \quad (4.11)$$

$$\|\partial_{nn}v_h\|_{\mathcal{F}_h \cap \Omega} \lesssim h^{-\frac{1}{2}} \|D^2 v_h\|_{\mathcal{T}_h}. \quad (4.12)$$

We aware that these inequalities also holds for the first order, that is.

$$\|\partial_n v_h\|_{\mathcal{T}_h \cap \Gamma} \lesssim h^{-\frac{1}{2}} \|\nabla v_h\|_{\mathcal{T}_h}, \quad (4.13)$$

$$\|\partial_n v_h\|_{\mathcal{F}_h \cap \Omega} \lesssim h^{-\frac{1}{2}} \|\nabla v_h\|_{\mathcal{T}_h}. \quad (4.14)$$

In fact, combining the second order inequalities we get the following identity.

$$h \|\partial_{nn}v_h\|_{\mathcal{F}_h \cap \Omega}^2 + h \|\partial_{nn}v_h\|_{\mathcal{T}_h \cap \Gamma}^2 \lesssim \|D^2 v_h\|_{\mathcal{T}_h}^2 \quad \forall v_h \in V_h. \quad (4.15)$$

For more information about the derivations of the inequalities, see the discussion in [1, Section 2.4].

We may introduce our first assumption on the ghost penalty. Inspired by the expansion for the H^1 -norm as detailed in [1, Equation 2.23], we adopt an analogous approach for the H^2 -norm in this scenario.

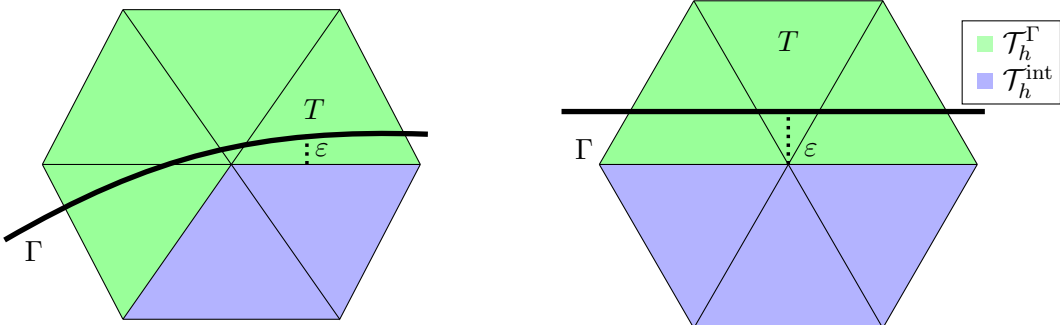


Figure 14: Illustration of two examples of bad cut cells with an arbitrary small length $\varepsilon \ll 1$. Let $T \in \mathcal{T}_h^\Gamma$ be a cut cell. On the left example, is it clear that $|\Gamma \cap T| \lesssim h^{d-1}$ and $|\Omega \cap T| \lesssim \varepsilon h^d$. However, in the right example, is it clear that $|\Gamma \cap T| \lesssim \varepsilon h^{d-1}$ and $|\Omega \cap T| \lesssim \varepsilon h^d$.

Assumption (EP1). *The ghost penalty g_h extends the H^2 norm such that*

$$\|D^2v\|_{\mathcal{T}_h}^2 \lesssim \|D^2v\|_\Omega^2 + |v|_{g_h}^2. \quad (4.16)$$

Combining the results, we get the following convenient corollary.

Corollary 4.1. *Let g_h satisfy Assumption EP1 (4.16), then*

$$h\|\partial_{nn}v_h\|_{\mathcal{F}_h \cap \Omega}^2 + h\|\partial_{nn}v_h\|_{\mathcal{T}_h \cap \Gamma}^2 \lesssim \|D^2v_h\|_\Omega^2 + |v_h|_{g_h}^2 \lesssim \|v_h\|_{A_h}^2 \quad \forall v_h \in V_h. \quad (4.17)$$

From this, it is also clear that

$$\|v_h\|_{a_h,*} \lesssim \|v_h\|_{A_h} \quad \forall v_h \in V_h. \quad (4.18)$$

Proof. The first result (4.17) is a direct result of (4.15), Assumption EP1 (4.16) and the definition of $\|\cdot\|_{A_h}$. The second result (4.18) is simply a observation that the terms in (4.17) appears in $\|\cdot\|_{a_h,*}$, hence, the inequality follows. \square

Remark. The alternative version of the Assumption EP1 (4.16) for the Laplace formulation (3.24) is simply $\|\Delta^2v_h\|_{\mathcal{T}_h}^2 \lesssim \|\Delta^2v\|_\Omega^2 + |v_h|_{g_h}^2$ and, similarly, is it then clear that $h\|\Delta v\|_{\mathcal{F} \cap \Omega}^2 + h\|\Delta^2v_h\|_{\mathcal{T}_h \cap \Gamma}^2 \lesssim \|\Delta^2v\|_\Omega^2 + |v_h|_{g_h}^2$ would follow as in (4.17).

Lemma 4.2. *The discrete form A_h is coercive, that is,*

$$\|v_h\|_{A_h}^2 \lesssim A_h(v_h, v_h) \quad \forall v_h \in V_h.$$

Proof. Let $v_h \in V_h$. Observe that

$$A_h(v_h, v_h) = a_h(v_h, v_h) + |v_h|_{g_h}^2. \quad (4.19)$$

Firstly, the ghost penalty term is already a part of the $\|\cdot\|_{A_h}$ norm, hence, it only remains to bound the $a_h(\cdot, \cdot)$ term properly from below.

$$\begin{aligned} a_h(v_h, v_h) &= \alpha\|v_h\|_\Omega^2 + \|D^2v_h\|_\Omega^2 + \frac{\gamma}{h}\|\llbracket \partial_n v_h \rrbracket\|_{\mathcal{F}_h}^2 + \frac{\gamma}{h}\|\partial_n v_h\|_\Gamma^2 \\ &\quad + 2(\llbracket \partial_{nn}v_h \rrbracket, \llbracket \partial_n v_h \rrbracket)_{\mathcal{F}_h \cap \Omega} + 2(\partial_{nn}v_h, \partial_n v_h)_\Gamma. \end{aligned} \quad (4.20)$$

We first focus on the last two terms in (4.20). Using Cauchy-Schwarz (2.10), we observe that

$$\begin{aligned} (\llbracket \partial_{nn}v_h \rrbracket, \llbracket \partial_n v_h \rrbracket)_{\mathcal{F}_h \cap \Omega} &\geq -\|h^{\frac{1}{2}}\llbracket \partial_{nn}v_h \rrbracket\|_{\mathcal{F}_h \cap \Omega}\|h^{-\frac{1}{2}}\llbracket \partial_n v_h \rrbracket\|_{\mathcal{F}_h \cap \Omega}, \\ (\partial_{nn}v_h, \partial_n v_h)_\Gamma &\geq -\|h^{\frac{1}{2}}\partial_{nn}v_h\|_\Gamma\|h^{-\frac{1}{2}}\partial_n v_h\|_\Gamma. \end{aligned} \quad (4.21)$$

Using inverse-inequalities (4.11) and (4.12) and the Corollary 4.1 we can easily observe that

$$\begin{aligned} \|h^{\frac{1}{2}}\llbracket \partial_{nn}v_h \rrbracket\|_{\mathcal{F}_h \cap \Omega}^2 &\leq C_1\|D^2v_h\|_{\mathcal{T}_h}^2 \lesssim \|D^2v_h\|_\Omega^2 + |v_h|_{g_h}^2, \\ \|\partial_{nn}v_h\|_\Gamma^2 &\leq C_2\|D^2v_h\|_{\mathcal{T}_h}^2 \lesssim \|D^2v_h\|_\Omega^2 + |v_h|_{g_h}^2. \end{aligned} \quad (4.22)$$

Thus, by applying Young's ε -inequality (2.13), it is natural to see that,

$$\begin{aligned} -C_1^{\frac{1}{2}}\|D^2v_h\|_{\mathcal{T}_h}\|h^{-\frac{1}{2}}\llbracket \partial_n v_h \rrbracket\|_{\mathcal{F}_h \cap \Omega} &\geq -\frac{1}{\varepsilon}C(\|D^2v_h\|_\Omega^2 + |v_h|_{g_h}^2) - \varepsilon\|h^{-\frac{1}{2}}\llbracket \partial_n v_h \rrbracket\|_{\mathcal{F}_h \cap \Omega}^2, \\ -C_2^{\frac{1}{2}}\|D^2v_h\|_{\mathcal{T}_h}\|h^{-\frac{1}{2}}\partial_n v_h\|_\Gamma &\geq -\frac{1}{\varepsilon}C(\|D^2v_h\|_\Omega^2 + |v_h|_{g_h}^2) - \varepsilon\|h^{-\frac{1}{2}}\partial_n v_h\|_\Gamma^2. \end{aligned} \quad (4.23)$$

Combining these ideas, we end up with the following inequality,

$$\begin{aligned} a_h(v_h, v_h) &\geq \alpha\|v\|_\Omega^2 + \|D^2v_h\|_\Omega^2 - \frac{1}{\varepsilon}4C(\|D^2v_h\|_\Omega^2 + |v_h|_{g_h}^2) \\ &\quad + (\gamma - 2\varepsilon)\left(\|h^{-\frac{1}{2}}\llbracket \partial_n v_h \rrbracket\|_{\mathcal{F}_h \cap \Omega}^2 + \|h^{-\frac{1}{2}}\partial_n v_h\|_\Gamma^2\right). \end{aligned} \quad (4.24)$$

This inequality is useful since by adding a ghost penalty on the left-hand side we get,

$$\begin{aligned} A_h(v_h, v_h) &= a(v_h, v_h) + |v_h|_{g_h}^2 \\ &\gtrsim \| |\alpha|^{\frac{1}{2}} v_h \|_{\Omega}^2 + (1 - \frac{1}{\varepsilon} 4C)(\| D^2 v_h \|_{\Omega}^2 + |v_h|_{g_h}^2) \\ &\quad + (\gamma - 2\varepsilon) \left(\| h^{-\frac{1}{2}} [\partial_n v_h] \|_{\mathcal{F}_h \cap \Omega}^2 + \| h^{-\frac{1}{2}} \partial_n v_h \|_{\Gamma}^2 \right). \end{aligned} \quad (4.25)$$

Setting $\varepsilon = 8C$ and $\gamma = 32C$ we arrive at the desired inequality,

$$\begin{aligned} A_h(v_h, v_h) &\gtrsim \| |\alpha|^{\frac{1}{2}} v_h \|_{\Omega}^2 + \frac{1}{2}(\| D^2 v_h \|_{\Omega}^2 + |v_h|_{g_h}^2) \\ &\quad + \frac{\gamma}{2} \left(\| h^{-\frac{1}{2}} [\partial_n v_h] \|_{\mathcal{F}_h \cap \Omega}^2 + \| h^{-\frac{1}{2}} \partial_n v_h \|_{\Gamma}^2 \right) \\ &\gtrsim \| v_h \|_{A_h}^2. \end{aligned} \quad (4.26)$$

□

Lemma 4.3. *The discrete bilinear form $A_h(\cdot, \cdot)$ is bounded*

$$A_h(v_h, w_h) \lesssim \| v_h \|_{A_h} \| w_h \|_{A_h} \quad \forall v_h, w_h \in V_h. \quad (4.27)$$

Moreover, for $v \in V_h \oplus V$ and $w_h \in V_h$ the discrete bilinear form $a_h(\cdot, \cdot)$ satisfies

$$a_h(v, w_h) \lesssim \| v \|_{a_h,*} \| w_h \|_{A_h}. \quad (4.28)$$

Proof. **Estimate (4.27).** We see that $|A_h(v_h, w_h)| \lesssim |a_h(v_h, w_h)| + |g_h(v_h, w_h)|$. By assumption the ghost penalty $g_h(\cdot, \cdot)$ is positive semi-definite, thus fulfills the Cauchy-Schwarz inequality,

$$|g_h(v_h, w_h)| \lesssim |v_h|_{g_h} |w_h|_{g_h}. \quad (4.29)$$

Hence, $|g_h(v_h, w_h)| \lesssim \| v_h \|_{A_h} \| w_h \|_{A_h}$ by definition of $A_h(\cdot, \cdot)$. It remains to show that the bilinear term $a_h(\cdot, \cdot)$ is bounded. We numerate the terms in this fashion.

$$\begin{aligned} a_h(v_h, w_h) &\leq \overbrace{(\alpha v_h, w_h)_{\mathcal{T}_h \cap \Omega}}^{\text{I}} + \overbrace{(D^2 v_h, D^2 w_h)_{\mathcal{T}_h \cap \Omega}}^{\text{II}} \\ &\quad + \overbrace{([\partial_n v_h], [\partial_n w_h])_{\mathcal{F}_h \cap \Omega}}^{\text{III}} + \overbrace{([\partial_{nn} v_h], [\partial_n v_h])_{\mathcal{F}_h \cap \Omega}}^{\text{IV}} + \overbrace{\frac{\gamma}{h} ([\partial_n v_h], [\partial_n w_h])_{\mathcal{F}_h \cap \Omega}}^{\text{V}} \\ &\quad + \overbrace{(\partial_{nn} v_h, \partial_n w_h)_{\Gamma}}^{\text{VI}} + \overbrace{(\partial_{nn} w_h, \partial_n v_h)_{\Gamma}}^{\text{VII}} + \overbrace{\frac{\gamma}{h} (\partial_n v_h, \partial_n w_h)_{\Gamma}}^{\text{VIII}} \\ &= \text{I} + \dots + \text{VIII}. \end{aligned} \quad (4.30)$$

The strategy is to bound each term individually using the Cauchy-Schwarz inequality (2.10). From this it is easy to see that $|\text{I}| + |\text{II}| \lesssim \| v_h \|_{a_h} \| w_h \|_{a_h}$. To the terms III and IV we apply the inequality (4.17) from the Corollary 4.1 to see that,

$$|\text{III}| \lesssim \| h^{\frac{1}{2}} \partial_{nn} v_h \|_{\mathcal{F}_h \cap \Omega} \| h^{-\frac{1}{2}} [\partial_n w_h] \|_{\mathcal{F}_h \cap \Omega} \lesssim \| v_h \|_{A_h} \| w_h \|_{a_h}. \quad (4.31)$$

The interior penalty can we easily see that,

$$|\text{V}| \lesssim \| h^{-\frac{1}{2}} [\partial_n v_h] \|_{\mathcal{F}_h \cap \Omega} \| h^{-\frac{1}{2}} [\partial_n w_h] \|_{\mathcal{F}_h \cap \Omega} \lesssim \| v_h \|_{a_h} \| w_h \|_{a_h}. \quad (4.32)$$

The remaining terms terms VI and VII can again be handles by Corollary 4.1, leading to

$$|\text{VI}| \lesssim \| h^{\frac{1}{2}} \partial_{nn} v_h \|_{\Gamma} \| h^{-\frac{1}{2}} \partial_n w_h \|_{\Gamma} \lesssim \| v_h \|_{A_h} \| w_h \|_{a_h}. \quad (4.33)$$

Finally, using the definition of the norm, it is easy to see that

$$|\text{VIII}| \lesssim \|\partial_n v_h\|_\Gamma \|\partial_n w_h\|_\Gamma \lesssim \|v_h\|_{a_h} \|w_h\|_{a_h}. \quad (4.34)$$

Hence, we can conclude

$$|a_h(v_h, w_h)| \leq \|v_h\|_{a_h} \|w_h\|_{a_h} \quad \forall v_h, w_h \in V_h. \quad (4.35)$$

Therefore, since $\|\cdot\|_{a_h} \lesssim \|\cdot\|_{A_h}$, it has been demonstrated that $a_h(\cdot, \cdot)$ is bounded within the $\|\cdot\|_{A_h}$ norm.

Estimate (4.28). Let $v \in V_h \oplus V$ and $w_h \in V_h$. The only difference is that since v can have a contribution from V where no inverse estimate can be used to bound $\{\partial_{nn} v\}$, hence, we cannot apply to Corollary 4.1 on the estimates (4.31) and (4.33). However, this is not a problem since $\|h^{\frac{1}{2}} \{\partial_{nn} v\}\|_{\mathcal{F}_h \cap \Omega}$ and $\|h^{\frac{1}{2}} \partial_{nn} v\|_\Gamma$ are terms in the norm $\|v\|_{a_h,*}$. Thus, we know that

$$|a_h(v, w_h)| \leq \|v\|_{a_h,*} \|w_h\|_{A_h} \quad \forall v \in V_h \oplus V \text{ and } w_h \in V_h. \quad (4.36)$$

□

4.4 A priori error estimate

For the proposed method, we want to derive a priori error estimate with respect to both the $\|\cdot\|_{a_h,*}$ -norm and the $\|\cdot\|_\Omega$ -norm. These estimates are geometrically robust in that they remain unaffected by specific cut configurations, thanks to the ghost penalty they incorporate. First, we construct a suitable (quasi-)interpolation operator. Here we use the Clement quasi interpolation operator which, in contrast to the standard Lagrange nodal interpolation operator, is also defined for low regularity function $u \in L^2(\Omega)$. In combination with discrete coercivity, this allows us to derive an a priori error estimate in the energy norm. Finally, we use a standard duality argument, also known as Aubin-Nitsche trick, to derive the $L^2(\Omega)$ -error estimate.

Recall that for $v \in H^3(\mathcal{T}_h)$ the following inequalities.

$$\|\nabla v\|_{\partial T} \lesssim h_T^{-\frac{1}{2}} \|\nabla v\|_T + h^{\frac{1}{2}} \|D^2 v\|_T, \quad (4.37)$$

$$\|\nabla v\|_{\Gamma \cap T} \lesssim h^{-\frac{1}{2}} \|\nabla v\|_T + h_T^{\frac{1}{2}} \|D^2 v\|_T, \quad (4.38)$$

$$\|D^2 v\|_{\Gamma \cap T} \lesssim h^{-\frac{1}{2}} \|D^2 v\|_T + h_T^{\frac{1}{2}} \|D^3 v\|_T, \quad (4.39)$$

holds $\forall T \in \mathcal{T}_h$, for proof see [96, Lemma 4.2]. In this context is $D^3 v$ a tensor defined in Equation (2.8).

Assume that Ω has a boundary Γ in C^1 , then there exists a bounded extension operator,

$$(\cdot)^e : H^m(\Omega) \rightarrow H^m(\mathbb{R}^d), \quad (4.40)$$

for all $v \in H^m(\Omega)$ which satisfies

$$\begin{aligned} v^e|_\Omega &= v, \\ \|v^e\|_{m, \mathbb{R}^d} &\lesssim \|v\|_{m, \Omega}. \end{aligned} \quad (4.41)$$

For more information, see [97, Theorem 9.7] and [98, p.181, p.185]. For the notation we simply write $v := v^e$ for $v \in \mathbb{R}^d \setminus \Omega$.

Starting from Lemma 2.8, assume $v \in H^s(\Omega)$ and let $r = \min(s, k+1)$. Revisit the definition of V_h from (4.2), which is a polynomial of degree k . We can then employ the combination of the Clément interpolator with the extension operator to create $C_h^e : H^m(\mathbb{R}^d) \rightarrow V_h$, such that $C_h^e v := C_h v^e$. Next, recall that $\sum_{T \in \mathcal{T}_h} \|v\|_{s, \omega(T)} \leq C \|v\|_{s, \mathcal{T}_h}$ where C is some constant decided by shape regularity of the mesh and the maximal number of different patches a single element can

belong to. This also holds for the inequality $\sum_{T \in \mathcal{T}_h} \sum_{F \in \partial T} \|v\|_{s, \omega(F)} \leq C \|v\|_{s, \mathcal{T}_h}$. The following estimates are thereby established.

$$\|v - C_h^e v\|_{l, \mathcal{T}_h} \lesssim h^{r-l} \sum_{T \in \mathcal{T}_h} \|v\|_{r, \omega(T)} \lesssim h^{r-l-\frac{1}{2}} \|v\|_{r, \Omega}, \quad 0 \leq l \leq r, \quad (4.42)$$

$$\|v - C_h^e v\|_{l, \partial \mathcal{T}_h} \lesssim h^{r-l-\frac{1}{2}} \sum_{T \in \mathcal{T}_h} \sum_{F \in \partial T} \|v\|_{r, \omega(F)} \lesssim h^{r-l-\frac{1}{2}} \|v\|_{r, \Omega}, \quad 0 \leq l \leq r - \frac{1}{2}. \quad (4.43)$$

Lemma 4.4. Let $u \in H^s(\Omega)$ for $s \geq 3$ be the exact solution to (3.3) and let k be the polynomial order of V_h . Set $r = \min(s, k+1)$, then we have the interpolation estimates

$$\|u - C_h u\|_{a_h, *} \lesssim h^{r-2} \|u\|_{r, \Omega}. \quad (4.44)$$

Proof. By definition,

$$\begin{aligned} \|u - C_h^e u\|_{a_h, *}^2 &= \alpha \overbrace{\|(u - C_h^e u)\|_{\mathcal{T}_h \cap \Omega}^2}^{\text{I}} + \overbrace{\|D^2(u - C_h^e u)\|_{\mathcal{T}_h \cap \Omega}^2}^{\text{II}} \\ &\quad + \overbrace{\gamma \|h^{-\frac{1}{2}} [\partial_n(u - C_h^e u)]\|_{\mathcal{F}_h \cap \Omega}^2}^{\text{III}} + \overbrace{\gamma \|h^{-\frac{1}{2}} \partial_n(u - C_h^e u)\|_{\Gamma}^2}^{\text{IV}} \\ &\quad + \overbrace{\|h^{\frac{1}{2}} \{\partial_{nn}(u - C_h^e u)\}\|_{\mathcal{F}_h \cap \Omega}^2}^{\text{V}} + \overbrace{\|h^{\frac{1}{2}} \partial_{nn}(u - C_h^e u)\|_{\Gamma}^2}^{\text{VI}} \\ &= \text{I} + \dots + \text{VI}. \end{aligned} \quad (4.45)$$

The strategy is to bound each term individually. By initially focusing on the first two terms and employing equation (4.42), we can easily observe

$$\begin{aligned} \text{I} + \text{II} &\lesssim \|u - C_h^e u\|_{\mathcal{T}_h}^2 + \|D^2(u - C_h^e u)\|_{\mathcal{T}_h}^2 \\ &\lesssim (h^{2r} + h^{2(r-2)}) \|u\|_{r, \mathcal{T}_h}^2 \lesssim h^{2(r-2)} \|u\|_{r, \mathcal{T}_h}^2. \end{aligned} \quad (4.46)$$

From (2.12) is it clear that $\|\partial_n u\|_{\mathcal{F}_h} \lesssim \|\nabla u\|_{\partial \mathcal{T}_h}$. Hence, first applying the trace inequality (4.37) and then (4.42) is it clear that,

$$\begin{aligned} \text{III} &\lesssim h^{-1} \|\nabla(u - C_h^e u)\|_{\partial \mathcal{T}_h}^2 \lesssim h^{-2} \|\nabla(u - C_h^e u)\|_{\mathcal{T}_h}^2 + \|D^2(u - C_h^e u)\|_{\mathcal{T}_h}^2 \\ &\lesssim (h^{2(r-1)-2} + h^{2(r-2)}) \|u\|_{r, \mathcal{T}_h}^2 \lesssim h^{2(r-2)} \|u\|_{r, \mathcal{T}_h}^2. \end{aligned} \quad (4.47)$$

And for the boundary term we apply (4.38) and then (4.42)

$$\begin{aligned} \text{IV} &\lesssim h^{-1} \|\nabla(u - C_h^e u)\|_{\Gamma}^2 \lesssim h^{-2} \|\nabla(u - C_h^e u)\|_{\mathcal{T}_h}^2 + \|D^2(u - C_h^e u)\|_{\mathcal{T}_h}^2 \\ &\lesssim h^{2(r-2)} \|u\|_{r, \mathcal{T}_h}^2. \end{aligned} \quad (4.48)$$

Again, from (2.12) is it clear that $\|\{\partial_{nn} u\}\|_{\mathcal{F}_h} \lesssim \|D^2 u\|_{\partial \mathcal{T}_h}$, thus we see that,

$$\text{V} \lesssim h \|D^2(u - C_h^e u)\|_{\partial \mathcal{T}_h}^2 \lesssim h^{2(r-2)} \|u\|_{r, \mathcal{T}_h}^2. \quad (4.49)$$

The final term we apply (4.39) and then (4.42)

$$\begin{aligned} \text{VI} &\lesssim h \|D^2(u - C_h^e u)\|_{\Gamma}^2 \\ &\lesssim h^{-2} \|D^2(u - C_h^e u)\|_{\mathcal{T}_h}^2 + \|D^3(u - C_h^e u)\|_{\mathcal{T}_h}^2 \\ &\lesssim h^{-2} (h^{2(r-2-\frac{1}{2})} + h^{2(r-3-\frac{1}{2})}) \|u\|_{r, \Omega} \\ &\lesssim (h^{2r-5} + h^{2r-6}) \|u\|_{r, \Omega} \lesssim h^{2(r-2)} \|u\|_{r, \Omega}. \end{aligned} \quad (4.50)$$

Hence, we have $\|u - C_h^e u\|_{a_h, *} \lesssim h^{r-2} \|u\|_{r, \mathcal{T}_h}^2$. □

Lemma 4.5 (Weak Galerkin orthogonality). *Let $u \in H^s(\Omega)$, $s \geq 3$ be the exact solution to (3.3) and $u_h \in V_h$ is a discrete solution to (4.3). Then is*

$$a_h(u - u_h, v_h) = g_h(u_h, v_h) \quad \forall v_h \in V_h.$$

Proof. From the definition of the problem (4.3) and utilizing that for $u \in H^s(\Omega)$ we have the identity $A_h(u, v_h) = a_h(u, v_h) = l(v_h) \forall v_h \in V_h$. Consequently, it follows that

$$l(v_h) = A_h(u_h, v_h) = a_h(u, v_h) = a_h(u_h, v_h) + g_h(u_h, v_h) \quad \forall v_h \in V_h.$$

Hence, we have $a_h(u - u_h, v_h) = g_h(u_h, v_h)$. \square

Assumption (EP2). *For $v \in H^s(\Omega)$ and $r = \min\{s, k+1\}$, the semi-norm $|\cdot|_{g_h}$ is weakly consistent in the sense that*

$$|C_h^e v|_{g_h} \lesssim h^{r-2} \|v\|_{r,\Omega}. \quad (4.51)$$

Theorem 4.6. *Let $u \in H^s(\Omega)$, $s \geq 3$ be a solution to (3.3) and let $u_h \in V_h$ of order $k \geq 2$ be the discrete solution to (4.3). Then with $r = \min\{s, k+1\}$ the error $e = u - u_h$ satisfies*

$$\|e\|_{a_h,*} \lesssim h^{r-2} \|u\|_{r,\Omega}, \quad (4.52)$$

$$\|e\|_\Omega \lesssim h^{r-\max\{0, 3-k\}} \|u\|_{r,\Omega}. \quad (4.53)$$

Remark. Be aware that for $k = 2$ the estimate (4.53) is suboptimal with 1 order.

Proof. We will divide the proof into two steps.

Step 1. We want to prove that $\|e\|_{a_h,*} \lesssim h^{r-2} \|u\|_{r,\Omega}$. Decompose $e = u - u_h$ intro $e = e_\pi + e_h$, where we denote the discrete error $e_h = C_h^e u - u_h$ and the interpolation error $e_\pi = u - C_h^e u$. We can then observe that

$$\begin{aligned} \|u - u_h\|_{a_h,*} &\leq \|u - C_h^e u + C_h^e u - u_h\|_{a_h,*} \\ &\leq \|u - C_h^e u\|_{a_h,*} + \|C_h^e u - u_h\|_{a_h,*} \\ &\lesssim \|e_\pi\|_{a_h,*} + \|e_h\|_{A_h}. \end{aligned} \quad (4.54)$$

Using Lemma 4.4, is it clear that $\|e_\pi\|_{a_h,*} \lesssim h^{r-2} \|u\|_{r,\Omega}$ is already fulfilled, hence, it remains to estimate e_h . From Lemma 4.2 and 4.3, the weak Galerkin orthogonality and Assumption EP2 (4.51) is it natural to arrive at,

$$\begin{aligned} \|e_h\|_{A_h}^2 &\lesssim a_h(C_h^e u - u_h, e_h) + g_h(C_h^e u - u_h, e_h) \\ &= a_h(C_h^e u - u, e_h) + a_h(u - u_h, e_h) + g_h(C_h^e u - u_h, e_h) \\ &= a_h(C_h^e u - u, e_h) + g_h(C_h^e u, e_h). \end{aligned} \quad (4.55)$$

Hence, now utilizing the Assumption EP2 (4.51) is it clear that

$$\begin{aligned} a_h(C_h^e u - u, e_h) + g_h(C_h^e u, e_h) &\lesssim \|C_h^e u - u\|_{a_h,*} \|e_h\|_{a_h} + |C_h^e u|_{g_h} |e_h|_{g_h} \\ &\lesssim \|C_h^e u - u\|_{a_h,*} \|e_h\|_{a_h} + h^{r-2} \|u\|_{r,\Omega} |e_h|_{g_h} \\ &\lesssim (\|C_h^e u - u\|_{a_h,*} + h^{r-2} \|u\|_{r,\Omega}) \|e_h\|_{A_h} \\ &\lesssim h^{r-2} \|u\|_{r,\Omega} \|e_h\|_{A_h}. \end{aligned} \quad (4.56)$$

Here we noticed that $\|e_h\|_{a_h} + |e_h|_{g_h} \lesssim \|e_h\|_{A_h}$, and used that $\|C_h^e u - u\|_{a_h,*} \lesssim h^{r-2} \|u\|_{r,\Omega}$ from Lemma 4.4. Combining (4.55) and (4.56) and dividing by $\|e_h\|_{A_h}$ is it clear that

$$\|e_h\|_{A_h} \lesssim h^{r-2} \|u\|_{r,\Omega}. \quad (4.57)$$

Hence, inserting (4.57) into (4.54) we conclude the energy a priori estimate (4.52) holds.

Step 2. We want to show that $\|e\|_\Omega \lesssim h^{r-\max(0,3-k)} \|u\|_{r,\Omega}$. The idea is to apply the so-called Aubin-Nitsche duality trick while being aware of the ghost penalty g_h . Let us denote the following observation. Let $e := u - u_h \in L^2(\Omega)$ and $\psi \in H^4(\Omega)$. Then is the corresponding dual problem to (3.1) be

$$\begin{aligned} \Delta^2 \psi &= e && \text{in } \Omega, \\ \partial_n \psi &= 0 && \text{on } \Gamma, \\ \partial_n \Delta \psi &= 0 && \text{on } \Gamma. \end{aligned} \quad (4.58)$$

Here is the regularity of ψ and e a consequence of the assumptions of the regularity of u and u_h [2, pp. 113]. This implies that it exists a $\psi \in H^4(\Omega)$ such that $a_h(v, \psi) = (e, v)_\Omega \forall v \in V_h$. Hence, we can easily observe that from the Lemma 4.5, we have

$$\begin{aligned} \|e\|_\Omega^2 &= (e, e)_\Omega = (e, \Delta^2 \psi)_\Omega \\ &= a_h(e, \psi) = a_h(u - u_h, \psi) \\ &= a_h(u - u_h, \psi + C_h^e \psi - C_h^e \psi) \\ &= a_h(u - u_h, \psi - C_h^e \psi) + a_h(u - u_h, C_h^e \psi) \\ &= a_h(u - u_h, \psi - C_h^e \psi) + g_h(u_h, C_h^e \psi) \\ &= a_h(u - u_h, \psi - C_h^e \psi) + g_h(u_h - C_h^e u, C_h^e \psi) + g_h(C_h^e u, C_h^e \psi) \\ &= \text{I} + \text{II} + \text{III}. \end{aligned} \quad (4.59)$$

Let $\tilde{r} = \min(4, k+1)$. Additionally, we have the regularity estimate $\|\psi\|_{\tilde{r},\Omega} \lesssim \|e\|_\Omega$. Hence, by also utilizing the energy a priori estimate (4.52), we can observe

$$\begin{aligned} \text{I} &\lesssim \|u - u_h\|_{a_h,*} \|\psi - C_h^e \psi\|_{a_h,*} \\ &\lesssim h^{r-2} \|u\|_{r,\Omega} h^{\tilde{r}-2} \|\psi\|_{\tilde{r},\Omega} \\ &\lesssim h^{r-2} \|u\|_{r,\Omega} h^{\tilde{r}-2} \|e\|_\Omega. \end{aligned} \quad (4.60)$$

Specifically for the term II we apply Assumption EP2 (4.51) and the estimate (4.57)

$$\begin{aligned} \text{II} &\lesssim |u_h - C_h^e u|_{g_h} |C_h^e \psi|_{g_h} \\ &\lesssim \|u_h - C_h^e u\|_{A_h} |C_h^e \psi|_{g_h} \\ &\lesssim h^{r-2} \|u\|_{r,\Omega} h^{\tilde{r}-2} \|\psi\|_{\tilde{r},\Omega} \\ &\lesssim h^{r+\tilde{r}-4} \|u\|_{r,\Omega} \|e\|_\Omega. \end{aligned} \quad (4.61)$$

The third term is simply an application of Assumption EP2 (4.51), i.e.

$$\text{III} \lesssim |C_h^e u|_{g_h} |C_h^e \psi|_{g_h} \lesssim h^{r+\tilde{r}-4} \|u\|_{r,\Omega}. \quad (4.62)$$

Hence, combining (4.59), (4.60), (4.61), (4.62), and dividing by $\|e\|_\Omega$ on both sides can we conclude

$$\|e\|_\Omega \lesssim h^{r+\tilde{r}-4} \|u\|_{r,\Omega}. \quad (4.63)$$

Having a clear look at \tilde{r} , we see that

$$\tilde{r} = \min(4, k+1) = \begin{cases} 3, & k=2 \\ 4, & k \geq 3 \end{cases}. \quad (4.64)$$

So we have the following estimate,

$$\|e\|_\Omega \lesssim \|u\|_{r,\Omega} \begin{cases} h^{r-1}, & k=2 \\ h^{r-2}, & k \geq 3 \end{cases}, \quad (4.65)$$

or equivalently $\|e\|_\Omega \lesssim \|u\|_\Omega^{r-\max(0,k-3)}$.

□

4.5 Constructing ghost penalties

We have the following assumptions for the ghost penalty.

EP1 The ghost penalty $g_h(\cdot, \cdot)$ extends the H^2 norm such that

$$\|D^2v_h\|_{\mathcal{T}_h}^2 \lesssim \|D^2v_h\|_\Omega^2 + |v_h|_{g_h}^2 \quad \forall v_h \in V_h. \quad (4.66)$$

EP2 For $v \in H^s(\Omega)$ and $r = \min(s, k+2)$, the semi-norm $|\cdot|_{g_h}$ satisfies the following estimate,

$$|C_h^e v|_{g_h} \lesssim h^{r-2} \|v\|_{r,\Omega}. \quad (4.67)$$

This chapter aims to engineer a ghost penalty that fulfills these assumptions.

Let k be a positive integer. Recall the multi-index $\alpha = (\alpha_1, \dots, \alpha_d)$ of order $|\alpha| = \sum_i \alpha_i = k$ with a corresponding component-wise factorial $\alpha! = \alpha_1! \dots \alpha_d!$. Let $v \in C^k(\Omega)$. The generalization of the normal derivative is denoted as,

$$\partial_n^k v = \sum_{|\alpha|=k} \frac{\partial^\alpha v}{\alpha!} n^\alpha, \quad (4.68)$$

where the component-wise product of the normal vector is $n^\alpha = n_1^{\alpha_1} \dots n_d^{\alpha_d}$ and the derivative $\partial^\alpha v$ is as defined in Equation (2.1). Remark that $\partial_n^0 v = v$, $\partial_n^1 v = \nabla v$, $n = \partial_n v$ and $\partial_n^2 v = \frac{1}{2} n^T D^2 v$, $n = \frac{1}{2} \partial_{nn} v$.

The following result is the backbone of the face-based ghost penalty.

Lemma 4.7. *Let $T_1, T_2 \in \mathcal{T}_h$ be two elements sharing a common face F . Then for $v_h \in V_h$ with polynomial degree k we have*

$$\|v_h\|_{T_1} \lesssim \|v_h\|_{T_2} + \sum_{0 \leq j \leq k} h^{2j+1} ([[\partial_n^j v_h]], [[\partial_n^j v_h]])_F. \quad (4.69)$$

Proof. See [1, Lemma 2.19]. □

We will now introduce the so-called ghost penalty faces, that is,

$$\mathcal{F}_h^g = \{F \in \mathcal{F}_h : T^+ \cap \Gamma \neq \emptyset \vee T^- \cap \Gamma \neq \emptyset\}.$$

This set is simply all facets that belong to all elements of the active mesh \mathcal{T}_h intersected with Γ , i.e., all triangles to the cut cells \mathcal{T}_h^Γ . For an illustration, see Figure 15.

Lemma 4.8. *Let $T_1, T_2 \in \mathcal{T}_h$ be two elements sharing a common face F . Then for $v_h \in V_h$ with polynomial degree k we have*

$$\|\partial_{x_i} v\|_{T_1} \lesssim \|\partial_{x_i} v_h\|_{T_2} + \sum_{0 \leq j \leq k} h^{2j-1} ([[\partial_n^j \partial_{x_i} v_h]], [[\partial_n^j \partial_{x_i} v_h]])_F, \quad (4.70a)$$

$$\|\nabla v\|_{T_1} \lesssim \|\nabla v_h\|_{T_2} + \sum_{0 \leq j \leq k} h^{2j-1} ([[\partial_n^j \nabla v_h]], [[\partial_n^j \nabla v_h]])_F. \quad (4.70b)$$

Similarly, this is generalized to

$$\|\Delta v\|_{T_1} \lesssim \|\Delta v_h\|_{T_2} + \sum_{0 \leq j \leq k} h^{2j-3} ([[\partial_n^j \Delta v_h]], [[\partial_n^j \Delta v_h]])_F, \quad (4.71a)$$

$$\|D^2 v\|_{T_1} \lesssim \|D^2 v_h\|_{T_2} + \sum_{0 \leq j \leq k} h^{2j-3} ([[\partial_n^j D^2 v_h]], [[\partial_n^j D^2 v_h]])_F. \quad (4.71b)$$

Proof. **Estimate (4.70a).** Let $w_h = w_h|_F$ and recall the projection (3.9), then is

$$\begin{aligned} \llbracket \partial_{x_i} w_h \rrbracket &= \llbracket \nabla w_h \rrbracket \cdot e_{x_i} = (P_F \llbracket \nabla w_h \rrbracket + Q_F \llbracket \nabla w_h \rrbracket) e_{x_i} \\ &= (\llbracket \partial_n w_h \rrbracket n + \sum_{j=1}^{d-1} \llbracket \llbracket \partial_{t_j} w_h \rrbracket t_j \rrbracket) e_{x_i}. \end{aligned} \quad (4.72)$$

Here is $e_{x_i}, i = 1, \dots, d$ one of the elementary unit vectors in \mathbb{R}^d . Since $|e_{x_i} \cdot n| \leq 1$ and $|e_{x_i} \cdot t_j| \leq 1 \forall i, j$ is it clear that this estimate holds.

$$\begin{aligned} \|\llbracket \partial_{x_i} w_h \rrbracket\|_F^2 &\lesssim \|\llbracket \partial_n w_h \rrbracket\|_F^2 + \sum_{j=1}^{d-1} \|\llbracket \llbracket \partial_{t_j} w_h \rrbracket\|_F^2 \\ &\lesssim \|\llbracket \partial_n w_h \rrbracket\|_F^2 + h^{-2} \|\llbracket w_h \rrbracket\|_F^2. \end{aligned} \quad (4.73)$$

Here we used the local inverse inequality (2.35) applied on the facet F , i.e. $\|\partial_{t_j} v_h\|_F \lesssim h^{-1} \|v_h\|_F$. Inserting $w_h = \partial_n^j v_h$ we conclude

$$\begin{aligned} \|\llbracket \partial_{x_i} \partial_n^j v_h \rrbracket\|_F^2 &\lesssim \|\llbracket \partial_n \partial_n^j v_h \rrbracket\|_F^2 + h^{-2} \|\llbracket \partial_n^j v_h \rrbracket\|_F^2 \\ &\lesssim \|\llbracket \partial_n^{j+1} v_h \rrbracket\|_F^2 + h^{-2} \|\llbracket \partial_n^j v_h \rrbracket\|_F^2. \end{aligned} \quad (4.74)$$

Next, we see that the Lemma 4.7 implies

$$\|\partial_{x_i} v_h\|_{T_1}^2 \lesssim \|\partial_{x_i} v_h\|_{T_2}^2 + h^{2j+1} \sum_{j=0}^k \|\llbracket \partial_n^j \partial_{x_i} v_h \rrbracket\|_F^2. \quad (4.75)$$

Hence, by using (4.74) can we rewrite the sum such that

$$\begin{aligned} \sum_{j=0}^k \|\llbracket \partial_n^j \partial_{x_i} v_h \rrbracket\|_F^2 &\lesssim \sum_{j=0}^k \|\llbracket \partial_n^{j+1} v_h \rrbracket\|_F^2 + h^{-2} \|\llbracket \partial_n^j v_h \rrbracket\|_F^2 \\ &\lesssim \sum_{j=1}^{k-1} \|\llbracket \partial_n^j v_h \rrbracket\|_F^2 + \sum_{j=0}^k h^{-2} \|\llbracket \partial_n^j v_h \rrbracket\|_F^2 \\ &\lesssim \sum_{j=0}^k h^{-2} \|\llbracket \partial_n^j v_h \rrbracket\|_F^2. \end{aligned} \quad (4.76)$$

Thus, combining (4.75) and (4.76) we get

$$\|\partial_{x_i} v_h\|_{T_1}^2 \lesssim \|\partial_{x_i} v_h\|_{T_2}^2 + h^{2j-1} \sum_{j=0}^k \|\llbracket \partial_n^j v_h \rrbracket\|_F^2. \quad (4.77)$$

Hence, estimate (4.70a) holds.

Estimate (4.70b). Using that $\|\nabla v\|_T^2 = \sum_{i=1}^d \|\partial_{x_i} v\|_T^2$, can we directly apply the estimate (4.70a) element-wise.

$$\begin{aligned} \|\nabla v\|_{T_1}^2 &= \sum_{i=1}^d \|\partial_{x_i} v_h\|_{T_1}^2 \lesssim \sum_{i=1}^d \|\partial_{x_i} v_h\|_{T_2}^2 + h^{2j-1} \sum_{j=0}^k \|\llbracket \partial_n^j v_h \rrbracket\|_F^2 \\ &= \|\nabla v_h\|_{T_2}^2 + h^{2j-1} \sum_{j=0}^k \|\llbracket \partial_n^j v_h \rrbracket\|_F^2. \end{aligned} \quad (4.78)$$

Hence, estimate (4.70b) holds.

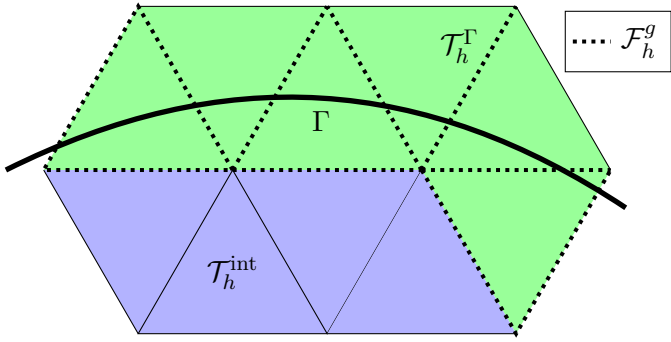


Figure 15: Illustration of \mathcal{F}_h^g denoted as the dotted lines. The set is defined as all facets which belong to cut cells \mathcal{T}_h^Γ sharing a node with interior elements $\mathcal{T}_h^{\text{int}}$.

Estimate (4.71a) and (4.71b). Following the same steps as in **Estimate (4.70a)**, but replacing Lemma 4.7 with estimate (4.70a), it is straight forward to conclude the following. For any $i_1, i_2 \in \{1, \dots, d\}$ we have,

$$\|\partial_{x_{i_1} x_{i_2}} v\|_{T_1} \lesssim \|\partial_{x_{i_1} x_{i_2}} v_h\|_{T_2} + \sum_{0 \leq j \leq k} h^{2j-3} (\llbracket \partial_n^j \partial_{x_{i_1} x_{i_2}} v_h \rrbracket, \llbracket \partial_n^j \partial_{x_{i_1} x_{i_2}} v_h \rrbracket)_F. \quad (4.79)$$

Finally, applying the element-wise argument, demonstrated in the proof for **Estimate (4.70b)**, for the Hessian and the Laplace operator, we conclude that (4.71a) and (4.71b) hold. \square

Now it remains to make this Lemma hold for the active mesh.

Lemma 4.9. *For $v_h \in V_h$ of polynomial degree k , the following estimates hold.*

$$\|v_h\|_{\mathcal{T}_h}^2 \lesssim \|v_h\|_\Omega^2 + \sum_{j=1}^k h^{2j+1} (\llbracket \partial_n^j v \rrbracket, \llbracket \partial_n^j v_h \rrbracket)_{\mathcal{F}_h^g}, \quad (4.80a)$$

$$\|D^2 v_h\|_{\mathcal{T}_h}^2 \lesssim \|D^2 v_h\|_\Omega^2 + \sum_{j=1}^k h^{2j-3} (\llbracket \partial_n^j v_h \rrbracket, \llbracket \partial_n^j v_h \rrbracket)_{\mathcal{F}_h^g}, \quad (4.80b)$$

$$\|\Delta v_h\|_{\mathcal{T}_h}^2 \lesssim \|\Delta v_h\|_\Omega^2 + \sum_{j=1}^k h^{2j-3} (\llbracket \partial_n^j v_h \rrbracket, \llbracket \partial_n^j v_h \rrbracket)_{\mathcal{F}_h^g}. \quad (4.80c)$$

Proof. **Estimate (4.80a).** This estimate is proven in [1, Lemma 2.20], but we will include it for completeness. First of all, notice that there is a patch $P(T)$ consisting of $\{T_i\}_{i=1}^l$ mesh elements such that each pair $\{T_i, T_{i+1}\}$ share a facet F_i and the last element T_l has a fat intersection.

Let us define the following norm

$$g_{F_i}^{L^2}(v_h, v_h) = \sum_{j=1}^k h^{2j+1} (\llbracket \partial_n^j v_h \rrbracket, \llbracket \partial_n^j v_h \rrbracket)_{F_i}. \quad (4.81)$$

where $F_i \in \mathcal{F}_h^g$ and polynomial degree k . Using Lemma 4.7 can we see that

$$\|v_h\|_{T_i} \lesssim \|v_h\|_{T_{i+1}}^2 + g_{F_i}^{L^2}(v, v). \quad (4.82)$$

By employing induction on each pair $\{T_i, T_{i+1}\}$ along with its corresponding F_i , we achieve the following outcome.

$$\|v_h\|_{T_1}^2 \leq C\|v_h\|_{T_2}^2 + g_{F_1}^{L^2}(v_h, v_h) \quad (4.83)$$

$$\leq C(C(\|v_h\|_{T_3}^2 + g_{F_2}^{L^2}(v_h, v_h)) + g_{F_1}^{L^2}(v_h, v_h)) \quad (4.84)$$

$$\lesssim \|v_h\|_{T_l}^2 + \sum_{i=1}^{l-1} g_{F_i}^{L^2}(v_h, v_h) \quad (4.85)$$

$$\lesssim \|v_h\|_{T_l \cap \Omega}^2 + \sum_{i=1}^{l-1} g_{F_i}^{L^2}(v_h, v_h). \quad (4.86)$$

Here the last steps arise from the fact that $\|v_h\|_{T_l} \lesssim \|v_h\|_{T_l \cap \Omega}$, which is a consequence of the fat intersection property. Summation over the cut elements \mathcal{T}_h^Γ implies,

$$\|v_h\|_{\mathcal{T}_h^\Gamma}^2 \lesssim \|v_h\|_{\mathcal{T}_h^\Gamma \cap \Omega}^2 + \sum_{i=1}^{l-1} g_{F_i}^{L^2}(v_h, v_h) \quad (4.87)$$

$$= \|v_h\|_{\mathcal{T}_h^\Gamma \cap \Omega}^2 + \sum_{j=0}^k h^{2j+1}(\llbracket \partial_n^j v_h \rrbracket, \llbracket \partial_n^j v_h \rrbracket)_{\mathcal{F}_h^g}. \quad (4.88)$$

And as a trivial extension, this now also holds for the active mesh \mathcal{T}_h , that is,

$$\|v_h\|_{\mathcal{T}_h}^2 \lesssim \|v_h\|_{\mathcal{T}_h \cap \Omega}^2 + \sum_{j=1}^k h^{2j+1}(\llbracket \partial_n^j v_h \rrbracket, \llbracket \partial_n^j v_h \rrbracket)_{\mathcal{F}_h^g}. \quad (4.89)$$

Hence, (4.80a) holds and the first part of the proof is complete.

Estimate (4.80b) and (4.80b). We simply use the exact same procedure as **Estimate (4.80a)** for the estimates with (4.71a) and (4.71b). Hence by defining the bilinear form $g_h(\cdot, \cdot)$ similarly. The proof is complete. \square

Finally, we now have the tools to construct a candidate for the ghost penalty that satisfies all assumptions.

Proposition 4.10 (Face-based ghost penalty). *Let $k \geq 2$ be the order of the polynomial basis in V_h . For any set of positive parameters $\{\gamma_j\}_{j=0}^k$, the ghost penalty defined as*

$$g_h(v_h, w_h) := \sum_{j=1}^k \sum_{F \in \mathcal{F}_h^g} \gamma_j h_F^{2j-3} (\llbracket \partial_n^j v_h \rrbracket, \llbracket \partial_n^j w_h \rrbracket)_F \text{ for any } v_h, w_h \in V_h, \quad (4.90)$$

satisfies the Assumption **EP1** and **EP2**.

Proof. From Lemma 4.9 is it clear that $\|D^2 v_h\|_{\mathcal{T}_h} \lesssim \|D^2 v_h\|_\Omega + |v_h|_{g_h}$, hence, Assumption **EP1** holds. Therefore, we only need to verify Assumption **EP2**, which states that $|C_h^e v|_{g_h} \lesssim h^{r-2} \|v\|_{r, \Omega}$. Let $v \in H^s(\Omega)$, $s \geq 3$, and $r = \min\{s, k+1\}$. We can see that from the definition is

$$\begin{aligned} |C_h^e v|_{g_h}^2 &= \sum_{j=0}^k \gamma_j h^{2j-3} \| \llbracket \partial_n^j C_h^e v \rrbracket \|_{\mathcal{F}_h^g}^2 \\ &= \sum_{j=0}^{r-1} \gamma_j h^{2j-3} \| \llbracket \partial_n^j (C_h^e v - v^e) \rrbracket \|_{\mathcal{F}_h^g}^2 + \sum_{j=r}^k \gamma_j h^{2j-3} \| \llbracket \partial_n^j C_h^e v \rrbracket \|_{\mathcal{F}_h^g}^2 = \text{I} + \text{II}. \end{aligned} \quad (4.91)$$

Here we added a zero term $v^e \in H^s(\Omega_h)$ since jump vanishes for the first $r-1$ terms, i.e. $\llbracket \partial_n^j v^e \rrbracket = 0 \forall j \leq r-1$. The given expression suggests that the first term can be readily estimated by utilizing the a priori estimate provided in equation (4.43).

$$\begin{aligned}
I &\lesssim \sum_{j=0}^{r-1} h^{2j-3} \| [\partial_n^j (C_h^e v - v^e)] \|_{\mathcal{F}_h^g}^2 \lesssim \sum_{j=0}^{r-1} h^{2j-3} \| D^j (C_h^e v - v^e) \|_{\partial \mathcal{T}_h}^2 \\
&\lesssim \sum_{j=0}^{r-1} h^{2j-3} h^{2r-2j-1} \| v \|_{r,\Omega}^2 \lesssim h^{2(r-2)} \| v \|_{r,\Omega}^2.
\end{aligned} \tag{4.92}$$

For the second term we are allowed to use the basic discrete inverse estimate (2.39) times since we work on the Clément operator,

$$\begin{aligned}
II &\lesssim \sum_{j=r}^k h^{2j-3} \| \partial_n^j C_h^e v \|_{\partial \mathcal{T}_h}^2 \lesssim \sum_{j=r}^k h^{2j-3} h^{2(r-j-\frac{1}{2})} \| D^r (C_h^e v) \|_{\Omega}^2 \\
&\lesssim h^{2(r-2)} \| C_h^e v \|_{r,\Omega}^2.
\end{aligned} \tag{4.93}$$

Hence, the estimate $|C_h^e v|_{g_h}^2 \lesssim h^{2(r-2)} \| v \|_{r,\Omega}^2$ holds. \square

4.6 Numerical experiments

We will investigate several numerical experiments for the Laplace and Hessian formulation to validate the proposed cut finite element methods for the biharmonic problem. We will provide numerical validation for the theoretical optimal a priori estimates presented in Theorem 4.6. We also demonstrate the effect ghost penalty of stabilization by translating the domain to trigger badly cut cells. Finally, we provide numerical validation of the expected convergence for the Cahn–Hilliard problem. We propose the following penalty parameters $\gamma = 20$ for the Hessian formulation (3.16) and the Laplace formulation (3.24), and $\gamma_1, \gamma_2 = 10, 0.5$ for the corresponding ghost penalty (4.90).

Condition numbers are essential to solve linear systems because they help us assess the accuracy and stability of the system's solutions. A large condition number indicates that the system is ill-conditioned, meaning the solution can be highly sensitive to small changes in the input data, potentially leading to inaccurate results. This underlines the importance of checking the conditional stability of cut cells, hence, motivating a so-called translation test with and without ghost penalty.

All numerical experiments are conducted using the open-source finite element method framework Gridap [99].

4.6.1 Numerical setup

For the convergence study, we will consider a square background domain $\tilde{\Omega}$ with side lengths L and a physical domain $\Omega \subset \tilde{\Omega}$ on the form $\Omega = \{(x, y) \mid \phi(x, y) \leq 0\}$, where $\phi : \mathbb{R}^2 \rightarrow \mathbb{R}$ is a given level set function. We will consider two cases; a circular domain,

$$\phi(x, y) = x^2 + y^2 - 1. \tag{4.94}$$

and a flower domain,

$$\phi(x, y) = \sqrt{x^2 + y^2} - r_0 - r_1 \cos(\text{atan2}(y, x)) \text{ where } r_0 = 0.3L \text{ and } r_1 = 0.1L. \tag{4.95}$$

For an illustration of the flower domain, see Figure 16.

We want to test spatial convergence for the method by doing numerous mesh refinements. Let $\tilde{\mathcal{T}}_h^j$ be the associated regular square mesh of the background domain $\tilde{\Omega}$ with the mesh size $h^j = L/2^{3+j}$ for the side length $L = 2.7$ and refinements $j = 1, \dots, 8$. This is illustrated in Figure 17 for the circular domain.

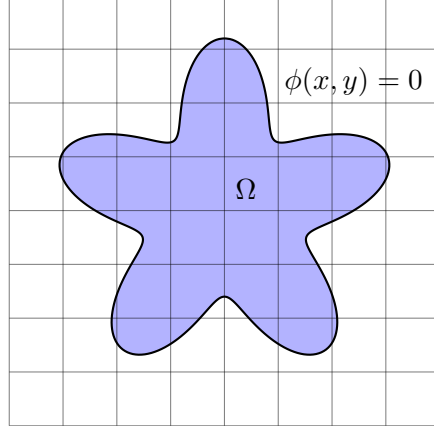


Figure 16: Illustration of the flower domain associated with the level set function (4.95).

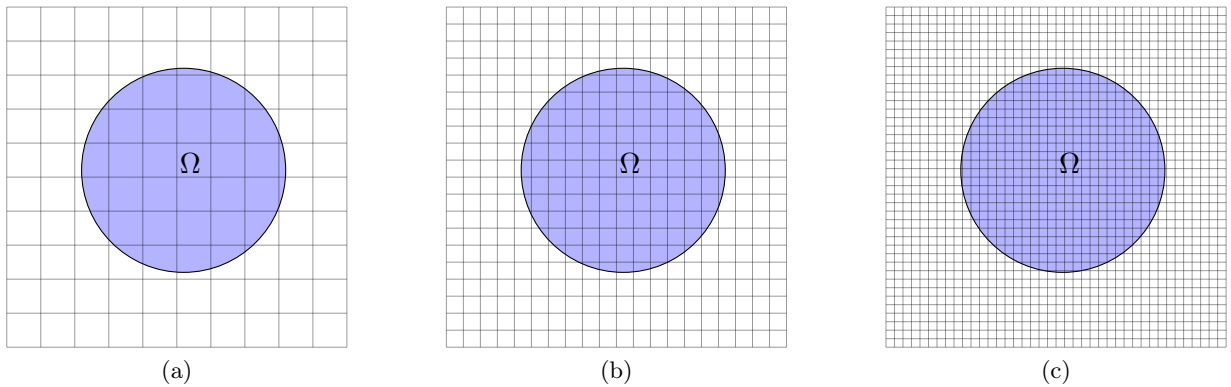


Figure 17: Illustration of the domain Ω defined as a circle with radius R . The regular square background mesh $\tilde{\mathcal{T}}_h^j$ with side lengths L with three refinements of the mesh size h^j .

On each mesh $\tilde{\mathcal{T}}_h^k$ we compute a numerical solution u_h^k , hence, motivating us to define the convergence rate. Let u be the exact solution, then do we define the so-called Experimental Order of Convergence (EOC) as

$$EOC(j) = \frac{\log\left(\frac{e^{j-1}}{e^j}\right)}{\log\left(\frac{h^{j-1}}{h^j}\right)}, \quad j = 2, \dots, 8. \quad (4.96)$$

Here we define the error $e^j = \|u - u_h^j\|$, where we choose to measure in the norms $\|\cdot\|_{L^2(\Omega)}$, $\|\cdot\|_{H^1(\Omega)}$ and $\|\cdot\|_{a_{h,*}}$. Recall the definition of the condition number $\kappa_\infty(A)$ from (2.30), where A is the system matrix defined in (2.27). We define A^j to the associated system matrix to the corresponding discrete solution u_h^j . Hence, when computing EOC specifically for the condition number we define,

$$EOC(j) = \frac{\log\left(\frac{\kappa_\infty(A^{j-1})}{\kappa_\infty(A^j)}\right)}{\log\left(\frac{h^{j-1}}{h^j}\right)}, \quad j = 2, \dots, 8. \quad (4.97)$$

4.6.2 Validation of the a priori estimates

Our goal it validate the a priori estimates presented in Theorem 4.6 for $k = 2$. The big-oh $O(h^r)$ is defined to be to be a upper bound such that it exists an $C > 0$ such that $\|e\| \leq C h^r$ for all h , where r is the order of convergence. Since we only will implement $k = 2$, we validate that it exists an upper bound $O(h)$ for $\|e\|_{L^2(\Omega)}$ and $O(h^2)$ for $\|e\|_{a_{h,*}}$. It has also been shown that for condition

number $\kappa_\infty(A)$ increases with the order of $O(h^{-4})$ [100], hence, we expect this also to hold for the methods we propose. We did the following convergence tests.

- **Convergence on circle domain** First, we consider the manufactured solution such that,

$$u(x, y) = (x^2 + y^2 - 1) \sin(2\pi x) \cos(2\pi y). \quad (4.98)$$

The result can be shown in Figure 18 and Table 1. Here we observe that for we clearly get optimal convergence, that is, we get a consistent EOC 1 and 2 for the respective norms $\|e\|_{a_h,*}$ and $\|e\|_{L^2(\Omega)}$. We also get a consistent EOC of 2 for $\|e\|_{H^1(\Omega)}$, even though we do not have theoretical a priori estimates of this norm. Since we expect the condition number $\kappa_\infty(A)$ to have a convergence rate of -4 , we observe a drop in the convergence rate of the discrete solution. This drop occurs for small values of $h \leq \frac{L}{512}$ because the condition number affects the convergence rate.

- **Convergence on flower domain** We consider the manufactured solution such that

$$u(x, y) = \sin(2\pi x) \cos(2\pi y). \quad (4.99)$$

In this case, we must assume non-homogeneous Neumann conditions, and thus we only test the numerical results for the Laplace formulation. The result can be shown in Figure 19 and Table 2. Here we observe that we get optimal convergence that is EOC of order 1 and 2 for $\|e\|_{a_h,*}$ and $\|e\|_{L^2(\Omega)}$ norm. Again, we see that the condition number $\kappa_\infty(A)$ has a EOC of order -4 and, thus, for small $h \leq \frac{L}{512}$ we see a drop in convergence rate for the $\|e_h\|_{L^2}$ norm.

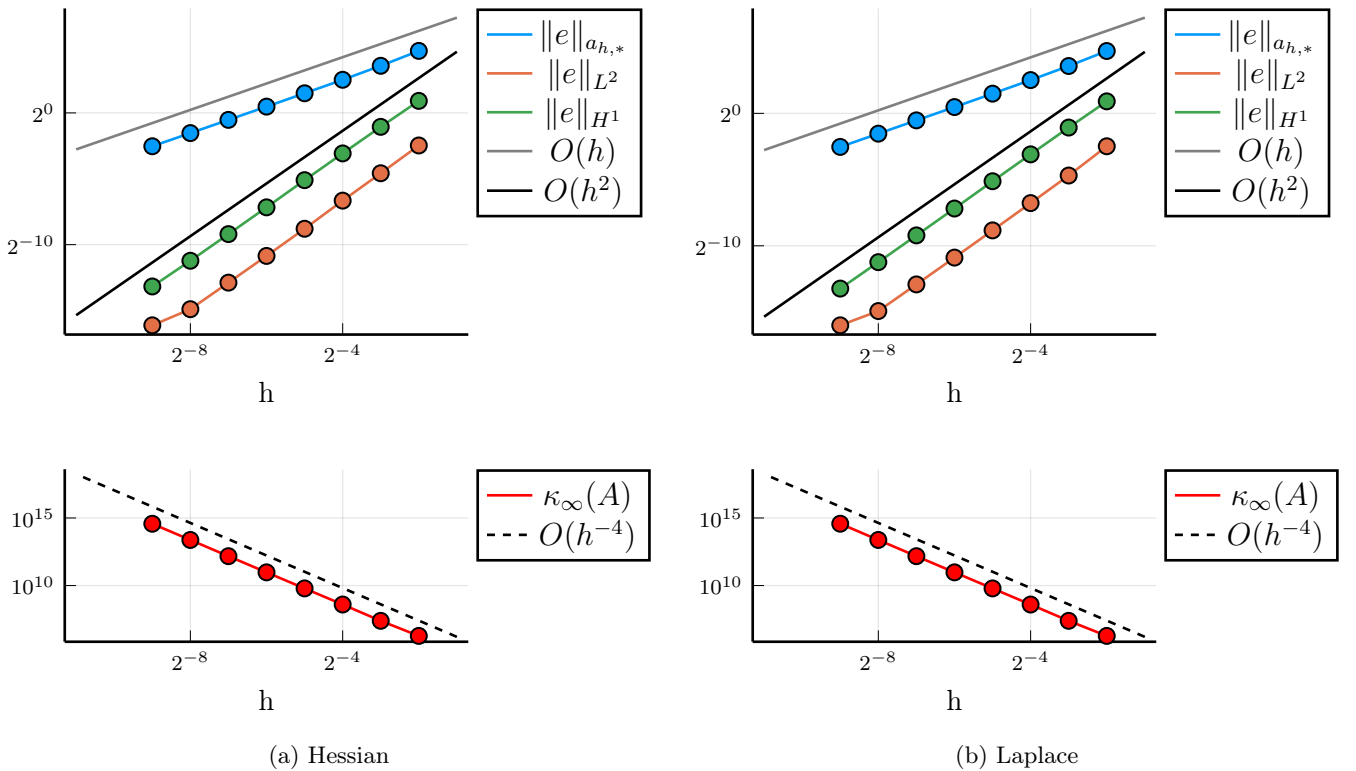


Figure 18: Convergence plots for the Hessian and the Laplacian method applied to the circular domain with side length $L = 2.7$, using parameters $\gamma = 20$, $\gamma_1 = 10$ and $\gamma_2 = 0.5$.

h/L	n	$\ e\ _{L^2}$	EOC	$\ e\ _{H^1}$	EOC	$\ e\ _{a_h,*}$	EOC	$\kappa_\infty(A)$	EOC	ndofs
1/8	8	1.8E-01	NaN	1.9E+00	NaN	2.6E+01	NaN	1.9E+06	NaN	1.7E+02
1/16	16	4.2E-02	2.11	4.8E-01	1.97	1.2E+01	1.13	2.5E+07	-3.70	5.8E+02
1/32	32	9.9E-03	2.08	1.2E-01	2.02	5.7E+00	1.06	4.0E+08	-4.01	2.0E+03
1/64	64	2.3E-03	2.13	2.9E-02	2.03	2.8E+00	1.02	6.1E+09	-3.96	7.6E+03
1/128	128	5.4E-04	2.06	6.9E-03	2.06	1.4E+00	1.01	9.5E+10	-3.95	2.9E+04
1/256	256	1.3E-04	2.03	1.7E-03	2.03	6.9E-01	1.01	1.5E+12	-3.97	1.2E+05
1/512	512	3.3E-05	2.02	4.2E-04	2.02	3.5E-01	1.00	2.4E+13	-3.99	4.6E+05
1/1024	1024	1.4E-05	1.22	1.1E-04	1.95	1.7E-01	1.00	3.7E+14	-3.98	1.8E+06

(a) Hessian

h/L	n	$\ e\ _{L^2}$	EOC	$\ e\ _{H^1}$	EOC	$\ e\ _{a_h,*}$	EOC	$\kappa_\infty(A)$	EOC	ndofs
1/8	8	1.8E-01	NaN	1.9E+00	NaN	2.6E+01	NaN	1.9E+06	NaN	1.7E+02
1/16	16	3.9E-02	2.21	4.8E-01	1.98	1.2E+01	1.13	2.5E+07	-3.70	5.8E+02
1/32	32	9.1E-03	2.08	1.2E-01	2.02	5.7E+00	1.06	3.9E+08	-4.00	2.0E+03
1/64	64	2.2E-03	2.06	2.9E-02	2.03	2.8E+00	1.02	6.1E+09	-3.96	7.6E+03
1/128	128	5.3E-04	2.05	6.9E-03	2.06	1.4E+00	1.01	9.5E+10	-3.95	2.9E+04
1/256	256	1.3E-04	2.03	1.7E-03	2.03	6.9E-01	1.01	1.5E+12	-3.97	1.2E+05
1/512	512	3.2E-05	2.01	4.1E-04	2.02	3.5E-01	1.00	2.4E+13	-3.99	4.6E+05
1/1024	1024	1.5E-05	1.08	1.0E-04	2.00	1.7E-01	1.00	3.8E+14	-3.99	1.8E+06

(b) Laplace

Table 1: EOC results for the Hessian and the Laplacian method applied to the circular domain with side length $L = 2.7$, using parameters $\gamma = 20$, $\gamma_1 = 10$ and $\gamma_2 = 0.5$.

h/L	n	$\ e\ _{L^2}$	EOC	$\ e\ _{H^1}$	EOC	$\ e\ _{a_h,*}$	EOC	$\kappa_\infty(A)$	EOC	ndofs
1/8	8	7.5E-01	NaN	3.9E+00	NaN	3.9E+01	NaN	3.4E+06	NaN	1.8E+02
1/16	16	1.9E-01	2.00	1.0E+00	1.90	1.8E+01	1.14	3.5E+07	-3.37	4.8E+02
1/32	32	4.5E-02	2.06	2.3E-01	2.16	7.4E+00	1.27	4.6E+08	-3.72	1.6E+03
1/64	64	1.1E-02	1.98	5.0E-02	2.22	3.4E+00	1.14	6.6E+09	-3.84	5.6E+03
1/128	128	2.1E-03	2.43	1.0E-02	2.29	1.6E+00	1.05	9.8E+10	-3.90	2.1E+04
1/256	256	4.8E-04	2.14	2.2E-03	2.19	8.0E-01	1.02	1.5E+12	-3.95	8.1E+04
1/512	512	1.5E-04	1.66	5.6E-04	2.00	4.0E-01	1.01	2.4E+13	-3.97	3.2E+05
1/1024	1024	5.2E-05	1.53	1.6E-04	1.81	2.0E-01	1.01	3.8E+14	-3.99	1.3E+06

Table 2: Convergence rates for the Laplacian-based method applied to the Flower domain with side length $L = 2.7$, using parameters $\gamma = 20$, $\gamma_1 = 10$, and $\gamma_2 = 0.5$

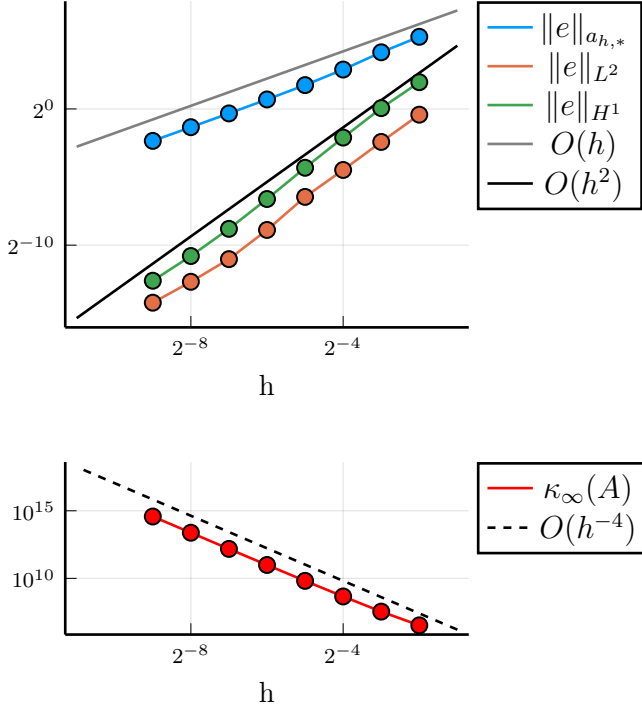


Figure 19: Convergence rates for the Laplacian-based method applied to the Flower domain with side length $L = 2.7$, using parameters $\gamma = 20$, $\gamma_1 = 10$, and $\gamma_2 = 0.5$

4.6.3 Translation test

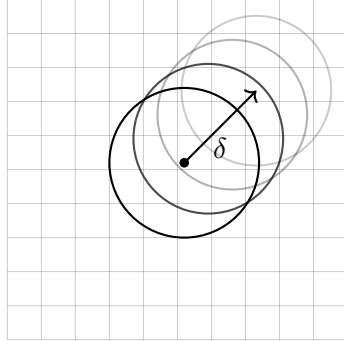


Figure 20: Illustration of several iterations of the translation test with translation distance δ from $(0, 2\sqrt{2}h)$. Remark that the circle is fixed in the origin, and the background mesh is translated diagonally.

In order to evaluate the robustness of the technique during adverse cut configurations (refer to Figure 14), we will incorporate what is known as a translation test. The fundamental concept involves conducting precise, iterative diagonal translations of the background mesh while keeping the domain fixed in origin, thereby intentionally inducing challenging cut cell scenarios. We denote the total length of the translation as δ . For this report, will we choose to do the test on the circle domain and translate a distance $\delta = 2\sqrt{2}h$ diagonally for 500 iterations for a background mesh $h = \frac{L}{n}$ where $n = 16$ using the manufactured solution (4.98). For a sketch of the experiment, see Figure 20.

In this context, due to the symmetry of the domain and background mesh, we expect a periodic pattern of bad cut configurations being triggered. This allows us to assess the impact of stabilization with and without the ghost penalty term. As illustrated in the numerical experiments provided

in Figure 21, the ghost penalty demonstrated significant enhancements regarding the stability of the system for both the Laplace and Hessian formulation. It is apparent that the error may not only magnify, but potentially exceed an order of magnitude if the ghost penalty is not considered. Hence, this demonstrates that the method is robust in handling bad cut configurations for both the Laplace and Hessian formulations.

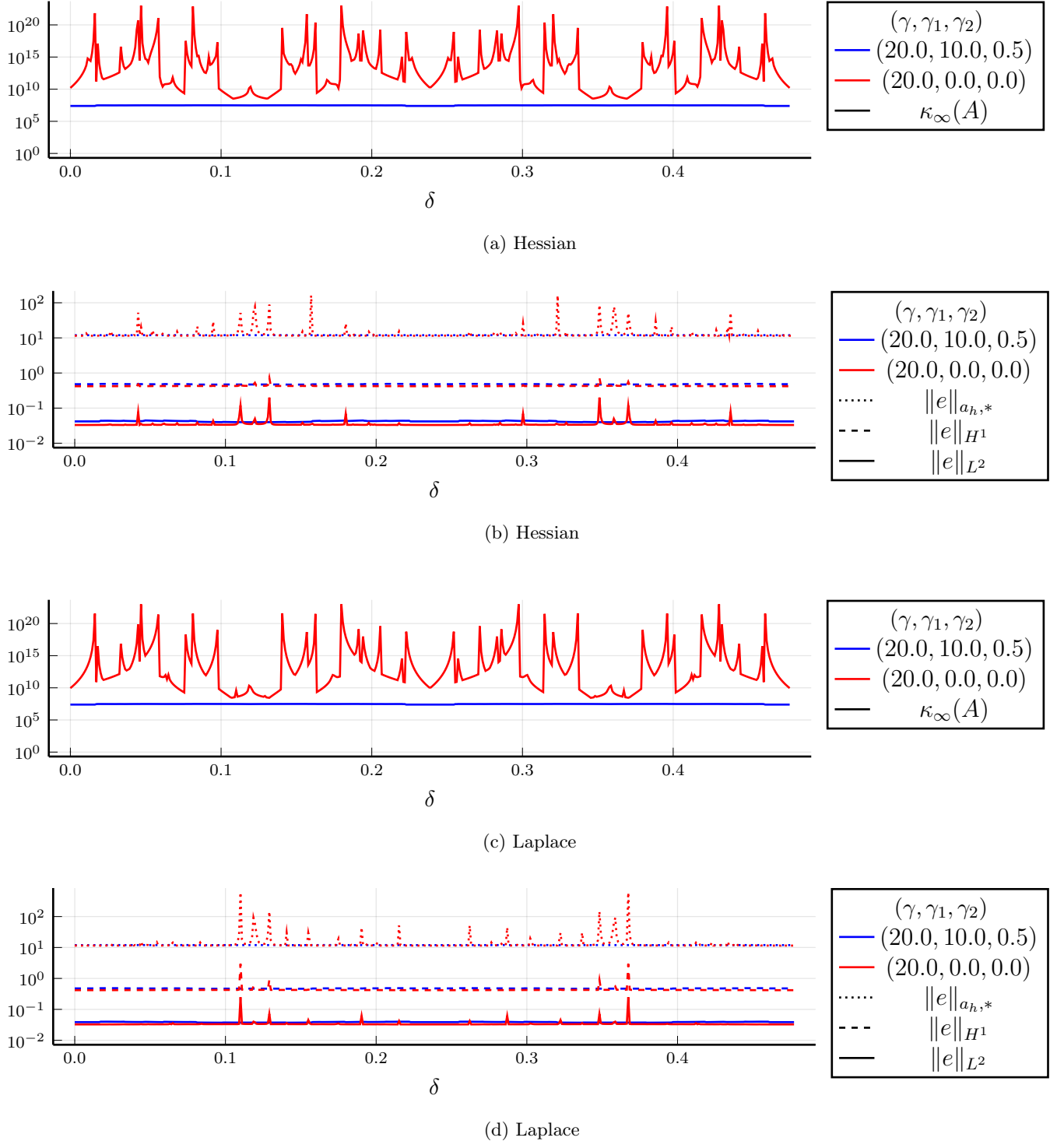


Figure 21: Translation results of the Laplace and Hessian formulations for $n=16$ and 500 iterations, with $\delta = (0, 2\sqrt{2}h)$ for $L=2.7$, inside a circle with radius $R=1$.

5 Applications to the Cahn-Hilliard equation

In this section, we will demonstrate that the proposed cut finite element method can be used to solve the Cahn-Hilliard problem. Firstly, we will recall the strong form and illustrate how it can be recast into a weak form following the approach in [3]. Subsequently, we will derive a simplistic numerical time iteration scheme to demonstrate that the solution to the problem can indeed be found. Again, all numerical experiments are conducted using the open-source finite element method (FEM) framework, Gridap, as documented in [99].

5.1 Deriving the discrete formulation of the Cahn-Hilliard equation

Recall the strong formulation of the Cahn-Hilliard equation. Let $u(x, 0) = u_0$ then is the dynamics on the form,

$$\partial_t u + \Delta (\varepsilon^2 \Delta u - f(u)) = 0 \quad \text{in } \Omega, \quad (5.1a)$$

$$\partial_n u = 0 \quad \text{on } \Gamma, \quad (5.1b)$$

$$\partial_n \Delta u = 0 \quad \text{on } \Gamma. \quad (5.1c)$$

Here we define $f(u) = u(u^2 - 1) = F'(u)$ where $F(u) = (1/4)(u^2 - 1)^2$. With the corresponding energy. We define the small parameter to be $\varepsilon = 1/100$.

$$E(u) = \int_{\Omega} \frac{\varepsilon^2}{2} |\nabla u|^2 + F(u) dx. \quad (5.2)$$

We also recall that the energy functional monotonically decreasing and that the global mass concentration is conserved, i.e.

$$\frac{d}{dt} E(u) < 0 \text{ and } \frac{d}{dt} \int_{\Omega} u dx = 0. \quad (5.3)$$

For convenience, we decompose the functional so that $E(u) = E_1(u) + E_2(u)$. Here, $E_1(u) = \int_{\Omega} \frac{\varepsilon^2}{2} |\nabla u|^2, dx$ represents the smoothing contribution, while $E_2(u) = \int_{\Omega} F(u), dx$ represents the separation contribution.

Now assume that $u \in L^2([0, T], H^4(\Omega))$ and $v_h \in V_h$ of order k . It is clear that the initial weak formulation is,

$$(\partial_t u, v_h)_{\Omega} + \varepsilon^2 (\Delta^2 u, v_h)_{\Omega} - (f(u), v_h)_{\Omega} = 0. \quad (5.4)$$

Given the appearance of the biharmonic equation, we can now utilize the cut finite element framework that was developed in Section 4. We define the discrete weak problem as follows.

$$\begin{aligned} \text{Find } u_h \in L^2([0, T], V_h) \text{ such that } \forall v_h \in V_h \\ (\partial_t u_h, v_h)_{\Omega} + \varepsilon^2 A_h(u_h, v_h) + c_h(u_h, v_h) = 0. \end{aligned} \quad (5.5)$$

Here we have followed the nonlinear weak formulation [3, Equation 4.2] and the cut finite element bilinear form for the biharmonic equation proposed in Equation (4.3) such that

$$c_h(u_h, v_h) = (f(u_h), \Delta v_h)_{\Omega} + (f(u_h), \partial_n v)_{\mathcal{F}_h}, \quad (5.6)$$

$$A_h(u_h, v_h) = a_h(u_h, v_h) + g_h(u_h, v_h). \quad (5.7)$$

The primary aim is to demonstrate that this problem can be solved using a simple time-integration scheme. Define the index $m = 0, 1, \dots, M$. This index corresponds to uniformly distributed time points t_m , which are subject to the boundary conditions $t_0 = 0$ and $t_M = M\tau$. Here, we denote the time step as $\tau = \varepsilon^2$. Each time step u_h^m is an element of the discrete space V_h

, i.e. $u_h^m \in V_h$ with the initial condition defined as $u^0 = u(t_0, x)$. Following this, we establish the forward difference operator, which is determined by the time step τ .

$$\bar{\partial}_t u_h^m = \frac{u_h^m - u_h^{m-1}}{\tau}. \quad (5.8)$$

We define the implicit explicit time step scheme (IMEX) scheme to have the following discretization,

$$(\bar{\partial}_t u_h^m, v_h)_\Omega + \varepsilon^2 A_h(u_h^m, v) + c_h(u_h^{m-1}, v_h) = 0, \quad \forall v_h, u_h^m \in V_h. \quad (5.9)$$

which equivalently can be rewritten as

$$(u_h^m, v)_\Omega + \tau \varepsilon^2 A_h(u_h^m, v) = (u_h^{m-1}, v)_\Omega - \tau c_h(u_h^{m-1}, v). \quad (5.10)$$

Hence, we have a complete space-time scheme.

5.2 Demonstration on the Cahn-Hilliard problem

We have no analytical solution for the strong form of the Cahn-Hilliard (5.1), hence, we cannot construct a manufactured solution. However, a way to check that the system does behave like expected based on the physical properties (5.2). In other words, we can check that our discrete solution satisfies the following conditions. We define the discrete values $E^m = E(u_h^m)$, $E_1^m = E_1(u_h^m)$ and $E_2^m = E_2(u_h^m)$ and the initial function $u_0 = u(x, 0)$. From the physical properties (5.2), we expect the discrete equivalent to hold, i.e.

$$E^m \leq E^{m-1} \text{ and } \int_{\Omega} u_h^m dx \approx \int_{\Omega} u_0 dx. \quad (5.11)$$

To test this, we check that $\delta E^m \geq 0$ generally holds, where

$$\delta E^m = E(u_h^{m-1}) - E(u_h^m). \quad (5.12)$$

Similarly, let us define the relative cumulative global mass error and local mass error.

$$\Delta u_h^m = \frac{|\int_{\Omega} (u_h^m - u_0) dx|}{|\int_{\Omega} u_0 dx|} \quad \text{and} \quad \delta u_h^m = \frac{|\int_{\Omega} (u_h^m - u_h^{m-1}) dx|}{|\int_{\Omega} u_0 dx|}. \quad (5.13)$$

To test mass conservation, we expect the error Δu_h^m and δu_h^m to be close to zero.

In our experiments, we defined the initial function $u_0(x)$ as the uniform samples from the interval $[-1, 1]$ for each node. That is, for each node a_i , $u_0(a_i)$ is a sample from the uniform distribution on the interval $[-1, 1]$. This applies for all $i = 1, \dots, N$, where N is the total number of degrees of freedom in our system. The node a_i is associated with the nodal basis for all N degrees of freedom, as discussed for the discrete system (2.26). We again used a square background mesh with length $L = 2.7$ and mesh size $h = \frac{L}{n}$ for $n = 2^7$. For an illustration of the active set \mathcal{T}_h (defined in Section 4.1), see Figure 25.

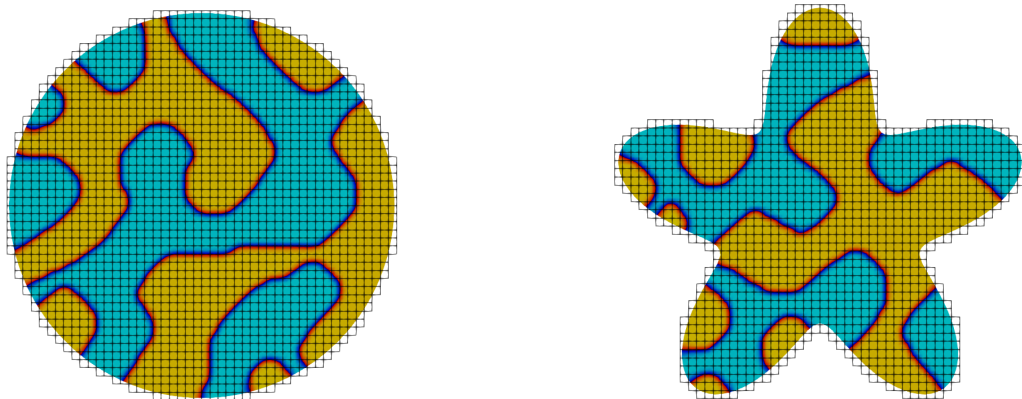


Figure 25: Illustration of the active mesh \mathcal{T}_h .

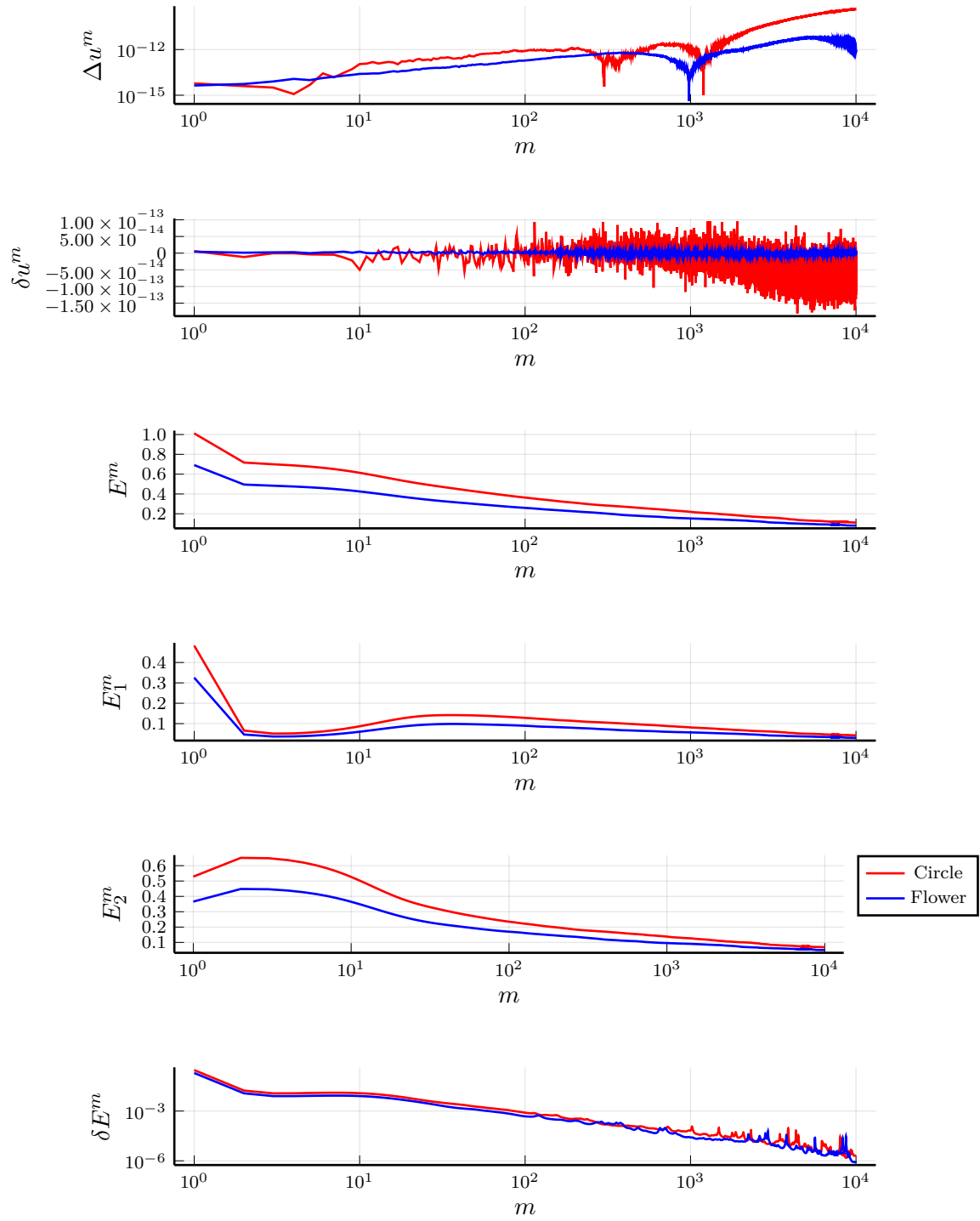


Figure 22: Consider time as $t^m = m\tau$ where $m = 0, \dots, M$, with $M = 10^4$ and timestep τ . The figure describes the evolution of the relative global mass error Δu^m and the local mass difference δu^m . It also demonstrates the total discrete energies E^m, E_1^m, E_2^m , along with the corresponding local energy difference δE^m . Simulations are conducted on both the circular and the flower domains.

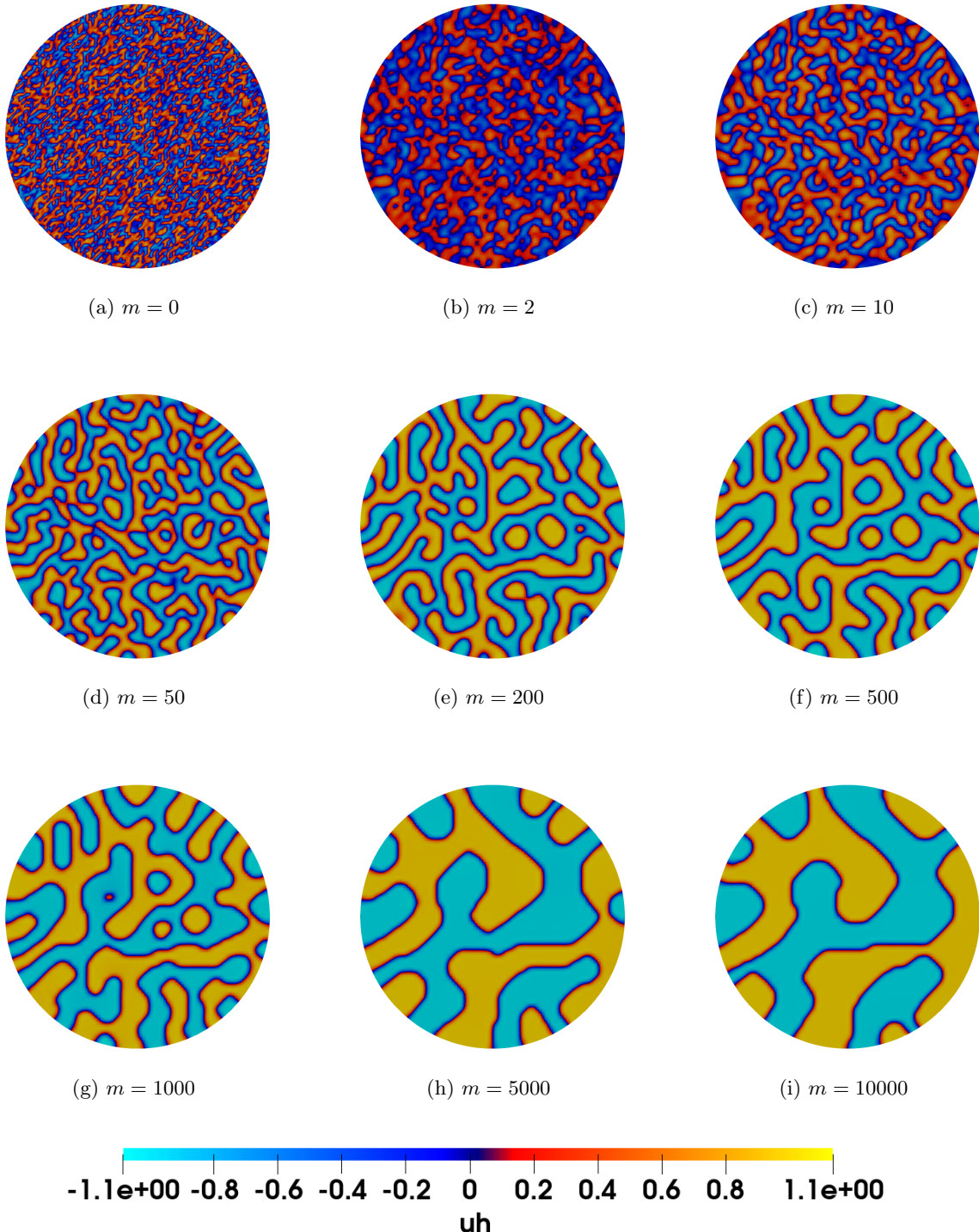


Figure 23: Illustration of a simulation of the Cahn-Hilliard equation on the circular domain for time $t_m = m\tau$, where τ is the timestep and $m = 0, \dots, M$, with $M = 10^4$.

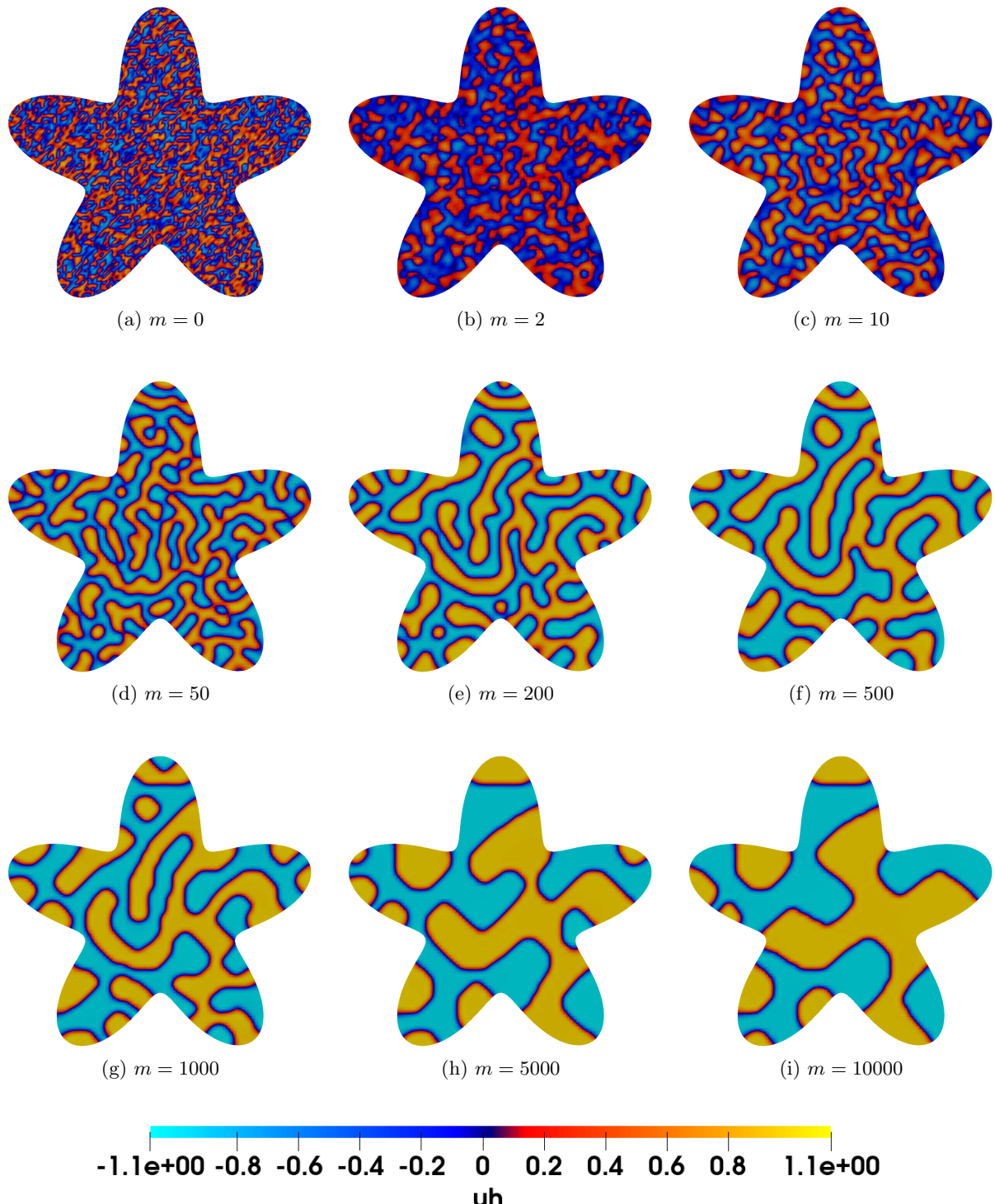


Figure 24: Illustration of a simulation of the Cahn-Hilliard equation on the flower domain for time $t_m = m\tau$, where τ is the timestep and $m = 0, \dots, M$, with $M = 10^4$.

We ran the simulation on the flower domain (4.95) and the circular domain (4.94), illustrated in Figure 24 and 23. The corresponding plots of the mass conservation and energy decrease are presented in the Figure 22, and confirm the expected physical properties of the Cahn-Hilliard equation. The global relative error Δu_h^m and δu_h^m demonstrating that the mass is conserved. We also observe that the energy functional $E(u_h)$ monotonically decreases over time and that $\delta E^m > 0$, signifying the systems tendency to seek a state of minimal energy. Take note that $E^m 1$ and $E^m 2$ are interconnected in such a way that if the value of one increases, the other will correspondingly decrease to maintain balance, and vice versa.

5.3 Note on the manufactured solution

While the report is not consisting of a numerical convergence analysis of the Cahn-Hilliard problem, we still present a framework for manufactured solutions for non-homogeneous boundary conditions. Let $u(x, 0) = u_0$ then is Cahn-Hilliard with non-homogeneous boundary conditions as follows,

$$\partial_t u + \Delta (\varepsilon^2 \Delta u - f(u)) = g_0(x) \quad \text{in } \Omega, \quad (5.14a)$$

$$\partial_n u = g_1(x) \quad \text{on } \Gamma, \quad (5.14b)$$

$$\partial_n \Delta u = g_2(x) \quad \text{on } \Gamma, \quad (5.14c)$$

where we defined $f(u) = F'(u) = u(u^2 - 1)$ for $F(u) = \frac{1}{4}(u^2 - 1)^2$ and the domain $\Omega \subset \mathbb{R}^d$ for $d = 2, 3$. In contrast to the standard version presented in the introduction (1.7), this version is generalized to also holds for functions $g_0, g_1, g_2 : \Omega \rightarrow \mathbb{R}$. While the standard version may be physical correct, this version creates flexibility so we can easily construct manufactured solutions on complex domains.

Designing a manufactured solution using $g_0(\cdot)$ may be tempting with the formulation (5.14a). However, observe that by expanding the Laplacian, we get

$$\begin{aligned} \Delta (\varepsilon^2 \Delta u - f(u)) &= \varepsilon^2 \Delta^2 u - \Delta f(u) \\ &= \varepsilon^2 \Delta^2 u - 3(2u\|\nabla u\|_2^2 + u^2 \Delta u). \end{aligned} \quad (5.15)$$

Here we applied the chain rule twice and inserted the derivatives.

$$\begin{aligned} \Delta f(u) &= \nabla \cdot \nabla f(u) = \nabla \cdot [f'(u)\partial_{x_1} u, \dots, f'(u)\partial_{x_d} u]^T \\ &= f''(u)((\partial_{x_1} u)^2 + \dots + (\partial_{x_d} u)^2) + f'(u)(\partial_{x_1 x_1} u + \dots + \partial_{x_d x_d} u) \\ &= f''(u)\|\nabla u\|_2^2 + f'(u)\Delta u = 6u\|\nabla u\|_2^2 + 3u^2 \Delta u. \end{aligned} \quad (5.16)$$

We now seek to find a weak form of the nonlinear term with non-homogeneous boundary conditions.

Lemma 5.1 (Semi-linear form). *Let $u \in H^4(\Omega)$ be solution to (5.14) and $v_h \in V_h$ the test function. Then can we rewrite the nonlinear term into the corresponding semi-linear form $c_h(\cdot, \cdot)$ for the nonlinear term $(-\Delta f(u), v_h)_\Omega$ into two consistent formulations.*

$$c_h^1(u, v_h) = (f'(u)\nabla u, \nabla v_h)_\Omega - (f'(u)g_1, v_h)_\Gamma, \quad (5.17)$$

$$c_h^2(u, v_h) = -(f(u), \Delta v_h)_\Omega + (f(u), [\partial_n v_h])_{\mathcal{F}_h^{int}} + (f(u), \partial_n v_h)_\Gamma - (f'(u)g_1, v_h)_\Gamma. \quad (5.18)$$

Proof. Derivation of (5.17). We want to construct the first formulation. Let T be an element in \mathcal{T}_h . From the Greens theorem it is easy to see that

$$-(\Delta f(u), v_h)_T = (\nabla f(u), \nabla v_h)_T - (\partial_n f(u), v_h)_{\partial T}. \quad (5.19)$$

First by utilizing that $\nabla f(u) = f'(u)\nabla u$ and $\partial_n f(u) = f'(u)\partial_n u$ and doing a summation over the triangles is it clear that

$$(-\Delta f(u), v_h)_\Omega = (f'(u)\nabla u, \nabla v_h)_\Omega - (f'(u)\partial_n u, v_h)_{\partial \mathcal{T}_h}. \quad (5.20)$$

Iterating over the facets is it clear that

$$\begin{aligned}
(f'(u)\partial_n u, v_h)_{\partial\mathcal{T}_h} &= \sum_{F \in \mathcal{F}_h} \int_F [[f'(u)\partial_n u, v_h]] \\
&= ([[[f'(u)\partial_n u]], \{v_h\})_{\mathcal{F}_h^{int}} + (\{\{f'(u)\partial_n u\}\}, [v_h])_{\mathcal{F}_h^{int}} + (f'(u)\partial_n u, v_h)_\Gamma \\
&= (f'(u)\partial_n u, v_h)_\Gamma.
\end{aligned} \tag{5.21}$$

The jump terms vanishes by the regularity of u and v_h . Hence, by inserting g_1 we have shown that the first formulation holds.

Derivation of (5.18). Applying an extra iteration of the Greens theorem on (5.19) we get the following terms.

$$-(\Delta f(u), v_h)_T = -(f(u), \Delta v_h)_T + (f(u), \partial_n v_h)_{\partial T} - (f'(u)\partial_n u, v_h)_{\partial T}.$$

Now, by summatting all elements, it is clear that this holds.

$$-(\Delta f(u), v_h)_\Omega = -(f(u), \Delta v_h)_\Omega + (f(u), \partial_n v_h)_{\partial\mathcal{T}_h} - (f'(u)\partial_n u, v_h)_{\partial\mathcal{T}_h}. \tag{5.22}$$

It comes evident from the first step of the proof that $(f'(u)\partial_n u, v_h)_{\partial\mathcal{T}_h} = (f'(u)\partial_n u, v_h)_\Gamma$, hence, we only need to compute the term $(f(u), \partial_n v_h)_{\partial\mathcal{T}_h}$ on the facets.

$$\begin{aligned}
(f(u), \partial_n v_h)_{\partial\mathcal{T}_h} &= \sum_{F \in \mathcal{F}_h} \int_F [[f(u), \partial_n v_h]] \\
&= ([[[f(u)]], \{\partial_n v_h\})_{\mathcal{F}_h^{int}} + (\{\{f(u)\}\}, [\partial_n v_h])_{\mathcal{F}_h^{int}} + (f(u), \partial_n v_h)_\Gamma \\
&= (\{\{f(u)\}\}, [\partial_n v_h])_{\mathcal{F}_h^{int}} + (f(u), \partial_n v_h)_\Gamma.
\end{aligned} \tag{5.23}$$

Again one of the jump terms vanishes because of the regularity of u . Inserting the result into (5.22) we have shown that the second formulation also holds. \square

Combining the full general Cahn-Hilliard problem in (5.14) with the semi-linear forms(5.17) and the CutCIP biharmonic problem (4.3), we get the following scheme.

$$(\partial_t u_h, v_h)_\Omega + \varepsilon^2 A_h(u_h, v_h) + c_h(u_h, v_h) = l_h(v_h) \quad \forall u_h, v_h \in V_h. \tag{5.24}$$

To illustrate, assume we use the Laplace formulation presented in (3.24) integrated into (4.3), i.e. $A_h(u_h, v_h) = a_h^L(u_h, v_h) + g_h(u_h, v_h) = l_h^L(v_h)$. Due to the ε scaling, we ultimately arrive at the following modification.

$$l_h^L(v_h) = (g_0, v_h)_\Omega - \varepsilon^2 (g_2, v_h)_\Gamma - \varepsilon^2 (g_1, \Delta v_h)_\Gamma + \varepsilon^2 \frac{\gamma}{h} (g_1, \partial_n v_h)_\Gamma. \tag{5.25}$$

Hence, we arrived at a system which can easily be used to construct manufactured solutions.

6 Conclusion

The primary goal of this thesis was to develop a cut finite element method for discretizing the biharmonic problem in its primal formulation on unfitted meshes, and to apply the resulting scheme to the Cahn-Hilliard equation. Inspired by the theoretical discontinuous Galerkin framework for the Poisson problem proposed in [1], we managed to show that our method is well-posed and that the stability and convergence properties from the original fitted formulation are maintained. Thanks to the design of suitable ghost penalties, we could also show that all presented theoretical properties are geometrically robust in the sense that the derived bounds are insensitive to how the domain boundary cuts the background mesh. The theoretical results are further substantiated by the numerical evidence presented. Additionally, we conducted supplementary tests to ensure the method's geometrical robustness, particularly in instances where the non-stabilized formulation fails. Finally, we demonstrated that our cut continuous interior penalty methods can successfully be applied to the nonlinear Cahn-Hilliard equation using a simple implicit-explicit time stepping method.

While the present thesis demonstrates that the ghost penalty techniques can be successfully used to design non-conform C^0 -CutFEMs for elliptic and parabolic 4th order problems, we have only scratched the surface of this research direction. First of all, in the numerical implementation of the biharmonic problem, we only considered elements of order $k = 2$, hence, it remains to exploit higher order, i.e. $k = 3, 4$. In the continuous interior penalty setting, as our theory already covers the $k \geq 2$ case, this amounts to implement higher order ghost penalty in our computational framework. Moreover, it would also be interesting to compare our method to other unfitted methods, including aggregated finite element methods [101] and conform immersogeometric methods based on C^1 -continuous B -splines [102].

Regarding the Cahn-Hilliard problem, we restricted ourselves to handle a constant mobility $M = 1$ and a polynomial approximation of the non-linearity $F(u) = \frac{1}{4}(u^2 - 1)^2$ in this report. Consequently, we need to extend and test our framework using more physically realistic formulations, including concentration-dependent mobilities as well as thermodynamically more relevant log-based Ginzburg-Landau free energy densities $F(u)$. From a numerical efficiency point of view, our proposed method could significantly benefit from including adaptivity in space and time to both resolve the locally high gradient in the phase transition zone and to account for the different time scales in the phase separation process.

References

- [1] Ceren Gürkan and André Massing. “A stabilized cut discontinuous Galerkin framework for elliptic boundary value and interface problems”. In: *Computer Methods in Applied Mechanics and Engineering* 348 (2019), pp. 466–499.
- [2] Susanne Brenner. *C⁰ Interior Penalty Methods*. Springer International Publishing, 2012.
URL: https://link.springer.com/content/pdf/10.1007/978-3-642-23914-4_2.pdf.
- [3] Xiaobing Feng and Ohannes Karakashian. “Fully discrete dynamic mesh discontinuous Galerkin methods for the Cahn-Hilliard equation of phase transition”. In: *Mathematics of computation* 76.259 (2007), pp. 1093–1117.
- [4] John W Cahn and John E Hilliard. “Free energy of a nonuniform system. I. Interfacial free energy”. In: *The Journal of chemical physics* 28.2 (1958), pp. 258–267.
- [5] John W Cahn and John E Hilliard. “Free energy of a nonuniform system. III. Nucleation in a two-component incompressible fluid”. In: *The Journal of chemical physics* 31.3 (1959), pp. 688–699.
- [6] John W Cahn. “On spinodal decomposition”. In: *Acta metallurgica* 9.9 (1961), pp. 795–801.

- [7] Jessica Bosch and Martin Stoll. “A fractional inpainting model based on the vector-valued Cahn–Hilliard equation”. In: *SIAM Journal on Imaging Sciences* 8.4 (2015), pp. 2352–2382.
- [8] David J Eyre. “Systems of cahn–hilliard equations”. In: *SIAM Journal on Applied Mathematics* 53.6 (1993), pp. 1686–1712.
- [9] Gyula I Tóth, Mojdeh Zarifi, and Bjørn Kvamme. “Phase-field theory of multicomponent incompressible Cahn-Hilliard liquids”. In: *Physical Review E* 93.1 (2016), p. 013126.
- [10] Alain Miranville. “The Cahn–Hilliard equation and some of its variants”. In: *AIMS Mathematics* 2.3 (2017), pp. 479–544.
- [11] Ingo Steinbach. “Phase-field models in materials science”. In: *Modelling and simulation in materials science and engineering* 17.7 (2009), p. 073001.
- [12] Long-Qing Chen. “Phase-field models for microstructure evolution”. In: *Annual review of materials research* 32.1 (2002), pp. 113–140.
- [13] Vittorio E Badalassi, Hector D Ceniceros, and Sanjoy Banerjee. “Computation of multiphase systems with phase field models”. In: *Journal of computational physics* 190.2 (2003), pp. 371–397.
- [14] Qing Li et al. “Lattice Boltzmann methods for multiphase flow and phase-change heat transfer”. In: *Progress in Energy and Combustion Science* 52 (2016), pp. 62–105.
- [15] Junseok Kim. “Phase-field models for multi-component fluid flows”. In: *Communications in Computational Physics* 12.3 (2012), pp. 613–661.
- [16] Jie Shen and Xiaofeng Yang. “A phase-field model and its numerical approximation for two-phase incompressible flows with different densities and viscosities”. In: *SIAM Journal on Scientific Computing* 32.3 (2010), pp. 1159–1179.
- [17] Seong Gyo Kim, Won Tae Kim, and Toshio Suzuki. “Phase-field model for binary alloys”. In: *Physical review e* 60.6 (1999), p. 7186.
- [18] Blas Echebarria et al. “Quantitative phase-field model of alloy solidification”. In: *Physical review E* 70.6 (2004), p. 061604.
- [19] Charlotte Kuhn and Ralf Müller. “A continuum phase field model for fracture”. In: *Engineering Fracture Mechanics* 77.18 (2010), pp. 3625–3634.
- [20] Bin Li et al. “Phase-field modeling and simulation of fracture in brittle materials with strongly anisotropic surface energy”. In: *International Journal for Numerical Methods in Engineering* 102.3-4 (2015), pp. 711–727.
- [21] Andrea L Bertozzi, Selim Esedoglu, and Alan Gillette. “Inpainting of binary images using the Cahn–Hilliard equation”. In: *IEEE Transactions on image processing* 16.1 (2006), pp. 285–291.
- [22] Martin Burger, Lin He, and Carola-Bibiane Schönlieb. “Cahn–Hilliard inpainting and a generalization for grayvalue images”. In: *SIAM Journal on Imaging Sciences* 2.4 (2009), pp. 1129–1167.
- [23] Antun Lovro Brkić, Darko Mitrović, and Andrej Novak. “On the image inpainting problem from the viewpoint of a nonlocal Cahn-Hilliard type equation”. In: *Journal of Advanced Research* 25 (2020), pp. 67–76.
- [24] Scott Tremaine. “On the origin of irregular structure in Saturn’s rings”. In: *The Astronomical Journal* 125.2 (2003), p. 894.
- [25] Abramo Agosti et al. “A Cahn-Hilliard–type equation with application to tumor growth dynamics”. In: *Mathematical Methods in the Applied Sciences* 40.18 (2017), pp. 7598–7626.
- [26] Vittorio Cristini et al. “Nonlinear simulations of solid tumor growth using a mixture model: invasion and branching”. In: *Journal of mathematical biology* 58 (2009), pp. 723–763.

- [27] Ilya Levental, Kandice R Levental, and Frederick A Heberle. “Lipid rafts: controversies resolved, mysteries remain”. In: *Trends in cell biology* 30.5 (2020), pp. 341–353.
- [28] John F Hancock. “Lipid rafts: contentious only from simplistic standpoints”. In: *Nature Reviews Molecular Cell Biology* 7.6 (2006), pp. 456–462.
- [29] Sean Munro. “Lipid rafts: elusive or illusive?” In: *Cell* 115.4 (2003), pp. 377–388.
- [30] Kai Simons and Elina Ikonen. “Functional rafts in cell membranes”. In: *nature* 387.6633 (1997), pp. 569–572.
- [31] Ethan J Miller et al. “Divide and conquer: How phase separation contributes to lateral transport and organization of membrane proteins and lipids”. In: *Chemistry and Physics of Lipids* 233 (2020), p. 104985.
- [32] Harald Garcke et al. “A coupled surface-Cahn–Hilliard bulk-diffusion system modeling lipid raft formation in cell membranes”. In: *Mathematical Models and Methods in Applied Sciences* 26.06 (2016), pp. 1149–1189.
- [33] Vladimir Yushutin et al. “A computational study of lateral phase separation in biological membranes”. In: *International journal for numerical methods in biomedical engineering* 35.3 (2019), e3181.
- [34] Dongsun Lee et al. “Physical, mathematical, and numerical derivations of the Cahn–Hilliard equation”. In: *Computational Materials Science* 81 (2014), pp. 216–225.
- [35] Harald Garcke and Patrik Knopf. “Weak solutions of the Cahn–Hilliard system with dynamic boundary conditions: A gradient flow approach”. In: *SIAM Journal on Mathematical Analysis* 52.1 (2020), pp. 340–369.
- [36] Helmut Abels and Mathias Wilke. “Convergence to equilibrium for the Cahn–Hilliard equation with a logarithmic free energy”. In: *Nonlinear Analysis: Theory, Methods & Applications* 67.11 (2007), pp. 3176–3193.
- [37] Laurence Cherfils, Alain Miranville, and Sergey Zelik. “The Cahn–Hilliard equation with logarithmic potentials”. In: *Milan Journal of Mathematics* 79 (2011), pp. 561–596.
- [38] Charles M Elliott and Zheng Songmu. “On the cahn-hilliard equation”. In: *Archive for Rational Mechanics and Analysis* 96 (1986), pp. 339–357.
- [39] Daisuke Furihata. “A stable and conservative finite difference scheme for the Cahn–Hilliard equation”. In: *Numerische Mathematik* 87.4 (2001), pp. 675–699.
- [40] Kelong Cheng et al. “An energy stable fourth order finite difference scheme for the Cahn–Hilliard equation”. In: *Journal of Computational and Applied Mathematics* 362 (2019), pp. 574–595.
- [41] Chun Liu and Jie Shen. “A phase field model for the mixture of two incompressible fluids and its approximation by a Fourier-spectral method”. In: *Physica D: Nonlinear Phenomena* 179.3-4 (2003), pp. 211–228.
- [42] Li-ping He and Yunxian Liu. “A class of stable spectral methods for the Cahn–Hilliard equation”. In: *Journal of Computational Physics* 228.14 (2009), pp. 5101–5110.
- [43] Yibao Li et al. “A conservative numerical method for the Cahn–Hilliard equation with Dirichlet boundary conditions in complex domains”. In: *Computers & Mathematics with Applications* 65.1 (2013), pp. 102–115.
- [44] Jie Shen and Xiaofeng Yang. “An efficient moving mesh spectral method for the phase-field model of two-phase flows”. In: *Journal of computational physics* 228.8 (2009), pp. 2978–2992.
- [45] WM Feng et al. “A Fourier spectral moving mesh method for the Cahn–Hilliard equation with elasticity”. In: *Commun. Comput. Phys* 5.2-4 (2009), pp. 582–599.

- [46] Charles M Elliott and Donald A French. “Numerical studies of the Cahn–Hilliard equation for phase separation”. In: *IMA Journal of Applied Mathematics* 38.2 (1987), pp. 97–128.
- [47] Mario Kapl, Giancarlo Sangalli, and Thomas Takacs. “A family of C₁ quadrilateral finite elements”. In: *Advances in Computational Mathematics* 47 (2021), pp. 1–38.
- [48] Peter Percell. “On cubic and quartic Clough–Tocher finite elements”. In: *SIAM Journal on numerical analysis* 13.1 (1976), pp. 100–103.
- [49] John H Argyris, Isaac Fried, and Dieter W Scharpf. “The TUBA family of plate elements for the matrix displacement method”. In: *The Aeronautical Journal* 72.692 (1968), pp. 701–709.
- [50] Thomas JR Hughes, John A Cottrell, and Yuri Bazilevs. “Isogeometric analysis: CAD, finite elements, NURBS, exact geometry and mesh refinement”. In: *Computer methods in applied mechanics and engineering* 194.39–41 (2005), pp. 4135–4195.
- [51] Markus Kästner, Philipp Metsch, and Rene De Borst. “Isogeometric analysis of the Cahn–Hilliard equation—a convergence study”. In: *Journal of Computational Physics* 305 (2016), pp. 360–371.
- [52] Héctor Gómez et al. “Isogeometric analysis of the Cahn–Hilliard phase-field model”. In: *Computer methods in applied mechanics and engineering* 197.49–50 (2008), pp. 4333–4352.
- [53] Paola F Antonietti et al. “A C¹ virtual element method for the Cahn–Hilliard equation with polygonal meshes”. In: *SIAM Journal on Numerical Analysis* 54.1 (2016), pp. 34–56.
- [54] Susanne C Brenner et al. “A Quadratic C⁰ Interior Penalty Method for Linear Fourth Order Boundary Value Problems with Boundary Conditions of the Cahn–Hilliard Type”. In: *SIAM Journal on Numerical Analysis* 50.4 (2012), pp. 2088–2110.
- [55] Susanne C Brenner et al. “A quadratic C⁰ interior penalty method for the displacement obstacle problem of clamped Kirchhoff plates”. In: *SIAM Journal on Numerical Analysis* 50.6 (2012), pp. 3329–3350.
- [56] Lin Mu, Junping Wang, and Xiu Ye. “Weak Galerkin finite element methods for the biharmonic equation on polytopal meshes”. In: *Numerical Methods for Partial Differential Equations* 30.3 (2014), pp. 1003–1029.
- [57] Emmanuil H Georgoulis and Paul Houston. “Discontinuous Galerkin methods for the biharmonic problem”. In: *IMA journal of numerical analysis* 29.3 (2009), pp. 573–594.
- [58] Amanda E Diegel and Natasha S Sharma. “A C⁰ interior penalty method for the phase field crystal equation”. In: *Numerical Methods for Partial Differential Equations* 39.3 (2023), pp. 2510–2537.
- [59] Daniele Antonio Di Pietro and Alexandre Ern. *Mathematical aspects of discontinuous Galerkin methods*. Vol. 69. Springer Science & Business Media, 2011.
- [60] Garth N Wells, Ellen Kuhl, and Krishna Garikipati. “A discontinuous Galerkin method for the Cahn–Hilliard equation”. In: *Journal of Computational Physics* 218.2 (2006), pp. 860–877.
- [61] Richard S Falk. “Approximation of the biharmonic equation by a mixed finite element method”. In: *SIAM Journal on Numerical Analysis* 15.3 (1978), pp. 556–567.
- [62] Philippe G Ciarlet and Pierre-Arnaud Raviart. “A mixed finite element method for the biharmonic equation”. In: *Mathematical aspects of finite elements in partial differential equations* (1974), pp. 125–145.
- [63] Thirupathi Gudi, Neela Nataraj, and Amiya K Pani. “Mixed discontinuous Galerkin finite element method for the biharmonic equation”. In: *Journal of Scientific Computing* 37 (2008), pp. 139–161.

- [64] Xiao-liang Cheng, Weimin Han, and Hong-ci Huang. “Some mixed finite element methods for biharmonic equation”. In: *Journal of computational and applied mathematics* 126.1-2 (2000), pp. 91–109.
- [65] Volker John et al. *Finite element methods for incompressible flow problems*. Vol. 51. Springer, 2016.
- [66] Xiaobing Feng and Andreas Prohl. “Error analysis of a mixed finite element method for the Cahn–Hilliard equation”. In: *Numerische Mathematik* 99 (2004), pp. 47–84.
- [67] Eirik Valseth, Albert Romkes, and Austin R Kaul. “A stable FE method for the space-time solution of the Cahn–Hilliard equation”. In: *Journal of Computational Physics* 441 (2021), p. 110426.
- [68] Amanda E Diegel, Xiaobing H Feng, and Steven M Wise. “Analysis of a mixed finite element method for a Cahn–Hilliard–Darcy–Stokes system”. In: *SIAM Journal on Numerical Analysis* 53.1 (2015), pp. 127–152.
- [69] Susanne C Brenner, Amanda E Diegel, and Li-Yeng Sung. “A robust solver for a mixed finite element method for the Cahn–Hilliard equation”. In: *Journal of Scientific Computing* 77 (2018), pp. 1234–1249.
- [70] Florent Chave et al. “A Hybrid High-Order Method for the Cahn–Hilliard problem in Mixed Form”. In: *SIAM Journal on Numerical Analysis* 54.3 (2016), pp. 1873–1898.
- [71] Emmanuel Y Medina et al. “A stabilized hybrid discontinuous Galerkin method for the Cahn–Hilliard equation”. In: *Journal of Computational and Applied Mathematics* 406 (2022), p. 114025.
- [72] Erik Burman et al. “CutFEM: discretizing geometry and partial differential equations”. In: *International Journal for Numerical Methods in Engineering* 104.7 (2015), pp. 472–501.
- [73] Ying Cai, Jinru Chen, and Nan Wang. “A Nitsche extended finite element method for the biharmonic interface problem”. In: *Computer Methods in Applied Mechanics and Engineering* 382 (2021), p. 113880.
- [74] Stefano Zonca, Christian Vergara, and Luca Formaggia. “An unfitted formulation for the interaction of an incompressible fluid with a thick structure via an XFEM/DG approach”. In: (2018).
- [75] Ying Cai, Jinru Chen, and Nan Wang. “A Nitsche mixed extended finite element method for the biharmonic interface problem”. In: *Mathematics and Computers in Simulation* 203 (2023), pp. 112–130.
- [76] Yan Chen, Ruo Li, and Qicheng Liu. “An arbitrary order Reconstructed Discontinuous Approximation to Biharmonic Interface Problem”. In: *arXiv preprint arXiv:2305.03430* (2023).
- [77] Erik Burman, Peter Hansbo, and Mats G Larson. “Cut bogner-fox-schmit elements for plates”. In: *Advanced Modeling and Simulation in Engineering Sciences* 7.1 (2020), p. 27.
- [78] Efthymios N Karatzas and Gianluigi Rozza. “A reduced order model for a stable embedded boundary parametrized Cahn–Hilliard phase-field system based on cut finite elements”. In: *Journal of Scientific Computing* 89.1 (2021), p. 9.
- [79] Santiago Badia, Francesc Verdugo, and Alberto F Martín. “The aggregated unfitted finite element method for elliptic problems”. In: *Computer Methods in Applied Mechanics and Engineering* 336 (2018), pp. 533–553.
- [80] Santiago Badia, Eric Neiva, and Francesc Verdugo. “Linking ghost penalty and aggregated unfitted methods”. In: *Computer Methods in Applied Mechanics and Engineering* 388 (2022), p. 114232.

- [81] Ying Zhao, Dominik Schillinger, and Bai-Xiang Xu. “Variational boundary conditions based on the Nitsche method for fitted and unfitted isogeometric discretizations of the mechanically coupled Cahn–Hilliard equation”. In: *Journal of Computational Physics* 340 (2017), pp. 177–199.
- [82] Christopher Zimmermann et al. “An isogeometric finite element formulation for phase transitions on deforming surfaces”. In: *Computer Methods in Applied Mechanics and Engineering* 351 (2019), pp. 441–477.
- [83] Hammer I. *Solving the biharmonic equation using a continuous interior penalty finite element method*. Specialization project, Department of Mathematical Sciences, NTNU. 2022.
- [84] Alexandre Ern Daniele Antonio Di Pietro. “Mathematical Aspects of Discontinuous Galerkin Methods”. In: (2012). URL: https://link.springer.com/content/pdf/10.1007/978-3-642-23914-4_2.pdf.
- [85] Alexandre Ern and Jean-Luc Guermond. *Finite Elements I: Approximation and Interpolation*. Springer, 2021.
- [86] Philippe G Ciarlet. “Basic error estimates for elliptic problems”. In: (1991).
- [87] Endre Süli and David F Mayers. *An introduction to numerical analysis*. Cambridge university press, 2003.
- [88] A. Ern and J.L. Guermond. *Theory and Practice of Finite Elements*. Applied Mathematical Sciences. Springer New York, 2004, pp. 69–70. ISBN: 9780387205748. URL: <https://books.google.no/books?id=CCjm79FbJbcC>.
- [89] A. Quarteroni. *Numerical Models for Differential Problems, Third Edition 2017*. DOI: [10.1007/978-3-319-49316-9](https://doi.org/10.1007/978-3-319-49316-9). URL: <https://doi.org/10.1007/978-3-319-49316-9>.
- [90] Alexandre Ern and Jean-Luc Guermond. *Finite Elements II: Galerkin Approximation, Elliptic and Mixed PDEs*. Vol. 73. Texts in Applied Mathematics. Cham: Springer International Publishing, 2021. ISBN: 978-3-030-56922-8 978-3-030-56923-5. DOI: [10.1007/978-3-030-56923-5](https://doi.org/10.1007/978-3-030-56923-5). (Visited on 07/13/2023).
- [91] Joachim Nitsche. “Über ein Variationsprinzip zur Lösung von Dirichlet-Problemen bei Verwendung von Teilräumen, die keinen Randbedingungen unterworfen sind”. In: 36.1 (1971), pp. 9–15.
- [92] Ivo Babuška, J Osborn, and Juhani Pitkäranta. “Analysis of mixed methods using mesh dependent norms”. In: *Mathematics of Computation* 35.152 (1980), pp. 1039–1062.
- [93] Erik Burman. “Ghost penalty”. In: *Comptes Rendus Mathematique* 348.21-22 (2010), pp. 1217–1220.
- [94] Erik Burman, Peter Hansbo, and Mats G Larson. “CutFEM based on extended finite element spaces”. In: *Numerische Mathematik* 152.2 (2022), pp. 331–369.
- [95] Erik Burman and Peter Hansbo. “Fictitious domain finite element methods using cut elements: II. A stabilized Nitsche method”. In: *Applied Numerical Mathematics* 62.4 (2012), pp. 328–341.
- [96] Anita Hansbo, Peter Hansbo, and Mats G Larson. “A finite element method on composite grids based on Nitsche’s method”. In: *ESAIM: Mathematical Modelling and Numerical Analysis* 37.3 (2003), pp. 495–514.
- [97] Haim Brezis and Haim Brézis. *Functional analysis, Sobolev spaces and partial differential equations*. Vol. 2. 3. Springer, 2011.
- [98] Elias M Stein. *Singular integrals and differentiability properties of functions*. Vol. 2. Princeton university press, 1970.

- [99] Francesc Verdugo and Santiago Badia. “The software design of Gridap: a finite element package based on the Julia JIT compiler”. In: *Computer Physics Communications* 276 (2022), p. 108341.
- [100] Shuang Li and Kening Wang. “Condition Number Estimates for C0 Interior Penalty Methods”. In: (2007). Ed. by Olof B. Widlund and David E. Keyes, pp. 675–682.
- [101] Santiago Badia, Francesc Verdugo, and Alberto F Martín. “The Aggregated Unfitted Finite Element Method for Elliptic Problems”. In: *Comput. Methods Appl. Mech. Engrg.* 336 (2018), pp. 533–553.
- [102] Ying Zhao, Dominik Schillinger, and Bai-Xiang Xu. “Variational Boundary Conditions Based on the Nitsche Method for Fitted and Unfitted Isogeometric Discretizations of the Mechanically Coupled Cahn–Hilliard Equation”. In: *J. Comput. Phys.* 340 (2017), pp. 177–199. DOI: [10/f99hv6](https://doi.org/10/f99hv6).

